




Advanced Engineering Research

Theoretical and scientific-practical journal

Vol. 21

ISSN 2687-1653 

no. 2
2021

1

Mechanics

2

Machine Building and Machine Science

3

Information Technology, Computer Science, and Management

DOI 10.23947/2687-1653

vestnik-donstu.ru

Advanced Engineering Research

Vol. 21, no. 2

**Theoretical
and scientific-practical journal**

Published since 1999

4 issues a year
April-June 2021

ISSN 2687-1653
DOI: 10.23947/2687-1653

**Founder and publisher — Federal State Budgetary Educational Institution of Higher Education
Don State Technical University (DSTU)**

The journal was known as Vestnik of Don State Technical University (until August 2020)

Included in the list of peer-reviewed scientific editions where the basic research results of doctoral, candidate's theses should be published (State Commission for Academic Degrees and Titles List) in the following research areas:

01.02.01 – Analytical Mechanics (Engineering Sciences)
01.02.04 – Deformable Solid Mechanics (Engineering Sciences)
01.02.04 – Deformable Solid Mechanics (Physicomathematical Sciences)
01.02.06 – Dynamics, Strength of Machines, Gear, and Equipment (Engineering Sciences)
05.02.02 – Engineering Science, Drive Systems and Machine Parts (Engineering Sciences)
05.02.04 – Machine Friction and Wear (Engineering Sciences)
05.02.07 – Technology and Equipment of Mechanical and Physicotechnical Processing (Engineering Sciences)
05.02.08 – Engineering Technology (Engineering Sciences)
05.02.10 – Welding, Allied Processes and Technologies (Engineering Sciences)
05.02.11 – Testing Methods and Diagnosis in Machine Building (Engineering Sciences)
05.13.11 – Software and Mathematical Support of Machines, Complexes and Computer Networks (Engineering Sciences)
05.13.17 – Foundations of Information Science (Engineering Sciences)
05.13.18 – Mathematical Simulation, Numerical Methods and Program Systems (Engineering Sciences)

**The journal is indexed and archived in the Russian Science Citation Index (RSCI),
and in EBSCO International Database**

The journal is a member of Directory of Open Access Journals (DOAJ), Association of Science Editors and Publishers (ASEP) and CrossRef

Certificate of mass media registration ЭЛ № ФС 77 – 78854 of 07.08.2020 is issued by the Federal Service for Supervision of Communications, Information Technology, and Mass Media

The issue is prepared by:

Inna V. Boyko, Gennady I. Rassokhin, Marina P. Smirnova (English version)

Founder's, Publisher's and Printery Address:

Gagarin Sq. 1, Rostov-on-Don, 344003, Russia. Phone: +7 (863) 2-738-372

E-mail: vestnik@donstu.ru <http://vestnik-donstu.ru/>



The content is available under Creative Commons Attribution 4.0 License

Editorial Board

Editor-in-Chief — **Besarion Ch. Meskhi**, Dr.Sci. (Eng.), professor, Don State Technical University (Russian Federation);
deputy chief editor — **Valery P. Dimitrov**, Dr.Sci. (Eng.), professor, Don State Technical University (Russian Federation);
executive editor — **Manana G. Komakhidze**, Cand.Sci. (Chemistry), Don State Technical University (Russian Federation);
executive secretary — **Nadezhda A. Shevchenko**, Don State Technical University (Russian Federation);

Evgeny V. Ageev, Dr.Sci. (Eng.), professor, South-Western State University (Russian Federation);
Sergey M. Aizikov, Dr.Sci. (Phys.-Math.), professor, Don State Technical University (Russian Federation);
Kamil S. Akhverdiev, Dr.Sci. (Eng.), professor, Rostov State Transport University (Russian Federation);
Vladimir I. Andreev, member of RAACS, Dr.Sci. (Eng.), professor, National Research Moscow State University of Civil Engineering (Russian Federation);
Imad R. Antipas, Cand.Sci. (Eng.), Don State Technical University (Russian Federation);
Torsten Bertram, Dr.Sci. (Eng.), professor, TU Dortmund University (Germany);
Dmitry A. Bezuglov, Dr.Sci. (Eng.), professor, Rostov branch of Russian Customs Academy (Russian Federation);
Larisa V. Cherkesova, Dr.Sci. (Phys. -Math.), professor, Don State Technical University (Russian Federation);
Alexandr N. Chukarin, Dr.Sci. (Eng.), professor, Rostov State Transport University (Russian Federation);
Oleg V. Dvornikov, Dr.Sci. (Eng.), professor, Belarusian State University (Belarus);
Karen O. Eghiazaryan, Dr.Sci. (Eng.), professor, Tampere University of Technology (Tampere, Finland);
Sergey V. Eliseev, corresponding member of Russian Academy of Natural History, Dr.Sci. (Eng.), professor, Irkutsk State Railway Transport Engineering University (Russian Federation);
Victor A. Ereemeev, Dr.Sci. (Phys.-Math.), professor, Southern Scientific Center of RAS (Russian Federation);
Mikhail B. Flek, Dr.Sci. (Eng.), professor, "Rostvertol" JSC (Russian Federation);
Nikolay E. Galushkin, Dr.Sci. (Eng.), professor, Institute of Service and Business (DSTU branch) (Russian Federation);
LaRoux K. Gillespie, Dr.Sci. (Eng.), professor, President-elect of the Society of Manufacturing Engineers (USA);
Anatoly A. Korotkii, Dr.Sci. (Eng.), professor, Don State Technical University (Russian Federation);
Victor M. Kureychik, Dr.Sci. (Eng.), professor, Southern Federal University (Russian Federation);
Geny V. Kuznetzov, Dr.Sci. (Phys.-Math.), professor, Tomsk Polytechnic University (Russian Federation);
Vladimir I. Lysak, Dr.Sci. (Eng.), professor, Volgograd State Technical University, (Russian Federation);
Vladimir I. Marchuk, Dr.Sci. (Eng.), professor, Institute of Service and Business (DSTU branch) (Shakhty);
Igor P. Miroshnichenko, Cand.Sci. (Eng.), professor, Don State Technical University (Russian Federation);
Vladimir G. Mokrozub, Dr.Sci. (Eng.), associate professor, Rostov State Transport University (Russian Federation);
Murman A. Mukutadze, Cand.Sci. (Eng.), professor, Tambov State Technical University (Russian Federation);
Nguyen Dong Ahn, Dr.Sci. (Phys. -Math.), professor, Institute of Mechanics, Academy of Sciences and Technologies of Vietnam (Vietnam);
Petr M. Ogar, Dr.Sci. (Eng.), professor, Bratsk State University (Russian Federation);
Gennady A. Ougolnitsky, Dr.Sci. (Phys.-Math.), professor, Southern Federal University (Russian Federation);
Sergey G. Parshin, Dr.Sci. (Eng.), associate professor, St. Petersburg Polytechnic University (Russian Federation);
Valentin L. Popov, Dr.Sci. (Phys. -Math.), professor, Institute of Mechanics, Berlin University of Technology (Germany);
Nikolay N. Prokopenko, Dr.Sci. (Eng.), professor, Don State Technical University (Russian Federation);
Igor B. Sevostianov, Cand.Sci. (Phys. -Math.), professor, New Mexico State University (USA);
Vladimir N. Sidorov, Dr.Sci. (Eng.), Russian University of Transport (Russian Federation);
Arkady N. Solovyev, Dr.Sci. (Phys. -Math.), professor, Don State Technical University (Russian Federation);
Alexandr I. Sukhinov, Dr.Sci. (Phys.-Math.), professor, Don State Technical University (Russian Federation);
Mikhail A. Tamarkin, Dr.Sci. (Eng.), professor, Don State Technical University (Russian Federation);
Valery N. Varavka, Dr.Sci. (Eng.), professor, Don State Technical University (Russian Federation);
Igor M. Verner, Cand.Sci. (Eng.), Docent, Technion (Israel);
Batyr M. Yazyev, Dr.Sci. (Phys. -Math.), professor, Don State Technical University (Russian Federation);
Vilor L. Zakovorotny, Dr.Sci. (Eng.), professor, Don State Technical University (Russian Federation);

CONTENTS

MECHANICS

<i>Yazyev S. B., Andreev V. I., Chepurnenko A. S.</i> Stability analysis of wooden arches with account for nonlinear creep	114
<i>Lazarev S. I., Lomakina O. V., Bulanov V. E., Khorokhorina I. V.</i> Stress-strain state of a combined toroidal baromembrane apparatus	123
<i>Gaidzhurov P. P., Saveleva N. A., Dyaiachenkov V. A.</i> Finite element modeling of the joint action of flow slide and protective structure	133
<i>Vasiliev P. V., Senichev A. V., Giorgio I.</i> Visualization of internal defects using a deep generative neural network model and ultrasonic nondestructive testing	143

MACHINE BUILDING AND MACHINE SCIENCE

<i>Zakovorotny V. L., Gvindjiliya V. E., Zakalyuzhny A. A.</i> Influence of stiffness of the mechanical part of the drive and cutting parameters on the shaping elastic deformation control	154
<i>Lyudmirsky Y. G., Soloviev A. N., Soltovets M. V., Kotlyshev R. R., Kramskoy V. V., Mironov A. I.</i> Technology and equipment for friction stir preweld edge preparation	163
<i>Apryshkin D. S., Khazanovich G. Sh., Gutarevich V. O.</i> Improving the maintenance program for passenger elevators based on simulation of their operating modes	171
<i>Paleva-Kadiyska B., Roussev R., Galabov V.</i> Rational Possibility of Generating Power Laws in the Synthesis of Cam Mechanisms	184

INFORMATION TECHNOLOGY, COMPUTER SCIENCE, AND MANAGEMENT

<i>Lapshin V. L., Zenkov E. V.</i> Control algorithm for an elastic-viscoplastic model to study processes of shock interaction of bodies	191
<i>Zdor D. V.</i> Theoretical foundations of the organization of branches and repetitions in programs in the logic programming language Prolog	200
<i>Yadrovskaya M. V., Porksheyen M. V., Sinelnikov A. A.</i> Prospects of IoT technology	207

MECHANICS



UDC 624.04

<https://doi.org/10.23947/2687-1653-2021-21-2-114-122>

Stability analysis of wooden arches with account for nonlinear creep

S. B. Yazyev¹, V. I. Andreev², A. S. Chepurnenko¹¹ Don State Technical University (Rostov-on-Don, Russian Federation)² Moscow State University of Civil Engineering (Moscow, Russian Federation)

Introduction. The paper deals with the calculation of wooden arches taking into account the nonlinear relationship between stresses and instantaneous deformations, as well as creep and geometric nonlinearity, are considered. The analysis is based on the integral equation of the viscoelastoplastic hereditary aging model, originally proposed by A.G. Tamrazyan [1] to describe the nonlinear creep of concrete.

Materials and Methods. The creep measure is taken in accordance with the work of I.E. Prokopovich and V.A. Zedgenidze [2] as a sum of exponential functions. The transition from the integral form of the creep law to the differential form is shown. The relationship between stresses and instantaneous deformations for wood under compression is determined from the Gerstner formula, and elastic work is assumed under tension. The solution is carried out using the finite element method in combination with the Newton-Raphson method and the Euler method according to the scheme that involves a stepwise increase in the load with correction of the stiffness matrix taking into account the change in the coordinates of the nodes with the sequential calculation of additional displacements of the nodes, which are due to the residual forces. The proposed approach for increasing the accuracy of determination of creep deformations at each step provides using the fourth-order Runge-Kutta method instead of the Euler method.

Results. Based on the Lagrange variational principle, expressions are obtained for the stiffness matrix and the vector of additional dummy loads due to creep. The method developed by the authors is implemented in the form of a program in the MATLAB environment. Calculation examples are given for parabolic arches simply supported at the ends without an intermediate hinge and with an intermediate hinge in the middle of the span under the action of a uniformly distributed load. The results obtained are compared in the viscoelastic and viscoelastic formulation. The reliability of the results is validated through the calculation in the elastic formulation in the ANSYS software package.

Discussion and Conclusions. For the arches considered, it is found that even with a load close to the instant critical, the growth of time travel is limited. Thus, the nature of their work under creep conditions differs drastically from the nature of the deformation of compressed rods.

Keywords: creep, wooden arch, geometric nonlinearity, viscoelastic plasticity, finite element method.

For citation: S. B. Yazyev, V. I. Andreev, A. S. Chepurnenko. Stability analysis of wooden arches with account for nonlinear creep. Advanced Engineering Research, 2021, vol. 21, no. 2, pp. 114–122. <https://doi.org/10.23947/2687-1653-2021-21-2-114-122>

© Yazyev S. B., Andreev V. I., Chepurnenko A. S., 2021



Introduction. Wood refers to the materials that exhibit their non-linear properties, both under short-term and long-term exposure. Most existing rheological models of wood establish its instantaneous properties on the basis of Hooke's law; but for compressed wood, a nonlinear diagram of the elastoplastic type is typical [3]. K. P. Pyatikrestovsky was the first to investigate the issues of joint accounting of instantaneous elastoplastic properties of wood and its creep. He combined these properties on the basis of the method of modulus of long-term deformation [4–7]. In this method, the creep equation contains time explicitly, which significantly limits its use in the case of

complex loading modes and variable loads. There is a significant number of publications on the joint accounting of creep and instantaneous nonlinearity of wood deformation in the calculation of compressed rods [8–14]. In particular, [8] discusses the applicability of the Boltzmann superposition principle to the description of nonlinear wood creep. In [9], theoretical calculations are compared to experimental data for compressed rods; and in [10], in addition to the compressive longitudinal load, the transverse load is taken into account. In [11–13], the stability problem is solved for the rod elements in the frame structure. In paper [14], a long-term critical force is derived for compressed wooden elements, taking into account the nonlinear creep.

The problem of calculation with account for creep and instantaneous nonlinearity of deformation is a challenge not only for any particular rod and frame, but also for such rod systems as arches. This work objective is to develop a method for calculating arch structures taking into account the nonlinear properties of the material under short-term and long-term exposure, as well as geometric nonlinearity.

Materials and Methods. As a relation that determines the relationship between stresses and deformations, we use the equation of the viscoelastic model of hereditary aging:

$$\varepsilon(t) = \frac{f[\sigma(t)]}{E_0(t)} - \int_{\tau_0}^t f[\sigma(\tau)] \frac{\partial C(t, \tau)}{\partial \tau} d\tau, \quad (1)$$

This equation was first proposed in [1] for modeling the nonlinear creep of concrete. Here, the function $f(\sigma)$ establishes the relationship between stress and instantaneous strain, $C(t, \tau)$ — creep measure. The stress-strain diagram of compressed wood under short-term loading is well approximated by the Gerstner formula [15], which has the form:

$$\sigma = E_0 \varepsilon - \frac{E_0^2}{4R} \varepsilon^2. \quad (2)$$

The compressive stresses are used in the formula (2) with the sign “+”. When wood is stretched, there is a linear diagram up to the breaking point. Expressing the strain in terms of stress from (2), we obtain:

$$\varepsilon = \frac{2R}{E_0} \left(1 - \sqrt{1 - \frac{\sigma}{R}} \right). \quad (3)$$

Based on (3), the stress function $f(\sigma)$ can be written as:

$$f(\sigma) = 2R \left(1 - \sqrt{1 - \frac{\sigma}{R}} \right). \quad (4)$$

To measure the creep of wood, we use the formula proposed in the work of V. A. Zedgenidze and I. E. Prokopovich [2]:

$$C(t, \tau) = (C_0 + A_0 e^{-\gamma \tau}) [1 - B_1 e^{-\gamma_1(t-\tau)}], \quad (5)$$

where $C_0 = 2.87 \cdot 10^{-5} \text{ MPa}^{-1}$, $A_0 = 10.95 \cdot 10^{-5} \text{ MPa}^{-1}$, $B_1 = 1$, $\gamma = \gamma_1 = 0.15 \text{ day}^{-1}$.

Equation (1) can be presented in the form:

$$\varepsilon = \frac{\sigma}{E} + \varepsilon^*, \quad (6)$$

where $E = \frac{E_0 \sigma}{f(\sigma)}$ — secant modulus, $\varepsilon^* = - \int_{\tau_0}^t f[\sigma(\tau)] \frac{\partial C(t, \tau)}{\partial \tau} d\tau$ — creep deformation.

For the creep measure in the form (5), the creep strain can be written as the sum of two components:

$$\varepsilon^* = \varepsilon_1^* + \varepsilon_2^*, \quad \varepsilon_1^* = \gamma C_0 B_1 \int_{\tau_0}^t f[\sigma(\tau)] e^{-\gamma(t-\tau)} d\tau, \quad \varepsilon_2^* = A_0 \gamma \int_{\tau_0}^t f[\sigma(\tau)] e^{-\gamma \tau} d\tau. \quad (7)$$

Differentiating in time (7), we obtain expressions for the growth rates of each component:

$$\frac{\partial \varepsilon_1^*}{\partial t} = \gamma (C_0 B_1 f[\sigma(t)] - \varepsilon_1^*); \quad \frac{\partial \varepsilon_2^*}{\partial t} = A_0 \gamma f[\sigma(t)] e^{-\gamma t}. \quad (8)$$

On the basis of (6), we derive the relationship between internal forces and deformations for the element under the combined action of the longitudinal force and the bending moment. The elastic modulus is assumed to be a function of y coordinate, which varies from $-h/2$ to $h/2$ in the height of the cross section. Based on the hypothesis of flat sections, we write the total deformation in the form:

$$\varepsilon = \varepsilon_0 + y\chi, \quad (9)$$

where ε_0 — deformation of the middle layer $\chi = -\frac{d^2v}{dx^2}$ — change in curvature..

We then substitute (9) in (6). Expressing σ by ε , we obtain:

$$\sigma = E(y)(\varepsilon - \varepsilon^*) = E(y)(\varepsilon_0 + y\chi - \varepsilon^*). \quad (10)$$

The longitudinal force and bending moment in the element are related to the stress through the following integral dependences:

$$M = \int_A \sigma y dA; \quad N = \int_A \sigma dA. \quad (11)$$

Here, A — cross-sectional area of the rod.

Substitute (10) in (11) and convert the resulting equalities to the matrix form:

$$\begin{Bmatrix} N \\ M \end{Bmatrix} = [D] \begin{Bmatrix} \varepsilon_0 \\ \chi \end{Bmatrix} - \begin{Bmatrix} N^* \\ M^* \end{Bmatrix}, \quad (12)$$

where $N^* = \int_A E(y) \varepsilon^* dA$, $M^* = \int_A E(y) y \varepsilon^* dA$, $[D] = \begin{bmatrix} EA & ES \\ ES & EI \end{bmatrix}$ — the matrix of reduced stiffnesses, which are determined from the formulas:

$$EA = \int_A E(y) dA, \quad ES = \int_A E(y) y dA, \quad EI = \int_A E(y) y^2 dA. \quad (13)$$

The problem with account for the physical and geometric nonlinearity will be solved by the authors using the finite element method. The rod element shown in Fig. 1 is used. The axial strain, taking into account the geometric nonlinearity, is the sum of the linear and nonlinear components:

$$\varepsilon_0 = \varepsilon_0' + \varepsilon_0'' = \frac{du}{dx} + \frac{1}{2} \left(\frac{dv}{dx} \right)^2. \quad (14)$$

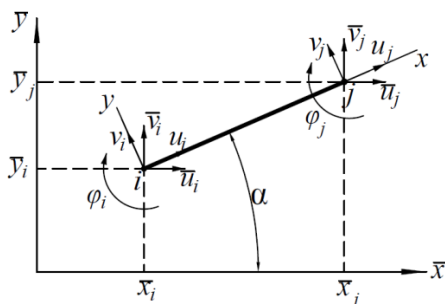


Fig. 1. Rod finite element

To obtain a system of FEM equations, we use the Lagrange variational principle. The strain potential energy (SPE) is written as:

$$\Pi = \frac{1}{2} \int_V \sigma \varepsilon^{el} dV = \frac{1}{2} \int_V E(y) (\varepsilon_0' + \varepsilon_0'' + y\chi - \varepsilon^*)^2 dV. \quad (15)$$

where ε^{el} — elastic strain, equal to the difference between total strain and creep strain.

We write (15) as the sum of four integrals:

$$\begin{aligned} \Pi = \frac{1}{2} & \left(\int_V E(y) \varepsilon_0' (\varepsilon_0' + \varepsilon_0'' + y\chi - \varepsilon^*) dV + \int_V E(y) \varepsilon_0'' (\varepsilon_0' + \varepsilon_0'' + y\chi - \varepsilon^*) dV + \right. \\ & \left. + \int_V E(y) y\chi (\varepsilon_0' + \varepsilon_0'' + y\chi - \varepsilon^*) dV - \int_V E(y) \varepsilon^* (\varepsilon_0' + \varepsilon_0'' + y\chi - \varepsilon^*) dV \right) \end{aligned} \quad (16)$$

The first integral in (16) is written as:

$$\int_V E(y) \varepsilon_0' (\varepsilon_0' + \varepsilon_0'' + y\chi - \varepsilon^*) dV = \int_0^l \varepsilon_0' \int_A E(y) (\varepsilon_0' + y\chi - \varepsilon^*) dA dx + \quad (17)$$

$$+\int_0^l \varepsilon_0' \cdot \varepsilon_0'' \int_A E(y) dA dx = \int_0^l \varepsilon_0' N dx + \int_0^l \varepsilon_0' \cdot \varepsilon_0'' \cdot E A dx,$$

where l — the length of the finite element.

The second integral in (16) is presented in the following form:

$$\begin{aligned} \int_V E(y) \varepsilon_0'' (\varepsilon_0' + \varepsilon_0'' + y\chi - \varepsilon^*) dV &= \int_0^l \varepsilon_0' \cdot \varepsilon_0'' \int_A E(y) dA dx + \int_V E(y) (\varepsilon_0'')^2 dV + \\ &+ \int_0^l \varepsilon_0'' \cdot \chi \int_A E(y) y dA dx - \int_0^l \varepsilon_0'' \int_A E(y) \varepsilon^* dA dx, \end{aligned} \quad (18)$$

The second term in the right-hand side of (18) can be neglected, given its higher order of smallness. The third integral in (16) is written as:

$$\begin{aligned} \int_V E(y) y \chi (\varepsilon_0' + \varepsilon_0'' + y\chi - \varepsilon^*) dV &= \int_0^l \chi \int_A E(y) y (\varepsilon_0' + y\chi - \varepsilon^*) dA dx + \\ &+ \int_0^l \varepsilon_0' \chi \cdot E S dx = \int_0^l M \chi dx + \int_0^l \varepsilon_0'' \chi \cdot E S dx. \end{aligned} \quad (19)$$

The fourth integral in (16) is presented in the following form:

$$\begin{aligned} \int_V E(y) \varepsilon^* (\varepsilon_0' + \varepsilon_0'' + y\chi - \varepsilon^*) dV &= \int_0^l \chi \int_A E(y) y \varepsilon^* dA dx + \\ &+ \int_0^l \varepsilon_0' \int_A \varepsilon^* E(y) dA dx - \int_V (\varepsilon^*)^2 E(y) dV + \int_0^l \varepsilon_0'' \int_A \varepsilon^* E(y) dA dx = \\ &= \int_0^l \chi M^* dx + \int_0^l \varepsilon_0' N^* dx + \int_0^l \varepsilon_0'' N^* dx - \int_V (\varepsilon^*)^2 E(y) dV. \end{aligned} \quad (20)$$

The summand $\int_V (\varepsilon^*)^2 E(y) dV$ when minimized over the vector of nodal displacements, will vanish. Finally, the expression for the SPE will take the form:

$$\begin{aligned} \Pi &= \frac{1}{2} \left(\int_0^l \varepsilon_0' N dx + 2 \int_0^l \varepsilon_0' \varepsilon_0'' E A dx + \int_0^l M \chi dx + 2 \int_0^l \varepsilon_0'' \chi E S dx - \int_0^l \chi M^* dx - \int_0^l \varepsilon_0' N^* dx + \right. \\ &\left. + 2 \int_0^l \varepsilon_0'' N^* dx \right) = \frac{1}{2} \int_0^l \left\{ \varepsilon_0' \quad \chi \right\}^T \left(\begin{Bmatrix} N \\ M \end{Bmatrix} - 2 \begin{Bmatrix} N^* \\ M^* \end{Bmatrix} \right) dx + N_{av} \int_0^l \varepsilon_0'' dx, \end{aligned} \quad (21)$$

where $N_{av} = \varepsilon_0' EA + \chi_{av} ES - N^*$ — the average axial force in the element, χ_{av} — the mean change in the curvature of the element.

Taking into account (12), formula (21) will take the form:

$$\Pi = \frac{1}{2} \int_0^l \left\{ \varepsilon \right\}^T \left([D] \left\{ \varepsilon \right\} - 2 \begin{Bmatrix} N^* \\ M^* \end{Bmatrix} \right) dx + N_{av} \int_0^l \varepsilon_0'' dx, \quad (22)$$

where $\left\{ \varepsilon \right\}^T = \left\{ \varepsilon_0' \quad \chi \right\}^T$.

For finite element displacements, we assume the following approximation:

$$u(x) = u_1 + \frac{u_2 - u_1}{l} x; \quad (23)$$

$$v(x) = \alpha_1 + \alpha_2 x + \alpha_3 x^2 + \alpha_4 x^3; \quad (24)$$

$$\varphi(x) = \frac{dv}{dx} = \alpha_2 + 2\alpha_3 x + 3\alpha_4 x^2. \quad (25)$$

The coefficients of polynomial (24) are determined through substituting the coordinates of the following nodes in (24) and (25):

$$\begin{bmatrix} 1 & 0 & 0 & 0 \\ 0 & 1 & 0 & 0 \\ 1 & l & l^2 & l^3 \\ 0 & 1 & 2l & 3l^2 \end{bmatrix} \cdot \begin{pmatrix} \alpha_1 \\ \alpha_2 \\ \alpha_3 \\ \alpha_4 \end{pmatrix} = \begin{pmatrix} v_1 \\ \varphi_1 \\ v_2 \\ \varphi_2 \end{pmatrix}. \quad (26)$$

From (26), vector $\{\alpha\} = \{\alpha_1 \ \alpha_2 \ \alpha_3 \ \alpha_4\}^T$ is expressed as follows:

$$\{\alpha\} = \begin{bmatrix} 1 & 0 & 0 & 0 \\ 0 & 1 & 0 & 0 \\ 1 & l & l^2 & l^3 \\ 0 & 1 & 2l & 3l^2 \end{bmatrix}^{-1} \cdot \begin{pmatrix} v_1 \\ \varphi_1 \\ v_2 \\ \varphi_2 \end{pmatrix} = \begin{bmatrix} 0 & 1 & 0 & 0 & 0 & 0 \\ 0 & 0 & 1 & 0 & 0 & 0 \\ 0 & -\frac{3}{l^2} & -\frac{2}{l} & 0 & \frac{3}{l^2} & -\frac{1}{l} \\ 0 & \frac{2}{l^3} & \frac{1}{l^2} & 0 & -\frac{2}{l^3} & \frac{1}{l^2} \end{bmatrix} \cdot \begin{pmatrix} u_1 \\ v_1 \\ \varphi_1 \\ u_2 \\ v_2 \\ \varphi_2 \end{pmatrix} = [\Phi]\{U\}. \quad (27)$$

Taking into account (27), formula (24) will take the form:

$$v = \{\Psi\}\{U\}, \quad (28)$$

$$\text{где } \Psi = \{1 \ x \ x^2 \ x^3\}[\Phi].$$

Vector $\{\varepsilon\}$ is written as:

$$\{\varepsilon\} = \begin{pmatrix} \frac{du}{dx} \\ -\frac{d^2v}{dx^2} \end{pmatrix} = \begin{bmatrix} -1/l & 0 & 0 & 1/l & 0 & 0 \\ -\frac{d^2\{\Psi\}}{dx^2} \end{bmatrix} \cdot \{U\} = [B]\{U\}. \quad (29)$$

After substituting (29) and (28) in (22), the SPE is written as:

$$\Pi = \frac{1}{2} \{U\}^T \int_0^l [B]^T [D] [B] dx \{U\} - \{U\}^T \int_0^l [B]^T dx \left\{ \begin{matrix} N^* \\ M^* \end{matrix} \right\} + \{U\}^T N_{av} \cdot \frac{1}{2} \int_0^l \frac{d\{\Psi\}^T}{dx} \frac{d\{\Psi\}}{dx} dx \{U\}. \quad (30)$$

After minimizing the Lagrange functional with respect to the nodal displacement vector, we arrive at a system of equations of the following form:

$$([K] + [K_g])\{U\} = \{F\} + \{F^*\}, \quad (31)$$

where $[K] = \int_0^l [B]^T [D] [B] dx$ — stiffness matrix, $[K_g] = N_{av} \int_0^l \frac{d\{\Psi\}^T}{dx} \frac{d\{\Psi\}}{dx} dx$ — geometric stiffness matrix,

$\{F^*\} = \int_0^l [B]^T dx \left\{ \begin{matrix} N^* \\ M^* \end{matrix} \right\}$ — contribution to the load vector of creep strains, $\{F\}$ — vector of external nodal forces.

A physically and geometrically nonlinear problem is solved using the Newton-Raphson method. The first step is the calculation at $t = 0$. The load increment is performed in quasi-statically small portions with the sequential calculation of additional displacements of the nodes, which are caused by the residual forces, the adjustment of the tangent modulus of elasticity and the coordinates of the nodes at each step.

Next, the time interval at which the calculation is performed is divided into a finite number of time steps. The creep calculation is performed in the same way as the static load calculation. The increment of creep deformations at the step $t + \Delta t$ can be determined using the Euler method

$$\Delta \varepsilon^* = \left(\frac{\partial \varepsilon_1^*}{\partial t} + \frac{\partial \varepsilon_2^*}{\partial t} \right) \Delta t. \quad (32)$$

Research Results. The presented equations and the calculation algorithm are implemented by the authors in the form of a program in the MATLAB environment. The calculation of a parabolic arch simply supported at the ends under the action of a load evenly distributed along the length was performed (Fig. 2) with the following initial data: $E_0 = 1.48 \cdot 10^4$ MPa, $R = 55$ MPa, $L = 16$ m, $f = 3.2$ m. The cross-section of the arch was assumed to be rectangular with dimensions $b = 10$ cm, $h = 15$ cm. The arch was divided into 40 finite elements in length, the section was divided into

100 segments in height, the number of steps in time was assumed to be 600, and in load — 200. The maximum number of iterations at each step is 20. Figure 3 shows the maximum deflection versus load graph. The dashed line corresponds to the calculation in the elastic formulation. To check the results, the solution to the elastic problem was also performed in the ANSYS software package using BEAM 188 rod finite elements. The number of finite elements was assumed to be the same as in MATLAB. There was no significant difference in the results. When calculating in the elastic formulation, a sharp increase in displacements corresponding to the loss of stability is observed at $q = 10.5$ kN/m, and when taking into account the instantaneous nonlinearity of deformation — at $q = 10$ kN/m.

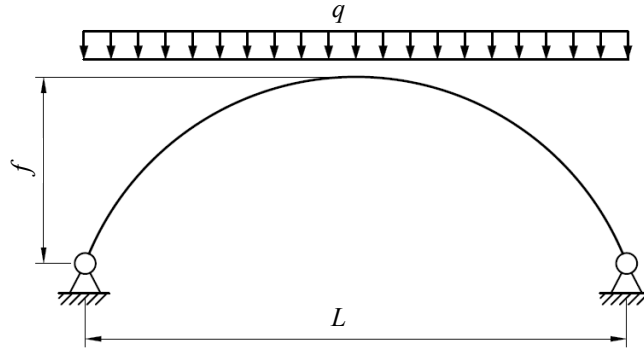


Fig. 2. Design scheme of the structure

q — distributed load on the arch, f — arch rise, L — arch span

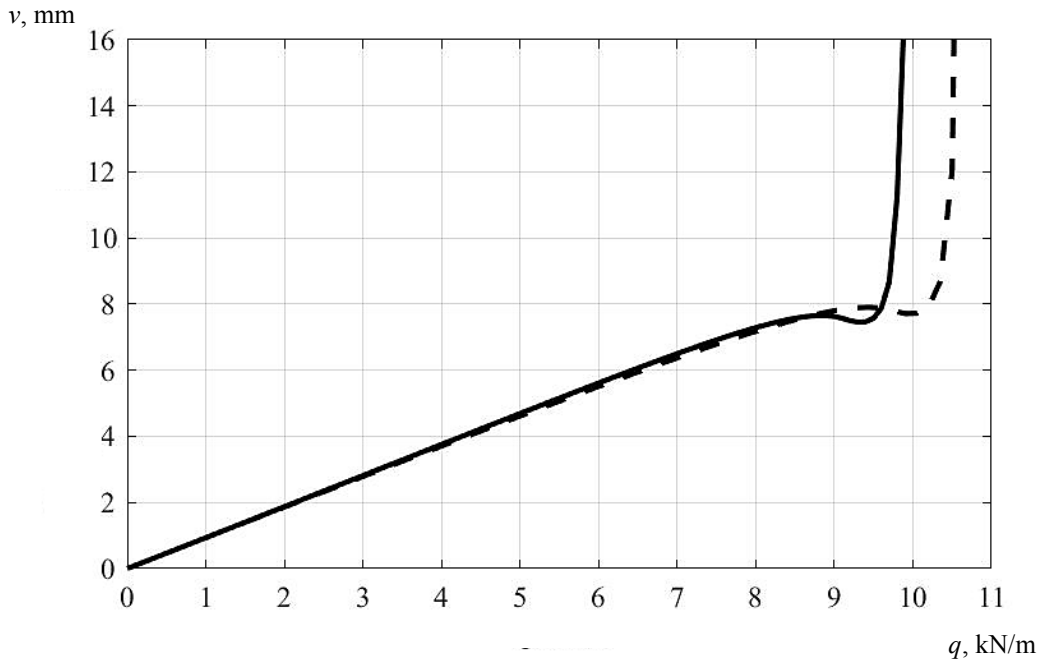


Fig. 3. Dependence of maximum arch deflection on the load under short-term loading

The creep calculation for this arch has shown that even at loads close enough to the instantaneous critical load, the growth of displacements is limited. Figure 4 shows a graph of the midspan deflection growth versus time under a load of $q = 8$ kN/m. The dashed line on this graph corresponds to the solution in the viscoelastic formulation. There was no significant difference in the results.

Also, with the above initial data, the calculation of a three-pinned arch with an intermediate hinge in the middle of the span was performed. In this case, the instantaneous critical load was significantly lower. When calculated in the elastic formulation, it was 4 kN/m, and with account for the instantaneous nonlinearity of deformation — 3.3 kN/m. As in the previous example, even when the load is close enough to the instantaneous critical, the creep decays. The curves of change in time of maximum deflection at $q = 3$ kN/m are shown in Fig. 5. The symbols are the same as in the previous graph.

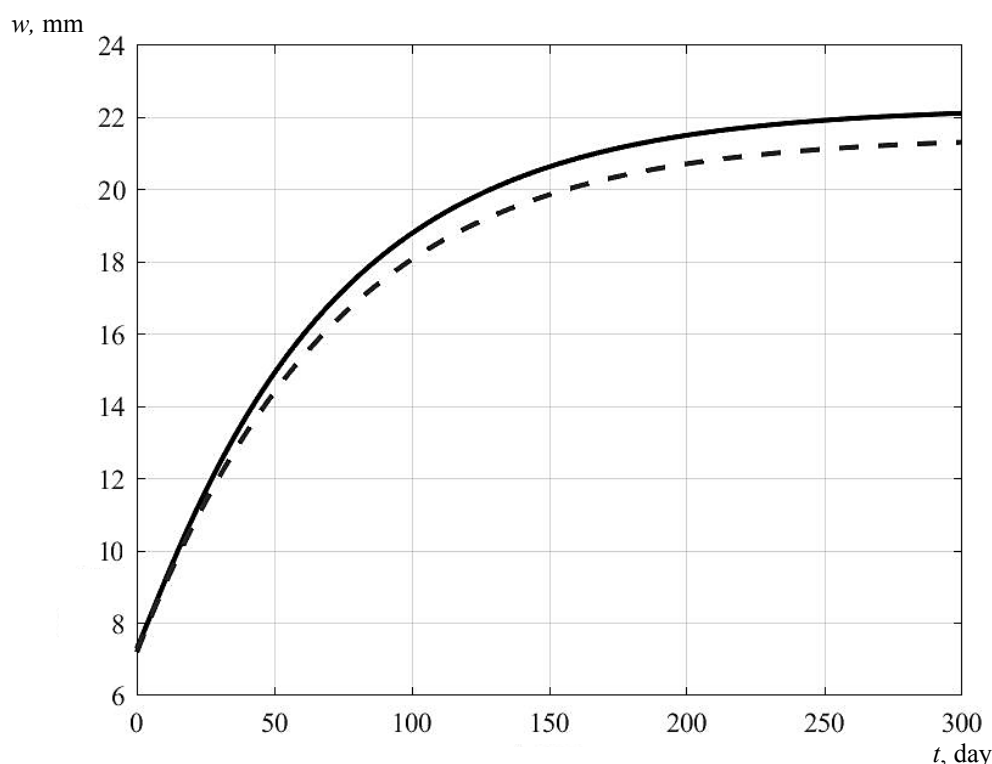


Fig. 4. Change in deflection in the middle of the span over time under load $q = 8 \text{ kN/m}$

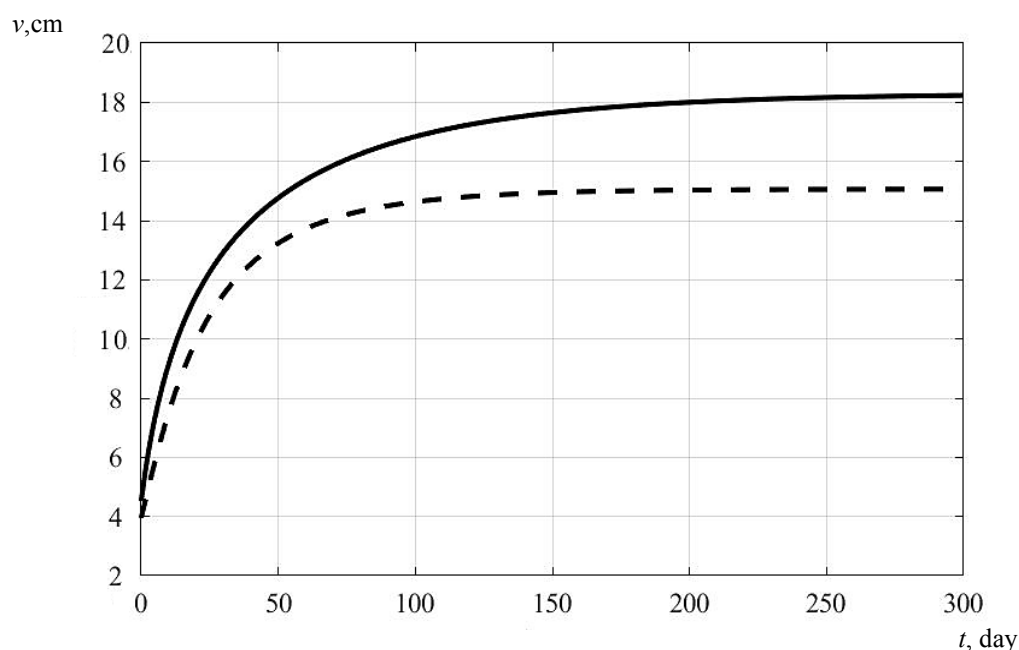


Fig. 5. The growth in time of maximum deflection for an arch with an intermediate hinge in the middle of the span at $q = 3 \text{ kN/m}$

Discussion and Conclusions. The resulting equations and the developed method are universal and provide the use of arbitrary dependences between stresses and instantaneous strains, as well as arbitrary expressions for the creep measure. This provides calculations of structures made not only of wood, but also of any other material. As a result of the analysis of the creep of wooden arches, it is found that, in contrast to compressed rods, creep is limited for them, even under loads close to the instantaneous critical load.

References

1. Tamrazyan AG, Esayan SG. Mekhanika polzuchesti betona [Mechanics of concrete creep]. Moscow: MGSU; 2011. 320 p. (In Russ.)
2. Prokopovich IE, Zedgenidze VA. Prikladnaya teoriya polzuchesti [Applied creep theory]. Moscow: Stroiizdat; 1980. 239 p. (In Russ.)

3. Varenik AS, Varenik KA. O polzuchesti drevesiny [Regarding creep of wood]. Modern Problems of Science and Education. 2014;2:88. URL: <http://www.science-education.ru/pdf/2014/2/429.pdf> (accessed: 19.03.2021). (In Russ.)
4. Pyatikrestovsky KP, Travush VI. O programmirovanii nelineinogo metoda rascheta derevyannykh konstrukttsii [Nonlinear method programming for calculations of statistically indeterminate wooden structures and software systems' communication to development of improved design standards]. Academia. Architecture and Construction. 2015;2:115–119. (In Russ.)
5. Pyatikrestovsky KP, Sokolov BS. Nonlinear analysis of statically indeterminate wooden structures and optimization of cross section dimensions of dome ribs. International Journal for Computational Civil and Structural Engineering. 2018;14(4):130–139.
6. Pyatikrestovsky KP, Travush VI, Pogoreltsev AA, et al. Development of structures from solid wood for objects of infrastructure. International Journal for Computational Civil and Structural Engineering. 2018;14(1):145–154. <https://doi.org/10.22337/2587-9618-2018-14-1-145-154>
7. Pyatikrestovsky KP, Sokolov BS. The Study of Complex Stress States of Elements Filling the Cells Between the Ribs of Wooden Large-Span Domes. International Journal for Computational Civil and Structural Engineering. 2019;15(1):140–152.
8. Varenik KA, Varenik AS, Sanzharovskij RS. Boltzmann principle of superposition in the theory of wood creep for deformations in time. IOP Conference Series: Materials Science and Engineering. 2018;441(1):012057. URL: <https://iopscience.iop.org/article/10.1088/1757-899X/441/1/012057/meta>
9. Varenik KA, Varenik AS, Kirillov AV, et al. Short-term and long-term longitudinal load tests of wooden rods. IOP Conference Series: Materials Science and Engineering. 2020;939(1):012080. URL: <https://iopscience.iop.org/article/10.1088/1757-899X/939/1/012080/meta>
10. Varenik AS, Varenik KA. Model of stress-strain state of wooden rod under eccentric compression and transverse load. IOP Conference Series: Materials Science and Engineering. 2019;656(1):012052. URL: <https://iopscience.iop.org/article/10.1088/1757-899X/656/1/012052/pdf>
11. Dubrakova KO, Dubakov SV, Altuhov FV, et al. The buckling of the physically nonlinear frame-rod structural systems. IOP Conference Series: Materials Science and Engineering. 2019;698(2):022007. <https://doi.org/10.1088/1757-899X/698/2/022007>
12. Dmitrieva KO. Voprosy ustoychivosti sterzhnevnykh ehlementov konstruktivnykh sistem iz drevesiny pri silovom i sredovom nagruzhenii [Issues of stability of core elements of structural systems made of wood under force and environmental loading]. Building and Reconstruction. 2016;4:13–18. (In Russ.)
13. Klyuyeva NV, Dmitrieva KO. Voprosy ustoychivosti sterzhnevnykh ehlementov konstruktivnykh sistem iz drevesiny razlichnykh porod pri silovom i sredovom nagruzhenii v usloviyakh povyshennoi vlazhnosti [Issues of sustainable rod elements design systems of different wood species in force and environmental loading moisture]. Building and Reconstruction. 2016;5:60–68. (In Russ.)
14. Varenik AS, Varenik KA. Dlitel'naya nesushchaya sposobnost' derevyannykh konstrukttsii [Long bearing capacity of wooden structure]. Structural Mechanics of Engineering Constructions and Buildings. 2014;2:23–30. (In Russ.)
15. Pyatikrestovsky KP. K voprosu o vybore modulei uprugosti pri raschete derevyannykh konstrukttsii na prochnost', ustoychivost' i po deformatsiyam [On the selection of elastic moduli in the calculation of wooden structures for strength, stability and deformations]. Structural Mechanics and Analysis of Constructions. 2012;6:73–79. (In Russ.)

Received 28.04.2021

Revised 02.06.2021

Accepted 04.06.2021

About the Authors:

Yazyev, Serdar B., associate professor of the Engineering Mechanics Department, Don State Technical University (1, Gagarin sq., Rostov-on-Don, RF, 344003), Cand.Sci. (Eng.), associate professor, ScopusID: [57190970024](https://orcid.org/0000-0002-7839-7381), ORCID: <http://orcid.org/0000-0002-7839-7381>, russiangel@mail.ru

Andreev, Vladimir I., Head of the Strength of Materials Department, Moscow State University of Civil Engineering (26, Yaroslavskoye Shosse, Moscow, RF, 129337), Dr.Sci. (Eng.), professor, member of Russian Academy of

Architecture and Construction Sciences, ResearcherID: [T-9006-2017](https://orcid.org/0000-0002-1057-4329), ScopusID: [57198780961](https://orcid.org/0000-0002-1057-4329), ORCID: <https://orcid.org/0000-0002-1057-4329>, asv@mgsu.ru

Chepurnenko, Anton S., associate professor of the Strength of Materials Department, Don State Technical University (1, Gagarin sq., Rostov-on-Don, RF, 344003), Cand.Sci. (Eng.), ResearcherID: [E-4692-2017](https://orcid.org/0000-0002-9133-8546), ScopusID: [56056531000](https://orcid.org/0000-0002-9133-8546), ORCID: <https://orcid.org/0000-0002-9133-8546>, anton_chepurnenk@mail.ru

Claimed contributorship

S. B. Yazyev: basic concept formulation; obtaining resolving equations; computational analysis; text preparation; formulation of conclusions. V. I. Andreev: academic advising; analysis of the research results; the text revision; correction of the conclusions. A. S. Chepurnenko: participation in the development of the calculation program; analysis of the research results; the text revision; correction of the conclusions.

All authors have read and approved the final manuscript.

MECHANICS



UDC 531

<https://doi.org/10.23947/2687-1653-2021-21-2-123-132>

Stress-strain state of a combined toroidal baromembrane apparatus



S. I. Lazarev, O. V. Lomakina, V. E. Bulanov, I. V. Khorokhorina

Tambov State Technical University (Tambov, Russian Federation)

Introduction. Currently, the purification of wastewater and technological solutions by membrane methods is considered a promising way to neutralize liquid waste. Therefore, the task of developing an engineering method for calculating baromembrane devices is a challenge. Studies on methods involving calculation of design and process variables, membrane equipment design, research of technological features of membrane devices, selection of design schemes, as well as methods of strength and rigidity analysis, are investigated.

Materials and Methods. Basic elements of the body of the combined membrane apparatus are considered, a design scheme is proposed, and a method for calculating the strength and rigidity of the main load-bearing element, the cover, is described.

Results. The methods determine the required dimensions of shells and plates for the development of a combined membrane apparatus, and evaluate the strength properties of the devices of this class. The construction elements of the apparatus (primarily, the load-bearing covers) must meet not only the requirements of efficiency and quality of separation and cleaning of solutions, but also the conditions for safe operation. Therefore, the design of the device covers should be based on the optimal design dimensions (thicknesses of round plates, toroidal shells, and support rings). To test the method, the stress-strain state of the membrane apparatus structure was calculated for strength and rigidity. As an example, we consider one cover presented in the form of an open toroidal shell. The evaluation of the application of this technique, taking into account the fact that the shell is mated with a round plate in the inner diameter, and with a ring in the outer diameter, has provided the determination of the required parameters.

Discussion and Conclusions. The obtained method of analytical description of the mechanical impact on the elements of the combined apparatus and the example of calculating the toroidal shell and plate, enables to evaluate the stress-strain state of the structure for strength and rigidity. The results of the calculation of covers made of various materials at different pressures are presented. Loading the combined apparatus with transmembrane pressure made it possible to determine the required dimensions of the shells and plates for its design and development.

Keywords: stress-strain state, toroidal plates, membrane apparatus, strength characteristics, design scheme.

For citation: S. I. Lazarev, O. V. Lomakina, V. E. Bulanov, I. V. Khorokhorina. Stress-strain state of a combined toroidal baromembrane apparatus. Advanced Engineering Research, 2021, vol. 21, no. 2, pp. 123–132. <https://doi.org/10.23947/2687-1653-2021-21-2-123-132>

© Lazarev S. I., Lomakina O. V., Bulanov V. E., Khorokhorina I. V., 2021



Introduction. Over the past 25 years, the development of membrane technology has accelerated significantly. Many scientific papers discuss the improvement of membrane installations and apparatuses. Thus, in [1], an original laboratory plant for membrane distillation planar geometry for future connection with solar energy was designed, built and tested. Although conceptually simple, the original geometry was developed to provide a multistage layout, compact design, internal heat recovery, and possible integration with a polymer heat exchanger for final heating of brine using

solar energy or waste heat. In addition, the effects of free air gap, permeable gap, and partial vacuum arrangement of air gaps were investigated.

In [2], the authors propose a multicriteria optimization method for determining the operating and geometric parameters of gas-jet apparatuses, and present the results of the two-stage installation calculations.

In paper [3], based on the concept of creating a directional movement of material flows in the apparatus, the possibility of intensifying the bulk material mixing processes through optimizing the apparatus design is considered. The results of experimental studies on a model of a centrifugal mixer with a rotor made in the form of a hollow truncated cone with a wavy upper edge are presented. It is shown that the rotor modernization provides upgrading the efficiency of the mixing process in intersecting flows of bulk material, and increases the smoothing capacity of the apparatus and the mixing intensity without additional energy costs.

Paper [4] discusses the recent developments to improve the design of the membrane module using 3D printing technology. Currently, there are standards for the design and calculation of the strength of high-pressure devices. Research paper [5] contains a general description of the developed standards, examines their structure, approaches, methods of calculation and design, as well as the main differences from previous regulatory documents. In [6], the authors consider the issues related to the calculation of the time of permeate release from the separation system during the operation of a baromembrane installation with the most common closed circulation loop. The engineering method for calculating the optimal design parameters of the flange of a flat-chamber electrobaromembrane device is described in paper [7]. The engineering method for calculating the optimal design parameters of the flange of a flat-chamber electrobaromembrane device is described in paper [7]. In [8–10], the authors developed the design of a tubular electrobaromembrane apparatus for purifying process solutions, and proposed modified equations for theoretical calculation and forecasting of the performance and quality of the electro-nanofiltration process. Paper [11] is devoted to the analysis of the stress-strain state, which takes into account the transformation of the structural form by folding repeated fragments in the plane of least rigidity. Also, for the analysis and modeling of the stress-strain state of various elements of the apparatus, the finite element method is often used. Thus, in [14], the process of interaction between an abrasive particle and the surface of a part is modeled, and its stress-strain state is analyzed. The results of numerical experiments are presented, which enable to determine how the equivalent plastic deformations are distributed at the penetration depths of the cone of 0.01 mm and 0.05 mm. Thus, the authors are studying the technological features of such devices, the selection of design schemes, methods for strength and stiffness calculations. In this paper, the authors propose to optimize the design in order to reduce material costs.

The review of sources [1–11] on methods for calculating structural and technological parameters and designing membrane equipment allowed us to formulate the research objective — to develop a promising design of the combined-type apparatus, to determine the mechanical loads on its parts, to develop recommendations for design. The structural elements of the device (above all, the load-bearing covers) must meet not only the requirements of efficiency and quality of separation and cleaning of solutions, but also the conditions of safe operation [12–13]. Therefore, the design of the device covers should be based on the optimal design dimensions (thicknesses of round plates, toroidal shells and support rings).

Materials and Methods. The basic elements of the housing of this device are the upper and lower covers. They are connected to each other by a bayonet locking ring (Fig. 1). Proceeding from the fact that the covers have the same geometric dimensions, and their loading differs only by the value of their own weight, we will consider only one — the upper cover.

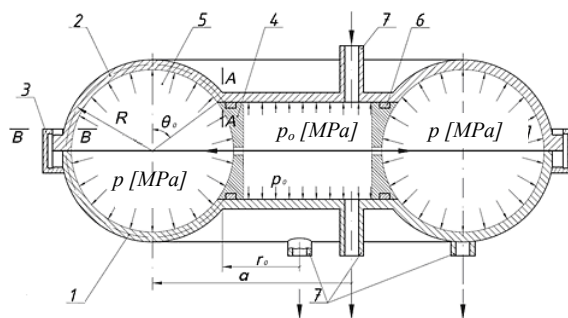


Fig. 1. Design of the baromembrane apparatus: 1 — lower cover; 2 — upper cover; 3 — bayonet lock ring; 4 — flat-chamber module; 5 — tubular module; 6 — seal; 7 — inlet and outlet pipes

Let us consider this design scheme (Fig. 2). The upper cover is under pressure on the round plate from the side of the flat-chamber module and on the wall of the toroidal shell from the side of the tubular module. We show the unknown internal forces in the sections: A–A (shell and round plate mating), B–B (shells and rings), axial force T_{MB} , shear forces, Q_A , Q_B , bending moments M_A .

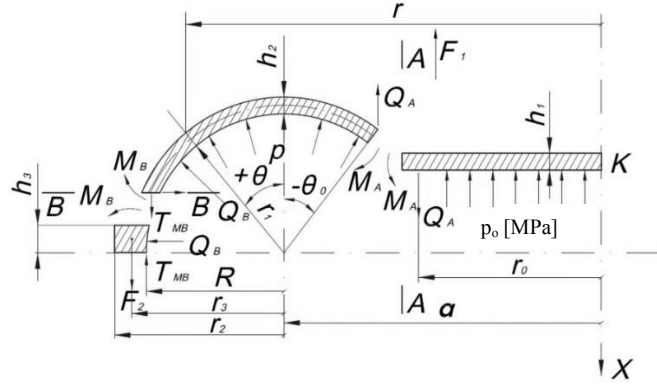


Fig. 2. Design scheme of the cover

These forces are circumferentially-spaced and, with the exception of T_{MB} , are unknown. They can be found from the condition of compatibility of deformations.

We introduce the notation: $N_\theta^*, N_\phi^*, Q^*, M_A^*$ — forces due to the action of pressure p and axial force F ; R — radius of the torus meridian; a — radius of the circular axis of the torus; r_0 — radius of the round plate; $F_1 = p_0 \pi r_0^2$ — direct force ($\theta = \theta_1$); θ_0 — angle at the interface of the toroidal shell and the round plate; θ — variable angle of the shell section; ϕ_B^K — angle of rotation of the ring; E, ν — elastic modulus of the shell material and the Poisson's ratio; ϑ_A^{III} — angle of rotation of the plate; h_2 — thickness of the shell; h_3 — thickness of the ring; p_0 — pressure on the plate; ξ_B^K — radial movement of the ring; $D_1 = \frac{Eh_1}{12(1-\nu^2)}$ — cylindrical stiffness of the plate;

$N = ph_3(a+R) + Q_B(a+R)$ — ring tangential force; $M = P(a+r_3)^2 - T_{MB}(a+R)^2 + M_B(a+R) + Q_B(a+R)\frac{h_3}{2}$ — annular bending moment; $F_2 = p_0 \pi r_0^2 + p\pi[(a+R)^2 - r_0^2]$ — axial force applied to the ring at $\theta = \theta_0$; $\alpha = \frac{R}{a}$; $\lambda = \sqrt[6]{12(1-\nu^2)} \cdot (\alpha\beta)^{1/3}$; $\beta = \frac{R}{h_2}$; $T_{MB} = \frac{F_2}{2\pi(a+R)}$; $I_1 = h_3 \ln\left(\frac{a+r_2}{a+R}\right)$; $I_3 = \frac{h_3^3}{12} \ln\left(\frac{a+r_2}{a+R}\right)$ — geometric characteristics of the annular section.

Section A–A (shell and round plate mating)

$$\left. \begin{aligned} u_A^* + \alpha_{11}(Q_A - Q_A^*) + \alpha_{12}(M_A - M_A^*) &= u_A^{III} \\ \vartheta_A^* + \alpha_{12}(Q_A - Q_A^*) + \alpha_{22}(M_A - M_A^*) &= -\vartheta_A^{III} \end{aligned} \right\}. \quad (1)$$

Section B–B (shell and ring)

$$\left. \begin{aligned} u_B^* + \alpha_{11}(Q_B - Q_B^*) + \alpha_{12}(M_B - M_B^*) &= \xi_B^K \\ \vartheta_B^* + \alpha_{12}(Q_B - Q_B^*) + \alpha_{22}(M_B - M_B^*) &= \phi_B^K \end{aligned} \right\}, \quad (2)$$

where the radial and angular displacements of the shell $u_A^*, u_B^*, \vartheta_A^*, \vartheta_B^*$ in sections A–A and B–B, caused by the internal pressure p , are determined from the formulas:

$$\begin{aligned} u^* &= \frac{a(1+\alpha \sin \theta)}{Eh_2} (N_\phi^* - \nu N_\theta^*); \\ \vartheta^* &= -\sqrt{12(1-\nu^2)} \frac{F_1 \cdot \lambda}{2\pi E h_2^2} \phi(\theta) \operatorname{Re}[-\lambda \omega(\theta)]; \end{aligned} \quad (3)$$

$$N_{\theta}^* = \frac{pR}{2} \left[\frac{2 + \alpha \sin \theta}{1 + \alpha \sin \theta} - \frac{\sin \theta_0}{\sin \theta} \cdot \frac{2 + \alpha \sin \theta_0}{1 + \alpha \sin \theta} \right] + \frac{F_1}{2\pi\alpha} \cdot \frac{1}{\sin \theta (1 + \alpha \sin \theta)} - \frac{F_1}{2\pi\alpha} \cdot \frac{\varphi(\theta) \cos \theta}{1 + \alpha \sin \theta} \cdot \left\{ \lambda I_m E[-\lambda \omega(\theta)] + \frac{1}{\omega(\theta)} \right\}. \quad (4)$$

$$N_{\varphi}^* = \frac{pR}{2} \left[1 + \frac{\sin \theta_0}{\alpha} \cdot \frac{2 + \alpha \sin \theta_0}{\sin^2 \theta} \right] - \frac{F_1}{2\pi r_1} \cdot \frac{1}{\sin^2 \theta} - \frac{F_1}{2\pi r_1} \times \left\{ -\lambda^2 \varphi(\theta) \omega'(\theta) I_m E'[-\lambda \omega(\theta)] + \lambda \varphi'(\theta) I_m E \left[-\lambda \omega(\theta) + \frac{\varphi'(\theta)}{\omega(\theta)} - \frac{\varphi(\theta) \omega'(\theta)}{\omega^2(\theta)} \right] \right\}, \quad (5)$$

$$Q_B^* = N_{\theta}^* \cos \theta - \frac{F_1 \lambda \sin^2 \theta}{2\pi a (1 + \alpha \sin \theta)} \left\{ I_m E[-\lambda \omega(\theta)] + \frac{1}{\lambda \omega(\theta)} \right\},$$

$$M_{\theta}^* = \frac{1}{\sqrt{12(1-\nu^2)}} \cdot \frac{F_1 h_1 \lambda^2}{2\pi R} \left[\varphi(\theta) \omega'(\theta) \cdot Re E'[-\lambda \omega(\theta)] \right], \quad (6)$$

$$M_{\varphi}^* = \nu M_{\theta}^*.$$

The shell can be considered long if the following inequality is satisfied:

$$|\omega(\theta_2) - \omega(\theta_1)| > \frac{3,0}{\lambda}. \quad (7)$$

For this type of toroidal shell, the coefficients at M and Q in equations (1)–(2) are determined from the formulas:

$$\alpha_{11} = \frac{a}{\alpha} \lambda \omega_0' (1 + \alpha \sin \theta_1)^2 + \frac{[Re h_{10}]^2 + [I_m h_{10}]^2}{Re h_{10} I_m h_{10}' - I_m h_{10} \cdot Re h_{10}'} \cdot \frac{1}{Eh_2}; \quad (8)$$

$$\alpha_{12} = -\sqrt{12(1-\nu^2)} \cdot a (1 + \alpha \sin \theta_1) \cdot \frac{Re h_{10} \cdot Re h_{10}' + I_m h_{10} \cdot I_m h_{10}'}{Re h_{10} I_m h_{10}' - I_m h_{10} \cdot Re h_{10}'} \cdot \frac{1}{Eh_2^2}; \quad (9)$$

$$\alpha_{22} = 12(1-\nu^2) \cdot \frac{R}{\lambda \omega_0'} \cdot \frac{[Re h_{10}]^2 + [I_m h_{10}]^2}{Re h_{10} \cdot I_m h_{10}' - I_m h_{10} \cdot Re h_{10}'} \cdot \frac{1}{Eh_2^3}. \quad (10)$$

Tables (1–5)¹ show the values of the functions $\phi(\theta), \omega(\theta), \omega'(\theta), Re h_1, Re h_1', Re[-\lambda \omega(\theta)], I_m E[-\lambda \omega(\theta)], I_m h_1, I_m h_1'$. These dependences will be valid for the case when $\lambda^3 > 5$. They can be obtained using the method of asymptotic integration [14].

The angular and linear displacements of the ring and the round plate can be expressed as

$$\vartheta_A^{III} = -\frac{P_0 r_0^3}{8D_1(1+\nu)} + \frac{M_A r_0}{D_1(1+\nu)}; \quad (11)$$

$u_A^{III} = 0$ — the plate is inextensible in its plane;

$$\xi_B^K = \frac{N}{EI_1} + \frac{\phi h_3}{2}; \quad (12)$$

$$\phi_B^K = \frac{M}{EI_3}, \quad (13)$$

Through determining the unknown forces at the interface points of the shell, plate, and ring M_A, Q_A, M_B, Q_B , it is possible to specify the stresses and deformations in any section of the cover: for the round plate

$$\sigma_{\phi max} = \frac{6M_{\phi}}{h_1^2}; \quad (14)$$

$$\sigma_{r max} = \frac{6Mr}{h_1^2} = \nu \cdot \sigma_{\phi max}; \quad (15)$$

for toroidal shell

$$\sigma_{\theta \max} = \sigma_{\theta \max}^{(u)} + \sigma_{\theta \max}^{(p)} = \frac{6M_0}{h_2^2} + \frac{1+0,5\alpha \cdot \sin \theta}{1+\alpha \cdot \sin \theta} \cdot \frac{pr_1}{h_2}, \quad (16)$$

$$\sigma_{\phi \max} = \sigma_{\phi \max}^{(u)} + \sigma_{\phi \max}^{(p)} = \frac{6M_\phi}{h_2^2} + \frac{pr_1}{h_2}, \quad (17)$$

where $\sigma_{\theta \max}^{(p)}, \sigma_{\phi \max}^{(p)}$ — tensile stresses found by the momentless theory; $\sigma_{\theta \max}^{(u)}, \sigma_{\phi \max}^{(u)}$ — bending stresses.

Maximum normal ring stresses

$$\sigma_{\max}^K = \frac{N}{(a+R)} + \frac{M \cdot h_3/2}{(a+R)I_3}. \quad (18)$$

For major stresses and displacements in the toroidal shell, we use the formulas [15]:
for the case $\theta_* = 0$,

$$\sigma_\phi^p = \sigma_v \cdot 2,15(1-\nu^2)^{1/3} \cdot \alpha^{-1/3} \cdot \beta^{2/3} + \frac{pR}{h_2},$$

at point $\theta_* = \pm \frac{1,225}{\lambda}$,

$$\sigma_\theta = \pm \sigma_v \cdot 2,99(1-\nu^2)^{-1/6} \cdot \alpha^{-1/3} \cdot \beta^{2/3} [\phi(\theta_*)\omega'(\theta_*)] + \frac{1+0,5\alpha \cdot \sin \theta_*}{1+\alpha \cdot \sin \theta_*} \cdot \frac{pR}{h_2}, \quad (19)$$

where $\sigma_v = \frac{F_0}{2\pi a h_2}$; $F_0 = p\pi r_0^2 + p_0\pi(a^2 - r_0^2)$.

Maximum axial displacement at point A ($\theta = \theta_1$) and maximum deflection at the center of the plate can be calculated from the formulas:

$$\delta_A = u_{xA} = \frac{2}{\lambda^3} \cdot \frac{12(1-\nu^2) \cdot R^3}{4Eh_2^3 \cdot a} \cdot F_1, \quad (20)$$

$$u_K^{III} = u_{xA} + \frac{(5+\nu)p_0r_0^4}{(1+\nu) \cdot 64D_1} + \frac{M_A \cdot r_0^2}{(1+\nu) \cdot 2D_1}. \quad (21)$$

The strength condition can be expressed (IV theory)

$$\sigma_{\sigma}^{IV} = \sqrt{\sigma_1^2 + \sigma_2^2 + \sigma_3^2 - \sigma_1\sigma_2 - \sigma_1\sigma_3 - \sigma_2\sigma_3} \leq [\sigma], \quad (22)$$

and rigidity condition

$$u_{x \max} \leq [u_x], \quad (23)$$

where $\sigma_1, \sigma_2, \sigma_3$ — primary stresses at dangerous points of the cover; $[\sigma]$ — permissible stress for the cover material;
 $[u_x]$ — permissible deflection for the cover in the axial direction.

Research Results. Figure 3 shows the design scheme of the toroidal shell.

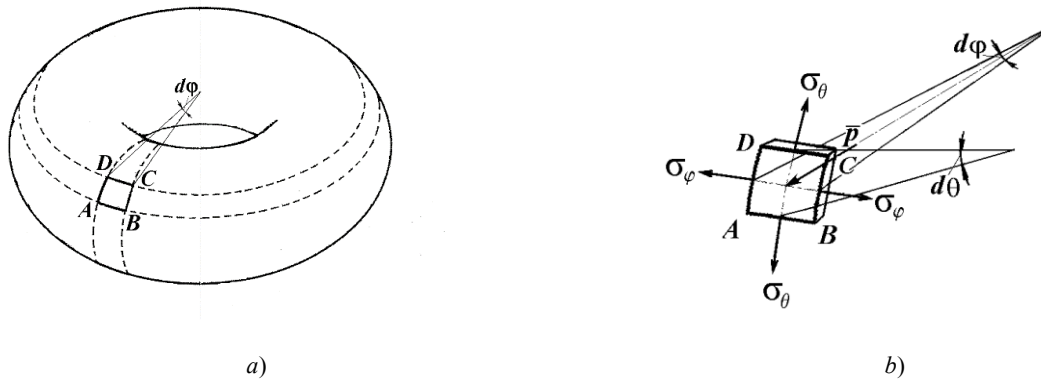


Fig. 3. Design scheme of the toroidal shell:
a) toroidal shell; b) pressurized sheathing element

During the operating process of the device, working pressure p_0 acts on the round plate from the side of the flat-chamber module; from the side of the tubular module, pressure p , which in its maximum value is about a third of the working pressure, acts on the walls of the shell.

In addition to the zones of attachment of the shell, in which there are significant stresses caused by the bending effect, given the thinness of the shell ($\frac{\delta}{R} \leq \frac{1}{20}$) it can be assumed that the stresses arising in the shell are constant in thickness. In this case the theory is called a momentless theory.

From the shell shown in Fig. 3a, we select the element $ABCD$ with two meridional planes (i.e., planes passing through the axis of rotation of the shell) with angle $d\phi$ between them and two planes perpendicular to the axis of the torus AB and CD .

Normal stresses acting on the faces of AC and BD , in the direction of the tangent to the circle, are called circumferential stresses σ_ϕ . Normal stresses acting along the faces of AB and CD in the meridional direction are called meridional stresses σ_θ . In addition to the stresses σ_ϕ and σ_θ , an internal overpressure p acts on the shell element perpendicular to the surface.

The equation connecting these three quantities is fundamental in the momentless theory of shells and is called the Laplace equation:

$$\frac{\sigma_\phi}{r} + \frac{\sigma_\theta}{R} = \frac{p}{\delta}, \quad (24)$$

where R — radius of the middle surface of the torus; r — distance to the axis of rotation; δ — thickness of the torus wall.

For the shell under consideration and when counting the angle from the vertical axis in [13], the following formulas are proposed:

for the outer part of the torus ($0 \leq \theta \leq 90^\circ$)

$$\begin{aligned} \sigma_\theta &= \frac{p}{2\delta} \left[\frac{(a + R \sin \theta)^2 - a^2}{(a + R \sin \theta) \sin \theta} \right], \\ \sigma_\phi &= \frac{p}{\delta} \left[(a + R \sin \theta) - \frac{(a + R \sin \theta)^2 - a^2}{2R \sin \theta} \right] \end{aligned} \quad (25)$$

for the inner part of the torus ($90^\circ \leq \theta \leq 180^\circ$)

$$\begin{aligned} \sigma_\theta &= \frac{p}{2\delta} \left[\frac{a^2 - (a + R \sin \theta)^2}{(a + R \sin \theta) |\sin \theta|} \right], \\ \sigma_\phi &= \frac{p}{\delta} \left[(a + R \sin \theta) + \frac{a^2 - (a + R \sin \theta)^2}{2R \sin \theta} \right]. \end{aligned} \quad (26)$$

where a — radius of the circular axis of the torus.

From the static equilibrium condition of a shell cut off by a cylindrical cross-section of radius a , given that the ring fibers do not deform $\sigma_\phi = 0$ at $\theta = 0^\circ$, and σ_θ can be found from the formula:

$$\sigma_\theta = \frac{pR}{\delta}, \quad (27)$$

for the stresses σ_ϕ , a simplified formula is proposed:

$$\sigma_\phi = pR \sin \frac{\theta}{2\delta}. \quad (28)$$

During the design calculation with an error of up to 5 %, the required thickness of the toroidal shell can be found

— by meridian stresses

$$\delta \geq \frac{pR}{[\sigma_p]} . \quad (29)$$

— by circumferential stresses

$$\delta \geq \frac{pR \sin \theta}{2[\sigma_p]} . \quad (30)$$

The higher value is selected from the obtained values.

At the same time, for vessels and devices operating under excessive pressure, the standard² recommends the following strength condition:

$$S \geq S_p + C , \quad (31)$$

where C — the sum of the increments to the calculated wall thicknesses, mm; S_p — the calculated wall thickness (in our case $S_p = \delta$).

The calculation of a round plate with a hole, loaded with internal pressure, is made according to the formulas (32)–(34).

Effective thickness of the plate:

$$S_{lp} = K \cdot K_0 \cdot D \sqrt{\frac{p}{[\sigma]}} . \quad (32)$$

Condition for the performance of the strength of the plate

$$S_l \geq S_{lp} + C . \quad (33)$$

Discussion and Conclusions. The value of coefficient K is determined depending on the type of connection of the cover parts and, for this option, corresponds to the values:

$$\frac{S-C}{S_l-C} \leq 0.5 ; K = 0.41$$

$$\frac{S-C}{S_l-C} \geq 0.5 ; K = 0.38$$

In all cases, the thickness of the round plate must be greater than or equal to the thickness of the toroidal part.

The value of the attenuation coefficient for the plates with one hole K_0 :

$$K_0 = \sqrt{1 + \frac{d}{D_p} + \left(\frac{d}{D_p}\right)^2} , \quad (34)$$

where d — the hole diameter.

If the inequality $\frac{S_l-C}{D} \geq 0.11$; $S_l - CD \geq 0.11$ is not satisfied, a correction factor is introduced:

$$K_p = \frac{2.2}{1 + \sqrt{1 + \left(6 \frac{S_l-C}{D}\right)^2}} ; \quad K_p = 2.21 + 1 + (6S_l - CD)2 .$$

It should be taken into account that the strength characteristics of fiberglass are in many respects higher than those of steel. The tensile stress (for metals — yield strength) for steel is 240 MPa, for aluminum — 50-440 MPa, for

²STP 10-04-02 Calculation of the strength of vessels and apparatuses. Vol. 1. Calculation of the strength of vertical and horizontal apparatuses. LLC NTP "Pipeline". Moscow, 2005. 190 p. (In Russ.)

fiberglass — 800-1700 MPa³. However, it is required to consider what is the binder. They can be polyester, phenol-formaldehyde, epoxy, organosilicon resins, polyamides, aliphatic polyamides, polycarbonates, etc. The choice of binder affects the strength limit of fiberglass.

Permissible excess internal pressure in the toroidal part:

$$[p] = \frac{[\sigma](S-C)}{R}. \quad (35)$$

The permissible pressure on the round plate is determined from the formula

$$[p] = \left(\frac{S_1 - C}{K \cdot K_0 \cdot D} \right)^2 \cdot [\sigma]. \quad (36)$$

In the future, the calculated value of the permissible overpressure is multiplied by this factor.

Using the data from the tables “Physical and mechanical characteristics of the composite material” and “Comparison of physical and mechanical parameters of various materials”, we will make a calculation.

Table 1 shows the results of calculating covers made of various materials at different pressures. The numerator shows the thickness of the toroidal part, and the denominator shows the thickness of the round plate.

Table 1

Calculating thickness of the covers

Pressure, MPa	Materials			
	PA 6–210/310 OST 6–06-C9–93	PA66-LTO-SV30	St. 3	Composite ⁴
0.5	0.62/3.46	0.31/2.45	0.25/2.19	0.22/2.14
1	1.24/4.89	0.62/3.45	0.50/3.09	0.45/2.92
2	2.48/6.92	1.24/4.87	0.99/4.36	0.89/4.04
3	3.69/8.47	1.85/5.96	1.49/5.35	1.34/5.02
5	6.18/10.93	3.09/7.71	2.47/6.91	2.23/6.53
10	12.32/15.46	6.16/10.91	4.93/9.77	4.48/9.23

In all cases, value c — the sum of the increments to the effective wall thicknesses (the value of STP 10-04-02 is not normalized) is added to these values.

The given method of analytical description of the mechanical impact on the elements of the combined apparatus, and the example of calculating the toroidal shell and plate provide evaluating the stress-strain state of the structure for strength and rigidity. When loading the combined apparatus with transmembrane pressure, it allowed the authors to determine the required dimensions of the shells and plates for its design and development.

References

1. Cipollina A, Sparti MGD, Tamburini A, et al. Development of a Membrane Distillation module for solar energy seawater desalination. Chemical Engineering Research and Design. 2012;90(12):2101–2121. <https://doi.org/10.1016/j.cherd.2012.05.021>
2. Yusupov TA, Yemelyanov VM, Gumerov AM, et al. Mnogokriterial'naya optimizatsiya parametrov gazostruiynykh apparatov [Multicriteria optimization of parameters of gas-jet apparatuses]. Herald of Kazan Technological University. 2003;2:131–136. (In Russ.)
3. Ivanets VN, Sibil' AV. Intensifikatsiya protsessa smeshivaniya putem optimizatsii konstruktssii apparata [Intensification of the mixing process by optimizing the machine design]. Izvestiya vuzov. Food Technology. 2010;4(316):66–67. (In Russ.)

³Comparative characteristics of the properties of fiberglass, steel and aluminum alloys. Available from: www.aquaprom24.ru (accessed: 22.03.2021). (In Russ.)

⁴Epoxy composite material (fiberglass) produced by LLC “Evolution Motors”. Available from: evolmotors.ru (accessed: 19.03.2021). (In Russ.)

4. Jian-Yuan Lee, Wen See Tan, Jia An, et al. The potential to enhance membrane module design with 3D printing technology. *Journal of Membrane Science*. 2016;499:480–490. <https://doi.org/10.1016/j.memsci.2015.11.008>
5. Volfson B. New Russian National Standards on Pressure Vessel and Apparatus Design and Strength Calculation. In: *Proc. ASME 2009 Pressure Vessels and Piping Conference*. Vol. 1: Codes and Standards. Prague, Czech Republic; 2009. P. 531–535. <https://doi.org/10.1115/PVP2009-77840>
6. Babyonyshev SP, Emelyanov SA, Zhidkov VE, et al. Teoreticheskie aspekty prognozirovaniya proizvoditel'nosti baromembrannykh ustanovok dlya razdeleniya zhidkikh polidispersnykh sistem [Theoretic aspects of forecasting the efficiency of baromembrane installations for separation liquid polydisperse systems]. *Science Review*. 2015;5:468–470. (In Russ.)
7. Kochetov VI, Popov VYu. Optimizatsiya konstruktivnykh parametrov flantsa ehlektrobaromembrannogo apparata ploskokamernogo tipa [Optimization of the design parameters of the flange of an electrobaromembrane apparatus of a flat-chamber type]. *Mechanical Engineers to XXI century*. 2012;11:92–96. (In Russ.)
8. Kovaleva O, Lazarev S, Kovalev S. Development and calculation of an electrobaromembrane apparatus for purifying process solutions. *Chemical and Petroleum Engineering*. 2017;53(1/2):21–25. <https://doi.org/10.1007/s10556-017-0287-9>
9. Kochetov VI, Lazarev SI, Kovalev SV, et al. Improved design of an electrobaromembrane apparatus and calculation of the parameters of the housing chamber when subjected to the effect of excess pressure. *Chemical and Petroleum Engineering*. 2018;54(1–2):82–86.
10. Lazarev SI, Kovalev SV, Kovaleva OA, et al. Flat-chamber electrobaromembrane apparatus with improved characteristics and its calculation method. *Chemical and Petroleum Engineering*. 2019;55(1–2):114–121.
11. Gaydzhurov PP, Iskhakova ER, Tsaritova NG. Study of stress-strain states of a regular hinge-rod constructions with kinematically oriented shape change. *International journal for computational civil and structural engineering*. 2020;16(1):38–47. <https://doi.org/10.22337/2587-9618-2020-16-1-38-47>
12. Soloviev AN, Tamarkin MA, Tho Nguyen Van. Metod konechnykh ehlementov v modelirovanii tsentrobezno-rotatsionnoi obrabotki [Finite element modeling method of centrifugal rotary processing]. *Advanced Engineering Research*. 2019;19(3):214–220. (In Russ.) <https://doi.org/10.23947/1992-5980-2019-19-2-214-220>
13. Boyarshinov SV. Osnovy stroitel'noi mekhaniki mashin [Fundamentals of construction mechanics of machines]. Moscow: Mashinostroenie; 1973. 456 p. (In Russ.)
14. Gevorkyan RS. Asimptoticheskie resheniya svyazannykh dinamicheskikh zadach termouprugosti dlya anizotropnykh v plane neodnorodnykh toroidal'nykh obolochek [Asymptotic solutions to coupled dynamic thermoelasticity problems for anisotropic inhomogeneous toroidal shells]. *World Science*. 2016;1(9):14–29. (In Russ.)
15. Legostaev VL, Mordovin ED. Metodika rascheta toroobraznykh obolochek po bezmomentnoi i momentnoi teoriyam prochnosti [Method of calculation of torus-shaped shells according to momentless and moment strength theories]. *Transactions of TSTU*. 2007.;13(3):795–801. (In Russ.)

Received 05.04.2021

Revised 26.04.2021

Accepted 30.04.2021

About the Authors:

Lazarev, Sergey I., Head of the Mechanics and Engineering Drawing Department, Tambov State Technical University (106, Sovetskaya St., Tambov, RF, 392000), Dr.Sci. (Eng.), professor, ORCID: <https://orcid.org/0000-0003-0746-5161>, sergey.lazarev.1962@mail.ru

Lomakina, Olga V., associate professor of the Mechanics and Engineering Drawing Department, Tambov State Technical University (106, Sovetskaya St., Tambov, RF, 392000), Cand.Sci. (Pedagogy), ORCID: <https://orcid.org/0000-0002-6908-6055>, lomakinaolga@mail.ru

Bulanov, Vladimir E., associate professor of the Mechanics and Engineering Drawing Department, Tambov State Technical University (106, Sovetskaya St., Tambov, RF, 392000), Cand.Sci. (Eng.), associate professor, ORCID: <https://orcid.org/0000-0002-8973-7513>, 0212vladimir@mail.ru

Khorohorina, Irina V., associate professor of the Mechanics and Engineering Drawing Department, Tambov State Technical University (106, Sovetskaya St., Tambov, RF, 392000), Cand.Sci. (Eng.), associate professor, ORCID: <https://orcid.org/0000-0002-8947-6181>, geometry@mail.nnn.tstu.ru

Claimed contributorship

S. I. Lazarev: setting the research objective and task; discussion of the results. O. V. Lomakina: conducting a review; selection of a solution method; text preparation. V. E. Bulanov: computational analysis; formulation of conclusions. I. V. Khorohorina: analysis of the research results; the release paper version revision.

All authors have read and approved the final manuscript.

MECHANICS



UDC 539.42

<https://doi.org/10.23947/2687-1653-2021-21-2-133-142>

Finite element modeling of the joint action of flow slide and protective structure



P. P. Gaidzhurov, N. A. Saveleva, V. A. Dyaichenkov

Don State Technical University (Rostov-on-Don, Russian Federation)

Introduction. In the context of the problem of plane deformation, a finite-element model of a natural landslide slope is developed. It allows for the joint work of a flow slide and a protective engineering structure. The Drucker-Prager model is used to take into account the physical nonlinearity of the slope layer material. To activate the kinematic instability, a viscoelastic interlayer is introduced into the design scheme, along which the landslide layer slides.

Materials and Methods. Numerical experiments were performed using the ANSYS Mechanical software package, which implements the finite element method in the form of the displacement method. Slope discretization is performed on the basis of PLANE42 flat four-node finite elements. To simulate the displacement of the landslide layer relative to the fixed base, the combined viscoelastic elements COMBIN14 were used.

Results. A physically nonlinear model of a natural landslide slope consisting of a base, a landslide layer, and a viscoelastic interlayer, is formalized. An engineering technique for analyzing the stress-strain state of the “slope-protective structure” system has been developed, taking into account the kinematic instability of the landslide layer. A series of computational experiments was carried out.

Discussion and Conclusion. Based on the calculations performed, it is shown that the proposed method enables to specify the force action of the landslide layer on the protective structure and, thereby, to increase the reliability of the risk assessment when activating the landslide process.

Keywords: finite element method, Drucker-Prager model, landslide process simulation, landslide protection engineering structures.

For citation: P. P. Gaidzhurov, N. A. Saveleva, V. A. Dyaichenkov. Finite element modeling of the joint action of flow slide and protective structure. Advanced Engineering Research, 2021, vol. 21, no. 2, pp. 133–142. <https://doi.org/10.23947/2687-1653-2021-21-2-133-142>

© Gaidzhurov P. P., Saveleva N. A., Dyaichenkov V. A., 2021



Introduction. The design of anti-landslide engineering structures is one of the most important areas in the construction science. At the same time, numerical modeling of the stability of natural landslide slopes is associated with uncertainty factors, such as instability of the physical and mechanical characteristics of the material and the variability of the fracture trajectories.

Nowadays, various variants of the limit equilibrium method and the method of reducing the shear strength of the material in combination with the finite element method are used to assess the slope stability [1–3]. The calculation result of the using the limit equilibrium method is the geometry of the “classical” circular sliding line. The method of reducing the strength provides more complete information about the sliding surface for the considered landslide area.

Particularly, we can distinguish the direction of the study of slope processes based on the model of the centroidal motion of particles that elastically interact with each other and the inclined surface [4]. Another approach based on block kinematics is the so-called discontinuous deformation analysis (DDA) method [5]. The DDA method has limitations regarding the interaction between adjacent blocks. The essence of these restrictions is the impossibility

of mutual penetration of the blocks and the absence of tensile stresses between the blocks. Figure 1 (taken from [5]) shows the block coupling scheme used in the ADD method for modeling rockfalls. In this Figure, k_x , k_y and c_x , c_y — are the stiffness and viscosity parameters, respectively, in the direction of the axes X and Y .

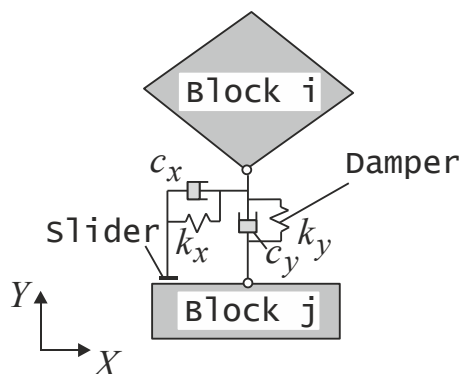


Fig. 1. Block diagram for modeling rockfalls

The disadvantage of the DDA method is the impossibility of introducing engineering structures into the design scheme that prevent the progressive destruction of the mountain range.

If, after assessing the natural slope stability, a decision is made on the feasibility of constructing landslide structures, then the data of engineering and geological surveys, as well as various scenarios of external force impacts on the landslide slope sections, are used as initial information for the design. Numerical simulation of the stress-strain state of a reinforced landslide slope is usually performed in a two-dimensional formulation within the framework of the nonlinear theory of elasticity using the finite element method. The ground pressure is assumed to be linearly distributed in depth. For engineering geotechnical calculations, specialized finite element software systems are used: Plaxis, MIDAS GTS, GEO5, which include the most common soil models. Modeling of complex geotechnical systems is carried out on the basis of the “heavy” software package ANSYS Mechanical [6].

It should be noted that in the papers devoted to the analysis of the stress-strain state of anti-landslide structures, there is no information on the use of models that take into account the direct sliding (creeping) of the landslide layer. In normal practice, design schemes are used, in which the joint (continuous) deformation of the entire soil mass is provided, up to the loss of the bearing capacity of the soil. This does not allow us to fully assess the force impact of the landslide layer on the structural elements.

Materials and Methods. The design scheme of the landslide slope is shown in Fig. 2 (dimensions are given in meters). Consider that the slope consists of two layers: S_1 — base of the slope (dense clay); S_2 — landslide layer (waterlogged loam). We assume that the position of the sliding line is known. The external impact is presented by the self-weight of the landslide layer S_2 and the evenly distributed pressure q .

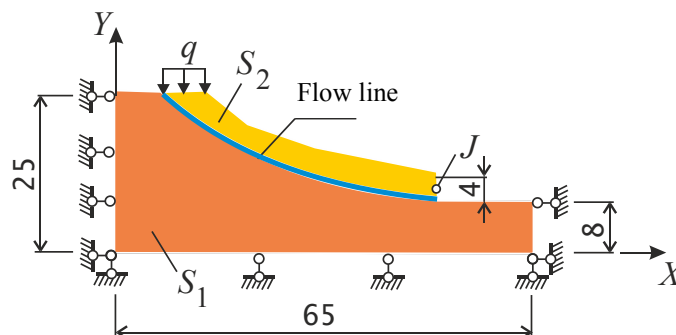


Fig. 2. Design scheme of landslide slope (dimensions are in meters)

The mechanical characteristics of the layer materials are given in Table 1.

Table 1

Mechanical characteristics of slope layers

Material	Deformation module E , MPa	Poisson's ratio ν	Angle of internal friction ϕ , deg.	Adhesion c , kPa	Density ρ , kg/m ³
layer S_1	21	0.30	15	45	1702
layer S_2	12	0.35	22	22	1800

Numerical simulation is performed using the ANSYS Mechanical software package. The finite element model of the slope is shown in Fig. 3. Two-dimensional 4-node finite elements PLANE42 are used for soil modeling. Moreover, the meshes of the layers S_1 and S_2 are topologically unrelated, i.e., along the flow line, each node has a double numbering. This will ensure to model the possible displacement of the layer S_2 relative to the layer S_1 .

To describe the behavior of the slope layers, we use the Drucker-Prager model of an elastic-perfectly-plastic material [7], which is included in the ANSYS Mechanical complex. The equation of the yield surface for this model has the form

$$F = \tau_i + 3\beta\sigma_m - \sigma_y = 0,$$

where τ_i — intensity of tangential stresses; σ_m — mean stress; β , σ_y — model parameters related to material constants C and ϕ ratios:

$$\beta = \frac{2 \sin \phi}{\sqrt{3}(3 - \sin \phi)}; \quad \sigma_y = \frac{6C \cos \phi}{\sqrt{3}(3 - \sin \phi)}.$$

Physical dependence linking stress and deformations for an elastic-perfectly-plastic material is described by the expression [8]

$$\tau_i = \frac{G \gamma_i}{1 + \gamma_i G / \tau_{np}},$$

where γ_i — the intensity of shear deformations; G — the shear modulus; the tangential stress corresponding to the material tensile strength (Fig. 4)

$$\tau_{np} = C + \sigma_m \operatorname{tg} \phi.$$

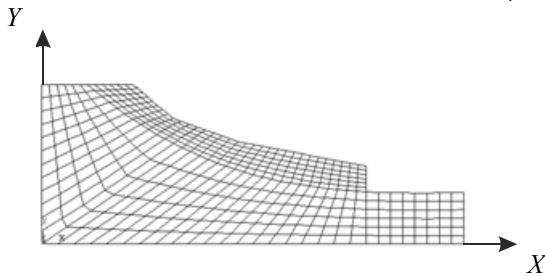
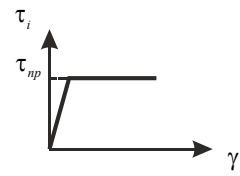


Fig. 3. Finite element model of the slope

Fig. 4. Graph $\tau_i \sim \gamma_i$

The effect of possible sliding of the layer S_2 relative to the layer S_1 is modeled using combined elements (CE) of spring type COMBIN14 (Fig. 5).

The equilibrium equation for a combined spring element (CE) has the form

$$[h]\{u\} = \{p\},$$

where $[h]$ — stiffness matrix; $\{u\}$, $\{p\}$ — vectors of the columns of nodal displacements and forces. Depending on the orientation of the spring element, we have:

— local CE axis ξ coincides with the axis x

$$[h] = k_x \begin{bmatrix} 1 & 0 & -1 & 0 \\ 0 & 0 & 0 & 0 \\ -1 & 0 & 1 & 0 \\ 0 & 0 & 0 & 0 \end{bmatrix}; \quad \{u\} = \{u_{ix} \ 0 \ u_{jx} \ 0\}^T;$$

$$\{p\} = \{p_{ix} \ 0 \ p_{jx} \ 0\}^T.$$

— local CE axis ξ coincides with the axis y

$$[h] = k_y \begin{bmatrix} 0 & 0 & 0 & 0 \\ 0 & 1 & 0 & -1 \\ 0 & 0 & 0 & 0 \\ 0 & -1 & 0 & 1 \end{bmatrix}; \quad \{u\} = \{0 \ u_{iy} \ 0 \ u_{jy}\}^T;$$

$$\{p\} = \{0 \ p_{iy} \ 0 \ p_{jy}\}^T.$$

Here, k_y , k_x — stiffness coefficients corresponding to the orientations of the spring along the axes x and y ;

T — symbol of the transpose operation.

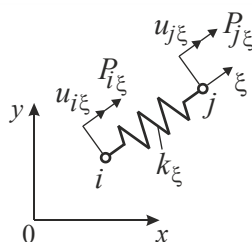


Fig. 5. Combined finite element COMBIN14

We take the following values of the elasticity coefficients:

$$k_y = 21 \text{ H/M}, \quad k_x = 100 \text{ H/M}.$$

Viscosity parameters: $c_x = c_y = 0.5 \text{ N}\cdot\text{s/m}$.

When assigning coefficients k_y and k_x , the aim was to bring the model of the slope under consideration closer to reality. In particular, along the flow line, we consider the shear strain resistance and elastic rebound of layer S_2 . A similar approach to modeling the “slipping” effect was used in [9]. Note that in the accepted layer discretization, the nodes i and j , belonging to the spring elements coincide. The design load includes the self-weight of the layer S_2 and the evenly distributed force q applied to the upper end of layer S_2 (Fig. 2).

To organize the computational process, we use the nonlinear “solver” of the ANSYS Mechanical complex, which implements the Newton-Raphson method.

To verify the finite element model, we estimate the slope stability under consideration through excluding the COMBIN14 elements from the design scheme and thus obtaining an unreduced model. By calculation, it is established that for an unweakened slope, the pressure limit value q , for the given mechanical characteristics of layers S_1 and S_2 , is 400 kPa. The operation process of the nonlinear solver is shown in the form of a graph in Fig. 6. Here, along the abscissa axis, the total number of iterations at each step of “Time” loading is plotted, along the ordinate axis, the corresponding norms of the residual forces “F” and displacements “U” are plotted. The “Time” parameter ranges from 0 to 1. The iterative process continues until the values “F”–“L2” are less than the values “F”–“CRIT”. The intersection of the peak of the sawtooth curve “F”–“L2” and the curve “F”–“CRIT” indicates that, in this example, the iterative process “converged” with the specified accuracy.

Figure 7 shows a picture of the distribution of horizontal displacements u_x in the body of an unweakened slope at $q = 400 \text{ kPa}$. As follows from the Figure, the loss of stability of the slope is local in nature. In this case, the circular-cylindrical type of the flow line is clearly traced. The corresponding distribution of the intensity field of plastic shear deformation γ_i is shown in Fig. 8.

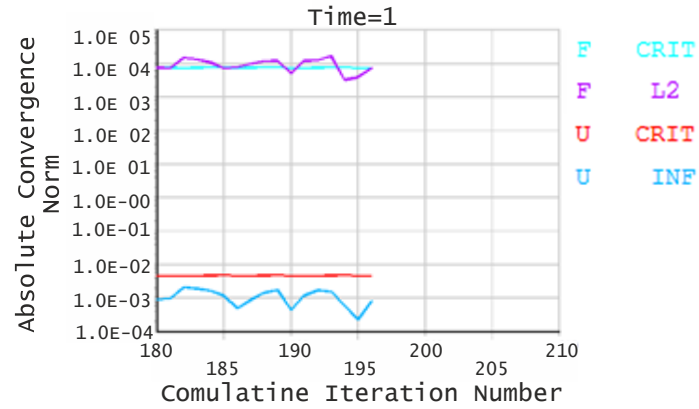


Fig. 6. Convergence graph of the Newton-Raphson procedure

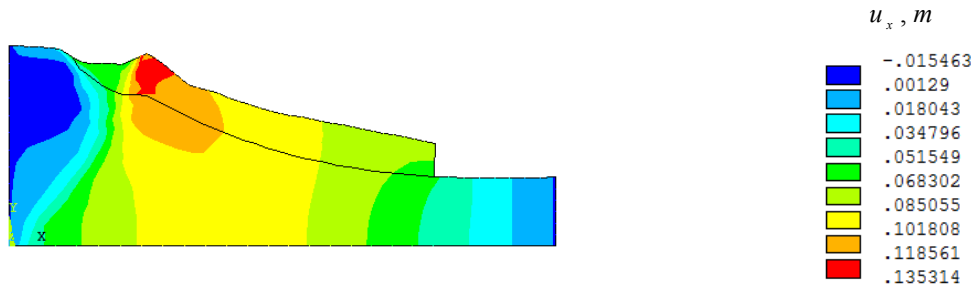


Fig. 7. Visualization of displacements u_x at $q=400$ kPa

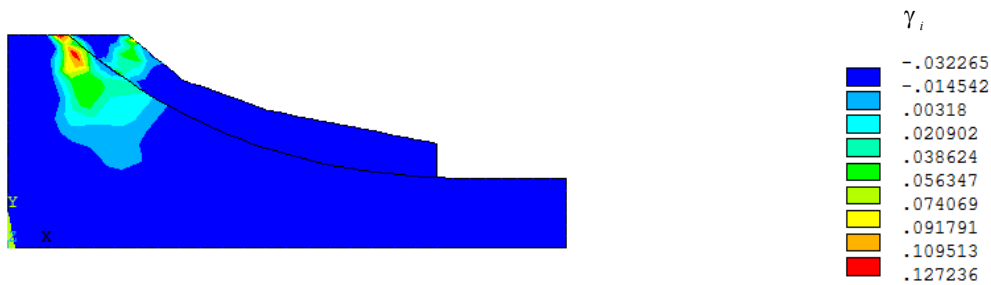


Fig. 8. Visualization of distribution γ_i at $q=400$ kPa

Research Results. To simulate the effect of kinematic instability of the landslide layer S_2 , we analyze the stress-strain state of the slope taking into account the weakening at different pressure values q . We emphasize that in this case, the elements of COMBIN14 are included. Fig. 9 shows the graph $u_x \sim q$, where u_x — the horizontal displacement of point J of the “tongue” of the landslide layer S_2 (Fig. 2).

Comparing the results of calculations for weakened and unweakened slopes, we come to the conclusion that the inclusion of a sliding layer in the design model significantly (by more than one order of magnitude) reduces the limit value q .

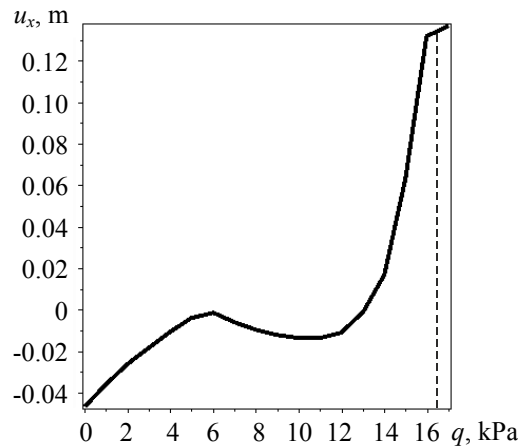


Fig. 9. Graph of the dependence of horizontal movement of point J of the “tongue” of landslide layer S_2 on pressure value q

The graph $u_x \sim q$ shows that, for the considered slope model, the landslide process has a pronounced nonlinear character. Moreover, in the pressure range from 6 kPa to 11 kPa, there is a displacement of the “tongue” of layer S_2 in the opposite direction to the expected landslide process. Fig. 10 shows a contrasting pattern of the distribution of the displacement field in the x - axis direction corresponding to the loading of layer S_2 with pressure $q=16.5$ kPa.

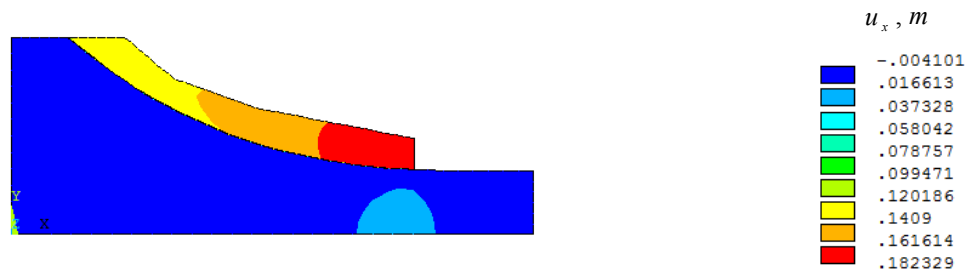


Fig. 10. Visualization of displacements u_x at $q=16.5$ kPa

A fragment of a finite element model of a landslide “tongue” in a deformed state at $q=16.5$ kPa is shown in Fig. 11.

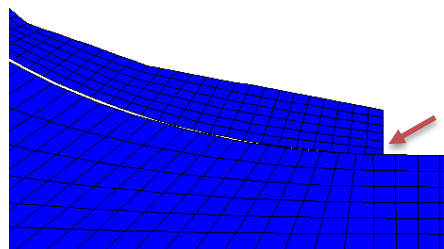


Fig. 11. Visualization of a finite element model of a slope fragment in a deformed state at $q=16.5$ kPa

As can be seen from Fig. 11, the proposed method allows you to simulate the effect of sliding of layer S_2 relative to layer S_1 . This effect is shown in the relative displacement of the grid nodes (shown by the arrow). Maximum relative displacement $u_{x \max}$ reaches 18.2 cm, which, from a physical point of view, is quite consistent with the landslide process onset.

Fig. 12 shows the considered variants of schemes of anti-landslide structures made of concrete. The following mechanical constants for concrete are accepted: $E_c = 3 \cdot 10^4$ MPa; $\nu_c = 0.2$; $\rho_c = 2446$ kg/m³. The design value of the height of the protective structures $h=2.6$ m. The depth of the pile foundation is 8 m (schemes b and c). Pressure value

$q = 16.5 \text{ kPa}$.

The pile foot (scheme *b*) and the sheet piling (scheme *c*) are presented by 2-node beam elements BEAM3. The diameter of the piles is assumed to be 0.35 m.

The visualization of the considered schemes of anti-landslide structures in the deformed state is shown in Fig. 13. From the above data, it follows that when modeling the landslide process, the “tongue” of layer S_2 is pressed into the foundation S_1 . This explains the “collapse” of anti-landslide structures towards the movement of layer S_2 .

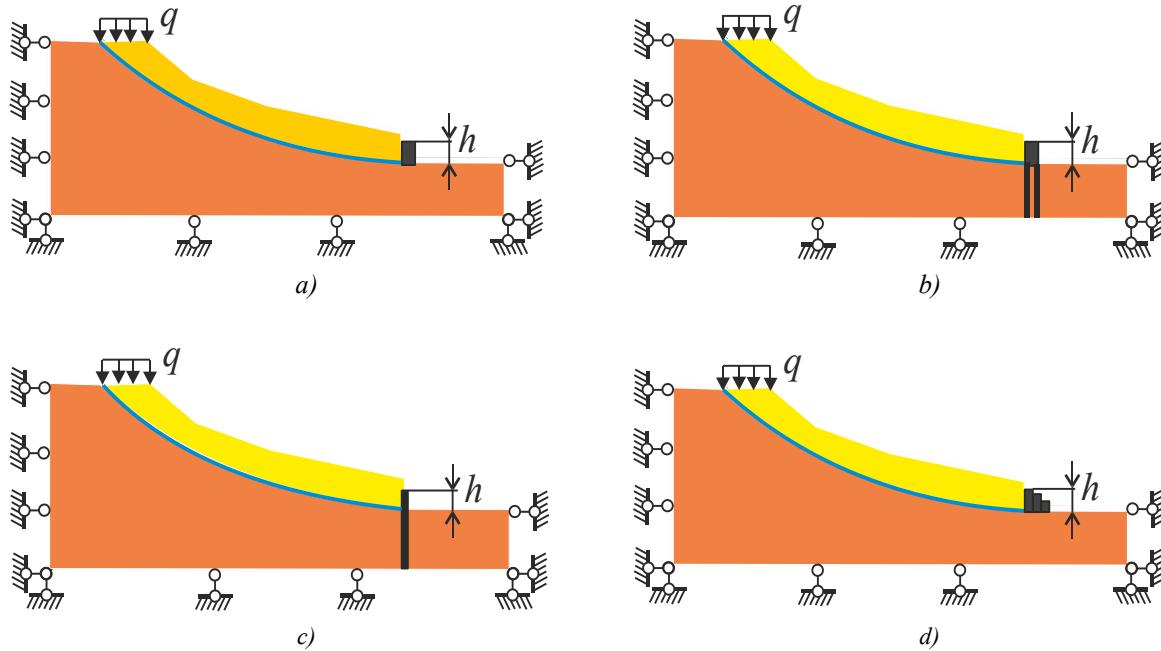


Fig. 12. Schemes of anti-landslide structures:

a) retaining wall, b) retaining wall on a pile foundation, c) sheet piling, d) gabion

Graphs of changes in horizontal displacements u_x and stresses σ_x along the height h of the considered protective structures are shown in Fig. 14.

Analyzing the results presented, we come to the conclusion that the most pronounced anti-landslide effect from an engineering point of view is scheme *b*, which provides a relatively uniform horizontal displacement of the retaining wall without “collapse”. In this case, maximum horizontal displacement of the wall is 16 mm. To increase the reliability of this design, you can use anchor ties [10].

A certain practical interest in the design of anti-landslide structures is the nature of the distribution of internal forces in the pile foundation. For scheme *b*, the diagrams of the bending moments M occurring in the left and right piles are shown in Fig. 15. The value of the maximum normal compression stress under bending for scheme *b* was $\sigma_{max} = 337 \text{ kN/m}^2$, which is significantly less than the compressive strength of concrete (25.5 MPa).

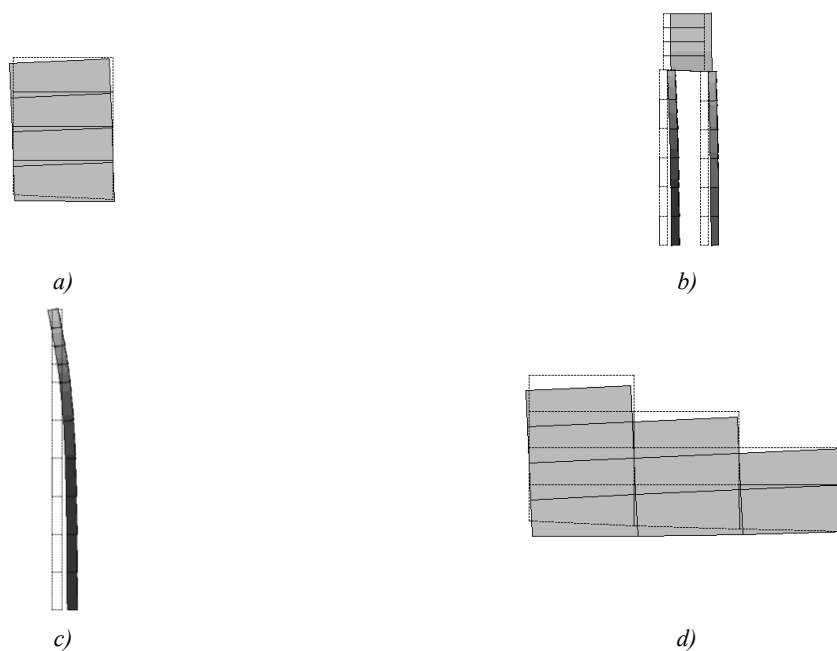


Fig. 13. Visualization of protective structures in the deformed state:
a) retaining wall, b) retaining wall on a pile foundation, c) sheet piling, d) gabion

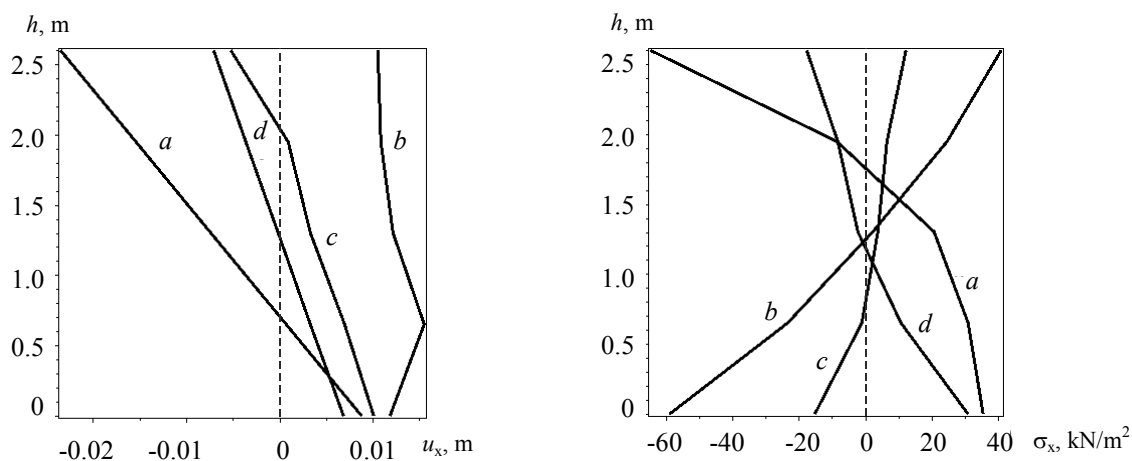


Fig. 14. Graphs $u_x \sim h$ and $\sigma_x \sim h$ for protective structures:
a) retaining wall, b) retaining wall on a pile foundation, c) sheet piling, d) gabion

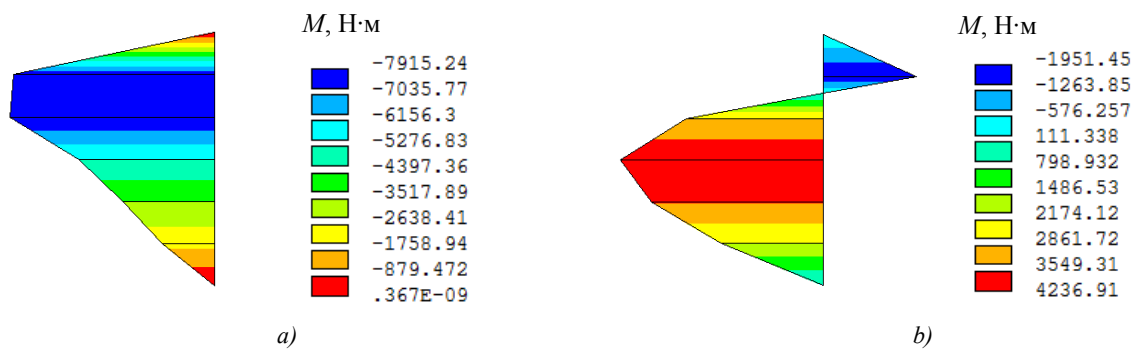


Fig. 15. Diagrams of bending moments in piles of scheme *b* in Fig.12:
a) left pile; b) right pile

Diagrams of shear forces Q in piles are shown in Fig. 16.

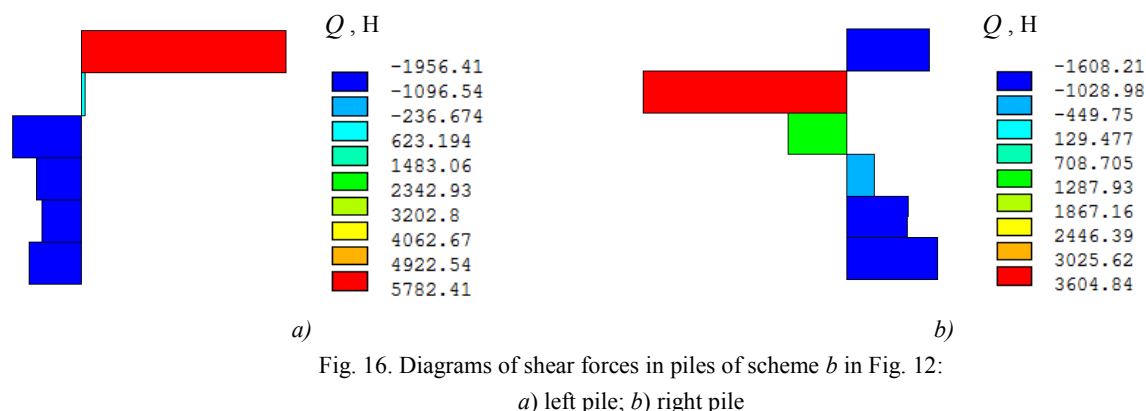


Fig. 16. Diagrams of shear forces in piles of scheme *b* in Fig. 12:

a) left pile; b) right pile

Fig. 16 shows that the cross-section of a possible pile cut is located below the zero mark of the structure.

Discussion and Conclusions. Under the problem of plane deformation, a finite element model is constructed that simulates the landslide process of a natural slope. In contrast to the existing methods of calculating landslide structures, this approach implements the concept of kinematic instability of the landslide layer, the essence of which is to use combined finite elements along the assumed sliding line. A series of numerical experiments was used to test the proposed method for studying the interaction of a sliding landslide and various types of protective structures. It is established that the most effective anti-landslide protection at the given geometric and physical parameters is provided by a combined structure consisting of a retaining wall and a pile foundation.

References

1. Seyed-Kolbadi SM, Sadoghi-Yazdi J, Hariri-Ardebili MA. An improved strength reduction-based slope stability analysis. *Geosciences*. 2019;9(1):55. <https://doi.org/10.3390/geosciences9010055>
2. Griffiths DV, Marquez RM. Three-dimensional slope stability analysis by elasto-plastic finite elements. *Geotechnique*. 2007;57(6):537–546. <https://doi.org/10.1680/geot.2007.57.6.537>
3. Jing Xi Chen, Peng Zhen Ke, Guang Zhang. Slope stability analysis by strength reduction elasto-plastic FEM. *Key Eng. Mater.* 2007;345:625–628. <https://doi.org/10.4028/www.scientific.net/KEM.345-346.625>
4. Mikhailov VO. Trekhmernaya matematicheskaya model' obval'nykh protsessov [3D mathematical model of landfall processes]. *Moscow University Bulletin. Series 5, Geography*. 2011;4:53–58. (In Russ.)
5. Yossef H. Hatzor, Guowei Ma, Gen-hua Shi. *Discontinuous Deformation Analysis in Rock Mechanics Practice*. ISRM, CRC Press, 2018. 410 p.
6. Morozov EM, Muzemnek AY, Shadskii AS. ANSYS v rukakh inzhenera. *Mekhanika razrusheniya [ANSYS is in the hands of an engineer. Destruction mechanics]*. Moscow: LENAND; 2008. 456 p. (In Russ.)
7. Drucker DC, Prager W. Soil Mechanics and plastic analysis or limit design. *Quarterly of Applied Mathematics*. 1952;10(2):157–165.
8. Fadeev AB. Metod konechnykh ehlementov v geomekhanike [Finite element method in Geomechanics]. Moscow: Nedra; 1987. 221 p. (In Russ.)
9. Gaigerov PP, Al-Jabobi Sami Fahl, Al-Yaj Mahmoud Abdo Hasa. Konechno-ehlementnoe modelirovanie peredachi usiliya natyazheniya stal'nogo kanata na beton [Finite element modeling of force transmission the tension of the steel tendon on the concrete]. *University News. North-Caucasian region. Technical Sciences Series*. 2017;2:73–78. (In Russ.)
10. Matsii SI, Ryabukhin AK. Svaino-ankernye protivopolznevye konstruksii [Pile-anchor anti-landslide structures]. Krasnodar: KubGAU; 2017. 189 p. (In Russ.)

Received 10.03.2021

Revised 08.04.2021

Accepted 13.04.2021

About the Authors:

Gaidzhurov, Petr P., professor of the Engineering Mechanics Department, Don State Technical University (1, Gagarin sq., Rostov-on-Don, RF, 344003), Dr.Sci. (Eng.), ORCID: <https://orcid.org/0000-0003-3913-9694>, gpp-161@yandex.ru

Saveleva, Nina A., senior lecturer of the Engineering Mechanics Department, Don State Technical University (1, Gagarin sq., Rostov-on-Don, RF, 344003), ORCID: <https://orcid.org/0000-0002-8702-5168>, ninasav86@mail.ru

Dyachenkov, Vladimir A., graduate student of the Engineering Mechanics Department, Don State Technical University (1, Gagarin sq., Rostov-on-Don, RF, 344003), snowflash88@gmail.com

Claimed contributorship

P. P. Gaidzhurov: task formulation; discussion of the results. N. A. Saveleva: conducting a review; selection of a method for solving the construction of a mathematical and computer model; computational analysis; computational analysis; discussion of the results. V. D. Dyachenkov: discussion of the results.

All authors have read and approved the final manuscript.

MECHANICS



UDC 004.85

<https://doi.org/10.23947/2687-1653-2021-21-2-143-153>

Visualization of internal defects using a deep generative neural network model and ultrasonic nondestructive testing

P. V. Vasiliev¹, A. V. Senichev¹, I. Giorgio²¹ Don State Technical University (Rostov-on-Don, Russian Federation)² Università degli Studi dell'Aquila (L'Aquila, Italy)

Introduction. The development of machine learning methods has given a new impulse to solving inverse problems in mechanics. Many studies show that along with well-behaved techniques of ultrasonic, magnetic, and thermal nondestructive testing, the latest methods are used, including those based on neural network models. In this paper, we demonstrate the potential application of machine learning methods in the problem of two-dimensional ultrasound imaging.

Materials and Methods. We have developed an experimental model of acoustic ultrasonic non-destructive testing, in which the probing of the object under study takes place, followed by the recording of the response signals. The propagation of an ultrasonic wave is modeled by the finite difference method in the time domain. An ultrasonic signal received at the internal points of the control object is applied to the input of the convolutional neural network. At the output, an image that visualizes the internal defect is generated.

Results. In the course of the performed complex of numerical experiments, a data set was generated for training a convolutional neural network. A convolutional neural network model, which is developed to solve the problem of visualizing internal defects based on methods of ultrasonic nondestructive testing, is presented. This model has a small size, which is 3.8 million parameters. Its simplicity and versatility provide high-speed learning and a wide range of applications in the class of related problems. The presented results show a high degree of information content of the ultrasonic response and its correspondence to the real form of an internal defect located inside the test object. The effect of geometric parameters of defects on the accuracy of the neural network model is investigated.

Discussion and Conclusion. The results obtained have established that the proposed model shows a high operating accuracy ($F1 > 0.95$) in cases when the wavelength of the probe pulse is tens of times less than the size of the defect. We believe that the combination of the proposed methods in this approach can serve as a good starting point for future research in solving flaw defection problems and inverse problems in general.

Keywords: ultrasonic nondestructive testing, defect, ultrasonic response, convolutional neural networks.

Funding information: the research is done with the financial support from RFFI within the framework of projects nos. 19-08-00074A and 20-31-90026.

For citation: P. V. Vasiliev, A. V. Senichev, I. Giorgio. Visualization of internal defects using a deep generative neural network model and ultrasonic nondestructive testing. Advanced Engineering Research, 2021, vol. 21, no. 2, pp. 143–153. <https://doi.org/10.23947/2687-1653-2021-21-2-143-153>

© Vasiliev P. V., Senichev A. V., Giorgio I., 2021



Introduction. In the paper, the authors investigate the possibilities of using neural network technology in solving inverse problems of mechanics, in particular, in the problem of two-dimensional visualization of internal defects. These methods are widely used in medicine, civil engineering, nondestructive testing and other fields.

Thus, in [1], a system was developed for detecting cracks in steel structures and assessing their depth based on two-dimensional images. The work objective is to develop an affordable and user-friendly control system instead of expensive measuring devices. A training strategy and several neural network structures were proposed. In process of training, the average intensity of the profiles of two-dimensional steel cracks was fed into the neural network along with the maximum depth of steel cracks measured using a laser microscope. The average error of the neural network is 18 % in the test sample, which is better in comparison to the previous studies of the authors. Improving the quality of determining the depth of defects is achieved through the use of a new training strategy and a tool for assessing the crack depth.

In [2], some deep learning methods were proposed for detecting defects in the images obtained through nondestructive testing. To apply such approaches, labeled data of images with defects is needed. The authors propose a deep-transfer learning model for extracting signs of internal defects on X-ray images of composite materials of the aviation industry. The method of automatic detection of inclusion defects on X-ray images was investigated using the proposed model. The experimental results show that the model can achieve a classification accuracy of 96 % (F1 metric) with satisfactory detection results.

In [3], a method for reconstructing and visualizing internal defects in the form of a three-dimensional image using an economical and fast pulse thermography technology is proposed. A new method of rapid assessment of the depth and thickness of the defect simultaneously based on a single one-sided check is presented. The feasibility and effectiveness of the proposed solution is demonstrated through examining composite and steel samples with semi-enclosed air gaps. For a composite sample, this method can provide a relatively low, within 10%, average relative error of the estimated total volume of 3D defects.

Paper [4] considers the main causes of failure of engines of solid-fuel rockets. Peeling at the propellant /sleeve /insulation interface is a critical moment for the integrity of the engines. Modern solutions are usually limited to methods of assessing the integrity of the design of rocket engines and visual inspection of their components.

This paper presents an improved algorithm for detecting sleeve surface defects that can disrupt the bond between solid rocket fuel and insulation. The use of local binary patterns (LBP) provides a structural and statistical approach to analyzing the texture of engine image samples. The neural network analyzes the engine image samples and classifies each pixel into one of three classes: serviceable, foreign object and defect. Several tests were conducted with varying different parameters to find the optimal configuration of the neural network. As a result, the best classification accuracy was obtained for the corresponding classes: 99.08 %, 90.66% and 99.48 %.

Paper [5] provides a brief overview of artificial intelligence algorithms applicable to nondestructive testing. It focuses on two methods: artificial neural networks and fuzzy logic. Selected examples of the application of these methods in digital radiography and the eddy current method are given.

In [6], the author explores the potential of deep learning methods for electromagnetic inversion. This approach does not require calculating the gradient and gives results immediately after training the network. Deep neural networks based on a fully convolutional architecture are trained on large sets of synthetic data obtained through full three-dimensional modeling. The method effectiveness is demonstrated on models of great practical importance, representing the scenario of monitoring the electromagnetic field of carbon dioxide accumulation underground with a controlled source on the surface.

Previously, the authors investigated some problems that combine modern methods of deep machine learning and well-proven classical approaches to identifying defects [7–9].

In this paper, a neural network model is considered as a pilot study, on the basis of which a two-dimensional acoustic visualization of internal defects is carried out. A trial model of nondestructive ultrasonic testing is constructed, on the basis of which a complex of numerical experiments is carried out. The results of these experiments serve as the basis for training a neural network and its validation.

Materials and Methods. A method for identifying and visualizing internal defects based on ultrasonic nondestructive testing and a generative neural network model is proposed. An ultrasonic signal received at the internal points of the control object is fed to the input of the convolutional neural network. At the output, an image is generated that visualizes an internal defect. The inner part of the steel plate was chosen as an object to demonstrate the possibility and prospects for the development of this research method. There may be a defect inside the strip, indicated by the lack of material. The shape, size and orientation of the defect may vary. The approach involves conducting a series of numerical experiments, on the basis of which it is possible to train a deep neural network model. A training set is created for each case through varying the geometric parameters of the defect and modeling the propagation of an acoustic ultrasonic wave. It is possible to build an optimal structure of a neural network model and train it on the basis of the collected data.

Finite difference-time domain method. This method was proposed by Kane Yee [10] and belongs to the class of grid methods for solving differential equations. At the moment, this method is widely used — from tasks of geophysics to solving problems in the optical range, as well as in a number of problems of modeling media with both dispersed and nonlinear properties. The finite difference-time domain method in the acoustic formulation is used to simulate the propagation of sound in fluid media, such as air or liquids. However, in some cases, to simplify the solution of problems, this method can also be used in elastic media. Within the framework of this method, the velocity and acoustic pressure of the particles of the simulated object are arranged alternately in the grid nodes. Then their values are calculated sequentially, which provides calculating the propagation of the sound field over time.

The basic equation of this acoustic model in a flat formulation is the following:

$$\frac{\partial p}{\partial t} = -k \left(\frac{\partial v_x}{\partial x} + \frac{\partial v_y}{\partial y} \right) \frac{\partial v_x}{\partial t} = -\frac{1}{\rho} \frac{\partial p}{\partial x}, \quad \frac{\partial v_y}{\partial t} = -\frac{1}{\rho} \frac{\partial p}{\partial y},$$

where p — pressure, v — velocity, k — volume modulus of elasticity, ρ — density of the medium.

The values of the spatial Δx and timing Δy resolutions affect how accurately and steadily the acoustic field will be calculated. These values cannot be set independently and must be selected taking into account each other.

First of all, you need to set value Δx based on accuracy considerations. At the same time, accuracy and stability are independent of each other. The simulation can be stable, but with low accuracy in the case of a coarse grid. The accuracy of the solution by this method depends on many factors. In this case, values Δx and Δy can be set as:

$$\Delta x = \frac{\lambda_{min}}{10} \sim \frac{\lambda_{min}}{20}, \Delta t \leq \frac{1}{\sqrt{d}} \frac{\Delta x}{c_{max}},$$

where λ_{min} — the wavelength that propagates in the simulated space, c_{max} — the largest value of the speed of sound in the simulated environment, d — the dimension value, for a flat problem $d = 2$.

A reference model of acoustic ultrasonic wave propagation is constructed in the COMSOL package. Accordingly, the solution is carried out by the finite element method and the finite difference method. Figure 1 below shows the normalized acoustic pressure values read at the model point. The model is a square area made of steel with a hole inside. Small differences in the signal shape are due to the way the source of ultrasonic vibrations is set. In the case of FEM — points are on the circle, in the case of FDTD — a point is in the grid node.

Comparison of ultrasonic wave propagation

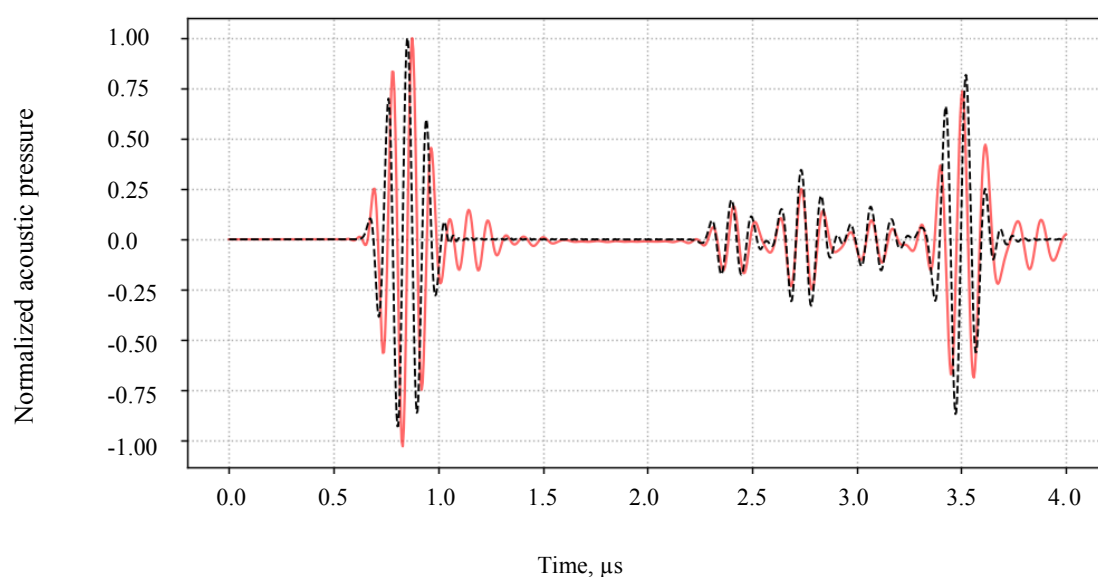


Fig. 1. Shape of the direct and reflected ultrasonic signal. The dashed line shows the values calculated using the FDTD method, the solid line shows the values calculated using the FEM

Since the grid has a limited size, it is not possible to simulate the propagation of acoustic waves outside this area, so special boundary conditions are applied. Moore's Absorbing Layers or Perfect Matched Layers (PML) are used [11]. These conditions reduce significantly the reflectivity of the boundaries of the area in which the simulation takes place and create the effect of waves passing beyond the boundaries of this area.

Nondestructive testing model. The inner part of the steel plate containing the defect was chosen as a trial model of nondestructive testing. The study area size is 20×20 mm. Defects are presented in the form of geometric shapes: ellipse, triangle, square, rectangle. Physical parameters of the defects vary relative to the simulated area within the following limits: the location of the defect — from 0.3 to 0.7; the size of the defect — from 0.1 to 0.35; the angle of defect inclination — from 0° to 360° . The input signal consists of a fixed number of discrete values specified by the experiment time. The time of the experiment was chosen in such a way that the probing pulse, having reflected from the defect, could cover the distance and return to the point of the initiating signal. The probing pulse frequency is 10 MHz.

Figure 2 shows the scheme of the numerical experiment. The defect is located in the center of the probed area with a given offset. The source of the ultrasonic signal is shown with red mark. The signal reading points are shown with green marks. The broken line shows the boundaries of the defect.

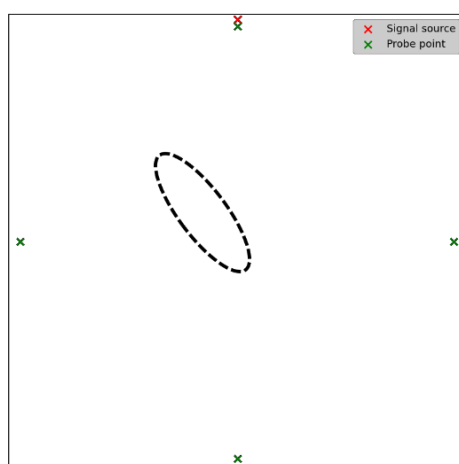


Fig. 2. Scheme of one of the conducted numerical experiments

The model provides evaluation of the possibility of using the proposed method and the further prospects for its application. The ultrasonic signal is set at the internal point of the control object. The points that simulate sensors that read the transmitted and reflected signals are located on different sides of the supposed location of the defect. Such a virtual model enables to evaluate the effect of some experimental parameters on the neural network quality. Based on the implemented approach, it is possible to build models that reflect real technical tasks. Figure 3 shows the propagation and reflection of an ultrasonic wave from a defect inside the study area.

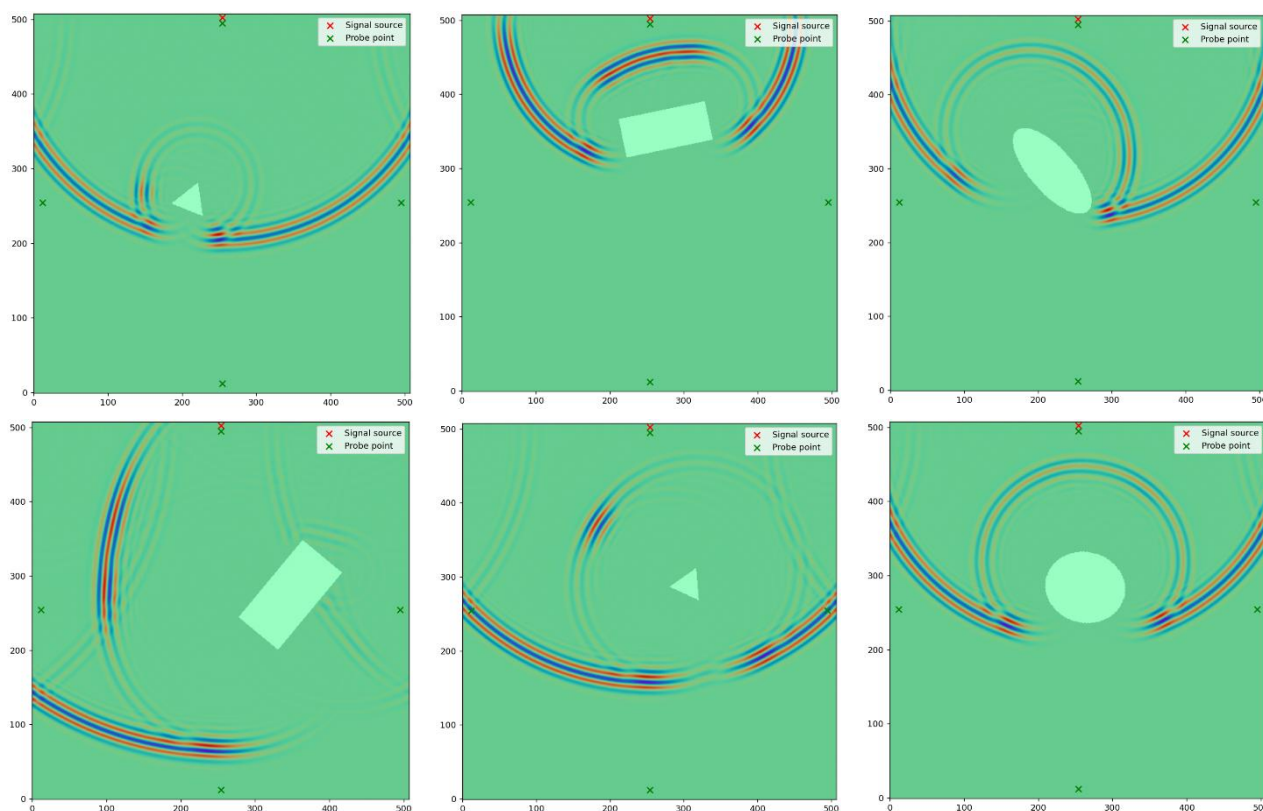


Fig. 3. Propagation of an ultrasonic wave and its reflection from various defects

Neural network model. Convolutional neural networks (CNN) are a special neural network tool for processing data with a grid structure (two-dimensional images, one-dimensional signals) [12]. At the moment, it is one of the most rapidly developing and promising deep learning tools [13–15].

They have also proved extremely successful in other practical applications, including video analysis and time-series data processing (the latter can be considered as a one-dimensional grid that processes samples at fixed time intervals). CNN is a key example of the successful application of ideas obtained under studying the brain (to some extent inspired by the structure of the mammalian visual system). As the name suggests, the convolutional network uses the convolution operation, i.e., filtering using a feature map or kernel, instead of the general matrix multiplication in fully connected networks (in fact, convolution corresponds to the product of a sparse matrix).

To solve the problem of defect visualization, the authors suggest using a convolutional neural network model. An ultrasonic signal received at the internal points of the control object is applied to the input of the model. The output generates an image with the expected shape, location and orientation of the defect. The input signal passes through layers of one-dimensional convolution (Conv1D) and subsampling (MaxPooling). After that, the data falls on a fully connected layer. This convolutional part of the network is used to extract features from the signal, on whose basis the defect will be visualized. The second part of the network generates images corresponding to the shape, location and orientation of the defect. Data from a fully connected layer is transformed and displayed on a two-dimensional layer. From this layer, after passing through a number of trained unfolding layers (Conv2D Transpose), the final image is obtained, which visualizes the internal defect. The model of the convolutional neural network used in this work is

shown in Fig. 4. Under each layer, the size of the input data and the number of convolution kernels are shown. For example, 504×32 means that 504 values are fed to this layer and 32 different convolutional filters are applied to them.

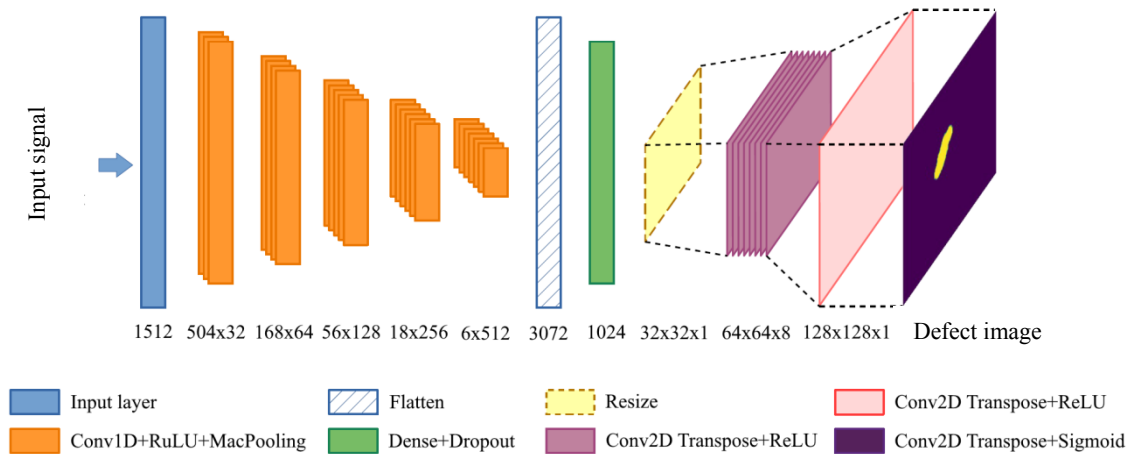


Fig. 4. Architecture diagram of a convolutional neural network

Model training and validation. Within the framework of a complex of numerical experiments, 17,000 problems with various geometric parameters of the defect were solved. 14,000 samples were used for training, 2,000 — for testing and 1,000 — for validation.

In training, the success rate is the training error. When checking the operation of a neural network model on test data that was previously unavailable to the network, its ability to generalize is determined. During the testing process, the testing error is calculated. Thus, the model performance can be judged by two key factors. The first is to achieve the smallest learning error. The second is to reduce the difference between the training and testing error.

There are several regularization techniques in the machine learning. When training neural networks, one of the problems is overtraining. It is expressed in the loss of the ability to generalize in the learning process. One of the most popular methods of preventing it is the use of Tikhonov regularization (ridge regression or L2), also called weight decay in machine learning.

One of the important stages of training a neural network model is the initialization of weights. One of the currently popular initialization methods is the Xavier method [16]. This method simplifies the signal transmission in case of forward and backward propagation of an error through the network layers. The method is suitable for both linear and sigmoid activation functions (its unsaturated section has a linear character).

The batch-normalization method was proposed by Ioffe and Szegedy [17]. During the propagation of the signal through the network layers, its distortion can occur both in terms of mathematical expectation and variance (this effect is known as an internal covariance shift). This may cause some discrepancy between the gradients at different network levels.

General regularization approaches are used when training a neural network model. The simplest of them are early stopping and the use of the dropout technique. These methods provide more stable training of the model. Due to the sufficient size of the training sample and the complexity of data augmentation, the latter is not performed.

As part of this work, the data set is not balanced. Below, in Fig. 5, you can see the distribution of defects depending on their size.

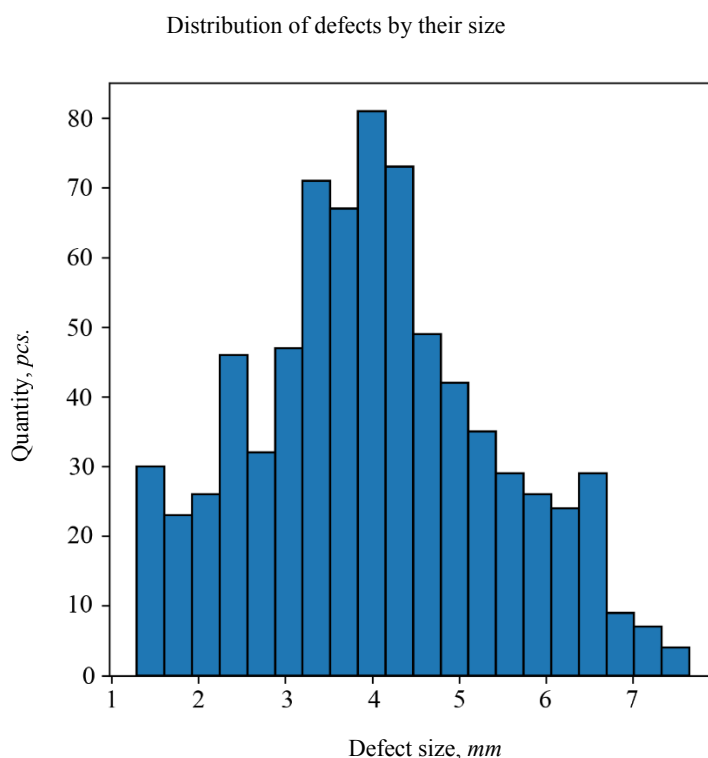


Fig. 5. Number of defects depending on their size in the training data set

Training a neural network is the equivalent of solving an optimization problem in which the minimum of the loss function is searched for. This function shows how well the model performs its task. The correct selection of the loss function has a great impact on the learning outcome. In this problem, the optimal choice is to use the Jaccard similarity coefficient (Intersection over Union). This factor is often used in computer vision problems and is defined as:

$$IoU = \frac{|A \cap B|}{|A \cup B|} = \frac{|A \cap B|}{|A| + |B| - |A \cap B|}$$

Accordingly, the loss function is defined as $1 - IoU$ and reflects the difference between the two samples. It is also known as the Jaccard distance. Also, to assess the quality of the neural network model, metric $F1 = \frac{2 \times IoU}{IoU + 1}$ is used, which reflects the harmonic mean between completeness and accuracy.

One of the most popular Adam algorithms [18] is used for training. The authors used the open TensorFlow library and the Keras framework. These software solutions include the majority of modern algorithms and models. It took 200 training epochs to achieve an acceptable level of the model performance.

Research Results. The use of a neural network approach to solving inverse problems has long proven itself [8, 19–20]. With the development of machine learning and the emergence of new techniques, new methods of data interpretation become available, and new opportunities for solving classical problems of mechanics and flaw detection appear.

The authors have presented a convolutional neural network model developed to solve the problem of visualization of internal defects based on methods of ultrasonic nondestructive testing. This model has a small size, which is 3.8 million parameters. Its simplicity and versatility provide high-speed learning and a wide range of applications in the class of related problems. The authors use the FDTD method for simulating the propagation of ultrasonic waves and compare its results with the results of the finite element method. The selection of this method made it possible to significantly increase the speed of calculating models, compared to the tasks solved earlier [21].

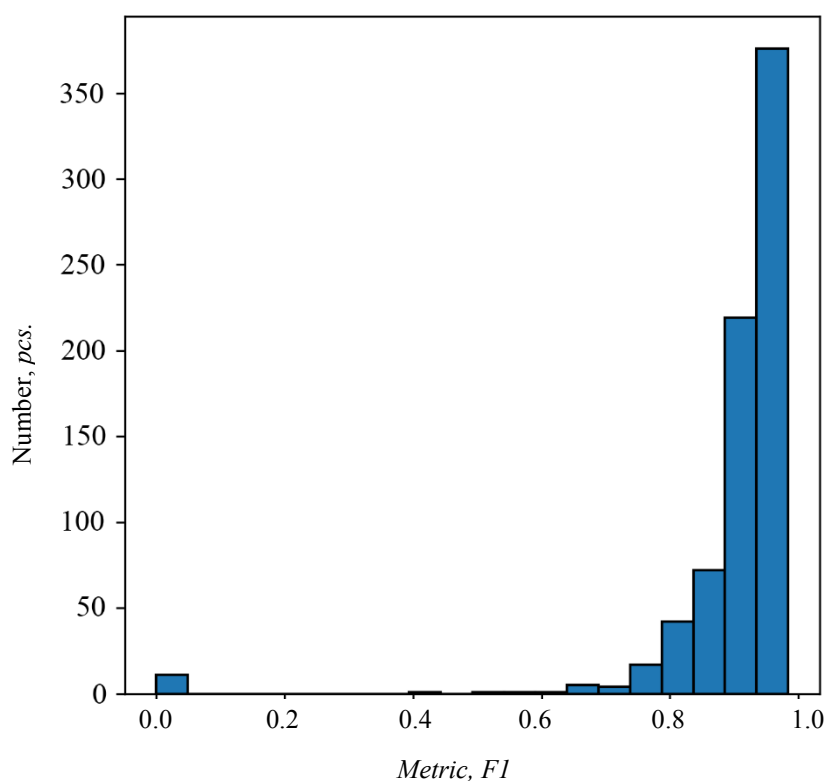


Fig. 6. Number of identified defects with a certain accuracy

After training the neural network model, its operation is validated on the corresponding data set. Metric F1, described above, is used to evaluate the overall performance of the model. In general, the accuracy of the proposed method is at a high level. The average value of F1 factor for the entire validation sample is 91 %. Figure 6 shows that some of the defects were not identified by the neural network model.

In Fig. 7, you can see how accurately the neural network model performs visualization of defects of various sizes. Visualization was performed on a validation data set.

The effect of the defect size on the visualization accuracy

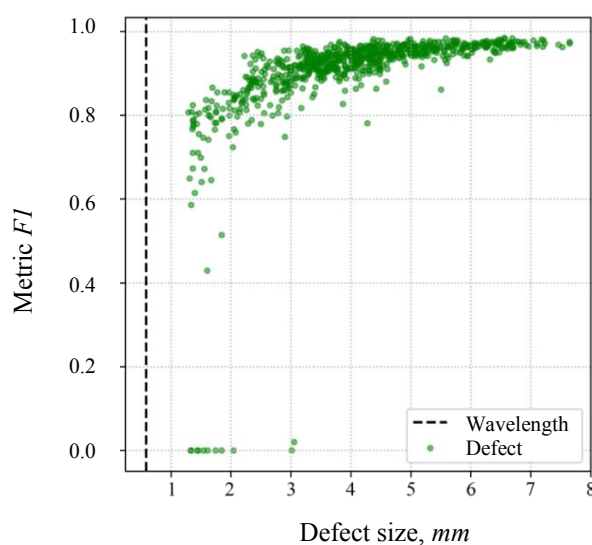


Fig. 7. Dependence of the visualization accuracy on the defect size

Figure 8 below shows the results of the neural network model operation. The images show the location, boundaries and shape of the alleged defect.

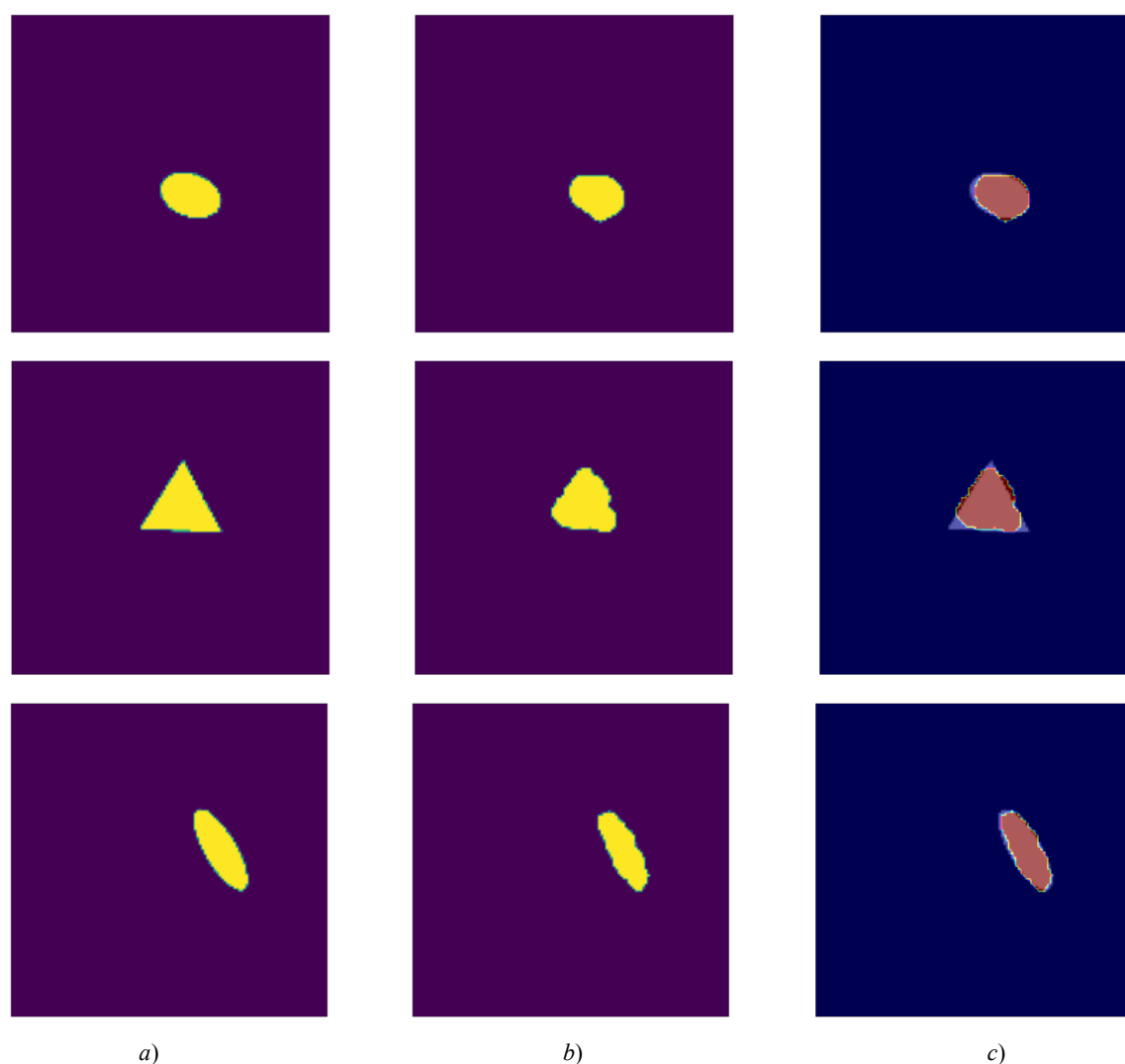


Fig. 8. The result of visualizing the defect with a neural network: a) original defect, b) defect visualization based on the ultrasonic response, c) difference between the original and restored samples

Discussion and Conclusions. In this paper, the potential of using machine learning methods in the problem of ultrasound imaging is shown. The authors have built a test model of nondestructive testing. Based on this model, a data set is prepared for training a neural network. A convolutional neural network model is proposed that provides predicting the shape, location and orientation of defects inside a solid body. The results obtained show a high degree of informativeness of the ultrasonic response and its correspondence to the real form of the internal defect.

Based on the results obtained, it is revealed that the proposed model shows high accuracy of work ($F1 > 0.95$) in cases when the wavelength of the probing pulse is ten times smaller than the size of the defect.

The authors believe that the combination of the proposed methods in this approach can serve as a good starting point for future research under solving problems of flaw detection and inverse problems in general.

References

1. Yasser S. Mohamed, Hesham M. Shehata, Mohamed Abdellatif, et al. Steel crack depth estimation based on 2D images using artificial neural networks. *Alexandria Engineering Journal*. 2019;58(4):1167–1174. <https://doi.org/10.1016/j.aej.2019.10.001>
2. Yanfeng Gong, Hongliang Shao, Jun Luo, et al. A deep transfer learning model for inclusion defect detection of aeronautics composite materials. *Composite Structures*. 2020;252:112681. <https://doi.org/10.1016/j.compstruct.2020.112681>

3. Adisorn Sirikham, Yifan Zhao, Haochen Liu, et al. Three-dimensional subsurface defect shape reconstruction and visualisation by pulsed thermography. *Infrared Physics & Technology*. 2020;104:103151. <https://doi.org/10.1016/j.infrared.2019.103151>
4. Luiz Felipe Simões Hoffmann, Francisco Carlos Parquet Bizarria, José Walter Parquet Bizarria. Detection of liner surface defects in solid rocket motors using multilayer perceptron neural networks. *Polymer Testing*. 2020;88:106559. <https://doi.org/10.1016/j.polymertesting.2020.106559>
5. Ryszard Sikora, Piotr Baniukiewicz, Tomasz Chady, et al. Artificial Neural Networks and Fuzzy Logic in Nondestructive Evaluation. *Studies in Applied Electromagnetics and Mechanics*. 2014;38:137–151. <https://doi.org/10.3233/978-1-61499-354-4-137>
6. Puzyrev V. Deep learning electromagnetic inversion with convolutional neural networks. *Geophysical Journal International*. 2019;218(2):817–832. <https://doi.org/10.1093/gji/ggz204>
7. Soloviev AN, Sobol BV, Vasiliev PV. Ultrasonic and Magnetic Flow Inspection Methods of Identification of Cracks in the Pipe Coupled with Artificial Neural Networks. *Advanced Materials. Springer Proceedings in Physics*. 2017;193:381–395.
8. Soloviev A, Sobol B, Vasiliev P, et al. Generative Artificial Neural Network Model for Visualization of Internal Defects of Structural Elements. *Advanced Materials. Springer Proceedings in Materials*. 2020;6:587–595. https://doi.org/10.1007/978-3-030-45120-2_48
9. Sobol BV, Soloviev AN, Rashidova EV, et al. Identification of crack-like defect and investigation of stress concentration in coated bar. *PNRPU Mechanics Bulletin*. 2019;4:165–174. <https://doi.org/10.15593/perm.mech/2019.4.16>
10. Kane Yee. Numerical solution of initial boundary value problems involving Maxwell's equations in isotropic media. *IEEE Transactions on Antennas and Propagation*. 1966;14(3):302–307. <https://doi.org/10.1109/TAP.1966.1138693>
11. Jean-Pierre Berenger. A perfectly matched layer for the absorption of electromagnetic waves. *Journal of Computational Physics*. 1994;114(2):185–200.
12. LeCun Y, Boser B, Denker JS, et al. Backpropagation applied to handwritten zip code recognition. *Neural Computation*. 1989;1(4):541–551. <https://doi.org/10.1162/neco.1989.1.4.541>
13. Goodfellow I, Bengio Y, Courville A. Deep learning. Vol. 1. Cambridge: MIT Press; 2016. 800 p.
14. Krizhevsky A, Sutskever I, Hinton GE. ImageNet classification with deep convolutional neural networks. *Advances in Neural Information Processing Systems*. 2012;25:1097–1105.
15. Kaiming He, Xiangyu Zhang, Shaoqing Ren, et al. Deep residual learning for image recognition. In: *Proc. IEEE Conference on Computer Vision and Pattern Recognition*, 2016. P. 770–778. <https://doi.org/10.1109/CVPR.2016.90>
16. Xavier Glorot, Yoshua Bengio. Understanding the difficulty of training deep feedforward neural networks. *JMLR Proceedings*. 2010;9:249–256.
17. Ioffe S, Szegedy Ch. Batch normalization: accelerating deep network training by reducing internal covariate shift. In: *Proc. the 32nd International Conference on International Conference on Machine Learning*. 2015;37:448–456.
18. Kingma DP, Ba J. Adam: A method for stochastic optimization. In: *Proc. 3rd International Conference for Learning Representations*, 2014. <https://arxiv.org/abs/1412.6980>
19. Puzyrev V. Deep learning electromagnetic inversion with convolutional neural networks. *Geophysical Journal International*. 2019;218(2):817–832. <https://doi.org/10.1093/gji/ggz204>
20. Nagatani Y, Okumura S, Wu S, et al. Two-dimensional Ultrasound Imaging Technique based on Neural Network using Acoustic Simulation. *Medical Physics*, 2020. <https://arxiv.org/abs/2004.08775v1>
21. Solov'ev AN, Sobol' BV, Vasil'ev PV. Ultrasonic Location of Inner Crack Defects in a Compound Elastic Cylinder Using an Artificial Neural-Network Apparatus. *Russian Journal of Nondestructive Testing*. 2016;52(3):119–124.

Received 26.02.2021

Revised 02.04.2021

Accepted 04.06.2021

About the Authors:

Vasiliev, Pavel V., senior lecturer of the Information Technologies Department, Don State Technical University (1, Gagarin sq., Rostov-on-Don, RF, 344003), Researcher ID: [P-8366-2017](https://orcid.org/0000-0003-4112-7449), Scopus ID: [57193327081](https://orcid.org/0000-0003-4112-7449), ORCID: <https://orcid.org/0000-0003-4112-7449>, lyftzeigen@mail.ru

Senichev, Alexander V., postgraduate student of the Information Technologies Department, Don State Technical University (1, Gagarin sq., Rostov-on-Don, RF, 344003), ORCID: <https://orcid.org/0000-0003-2001-8235>, alexandr.senichev@gmail.com

Giorgio, Ivan, professor of the Department of Civil, Construction-Architectural and Environmental Design, University of L'Aquila, researcher, M&MoCS International Research Center for the Mathematics & Mechanics of Complex Systems (Via Camponeschi, 19 Piazza Santa Margherita, 2 Palazzo Camponeschi, L'Aquila AQ, Italy, 67100), PhD (Theoretical and Applied Mechanics), Researcher ID: [E-9341-2010](https://orcid.org/0000-0002-0044-9188), Scopus ID: [24757867200](https://orcid.org/0000-0002-0044-9188), ORCID: <https://orcid.org/0000-0002-0044-9188>

Claimed contributorship

P. V. Vasiliev: basic concept formulation; research objectives and tasks. A. V. Senichev: computational analysis; text preparation; formulation of conclusions. I. Giorgio: the text revision; correction of the conclusions.

All authors have read and approved the final manuscript.

MACHINE BUILDING AND MACHINE SCIENCE



UDC 621.9:531.3

<https://doi.org/10.23947/2687-1653-2021-21-2-154-162>

Influence of stiffness of the mechanical part of the drive and cutting parameters on the shaping elastic deformation control



V. L. Zakovorotny, V. E. Gvindjiliya, A. A. Zakalyuzhny

Don State Technical University (Rostov-on-Don, Russian Federation)

Introduction. One of the ways to improve the accuracy of manufacturing parts by cutting is related to the control of elastic deformations of the tool and the workpiece. This is particularly true for slender parts, whose stiffness law along the tool path is given. In this case, the control parameter, as a rule, is the return flow rate, which affects the cutting forces, whose change causes variations in elastic deformations. To provide the specified accuracy of the diameter, it is required to coordinate the controlled trajectory of the feed drive speed with the feed rate and a priori given law of change in the stiffness of the workpiece or the law of variation of the cutting process parameters. To do this, it is required to determine the law of converting the engine speed into the feed rate, and, ultimately, into elastic deformations. This law depends on the stiffness of the mechanical part of the feed drive and the changing parameters of the cutting process.

Materials and Methods. The paper presents mathematical modeling and, on its basis, analysis of the conversion of the feed rate into cutting forces, taking into account the final stiffness value of the mechanical part of the drive and the evolutionary parameters of the cutting process.

Results. It is shown that, starting from a certain critical value, the law of converting the feed rate into cutting forces becomes fundamentally dependent on the stiffness of the mechanical part of the drive. At the same time, there is an increase in time for setting a new force value when the feed rate varies, which affects the accuracy of providing forces that are consistent with the stiffness law of the part. The paper presents algorithms for calculating elastic deformations for a given stiffness law, as well as algorithms for calculating the trajectory of the feed rate at which the deformations remain constant. It is shown that the law of conversion is also affected by variations in the cutting parameters.

Discussion and Conclusion. The frequency and time characteristics of the conversion are discussed. A conclusion is made about the accuracy of the diameter formed through cutting, depending on the stiffness of the mechanical part of the feed drive and on some parameters of the cutting process.

Keywords: cutting forces, control of elastic deformations, stiffness of the mechanical part of the feed drive.

For citation: V. L. Zakovorotny, V. E. Gvindjiliya, A. A. Zakalyuzhny. Influence of stiffness of the mechanical part of the drive and cutting parameters on the shaping elastic deformation control. Advanced Engineering Research, 2021, vol. 21, no. 2, pp. 154–162. <https://doi.org/10.23947/2687-1653-2021-21-2-154-162>

Funding information: The research is done with the financial support from RFFI (grants nos. 19-08-00022 and 20-38-90074).

© Zakovorotny V. L., Gvindjiliya V. E., Zakalyuzhny A. A., 2021



Introduction. The synergetic paradigm has provided a revision of many approaches to the analysis of the properties of systems interacting with different environments [1–19]. It is used under the study of the cutting process as a single nonlinear dynamic system, which considers various physical processes that characterize the state of the system [10–18]. The system-synergetic approach forms the basis of the synergetic control theory, as well as the control of processing on machine tools [18–24]. In this case, the external control is coordinated with the internal cutting dynamics [23–25]. The problems of synergetic matching are relevant when processing slender parts, for which the law of its change along the toolpaths is set a priori [13, 26–29]. In all these cases, it is required to control the elastic deformation displacements of the tool tip and the workpiece at the point of contact with the tool. It should be noted that the errors in the geometric topology of the part formed by cutting are 60–80% due to elastic deformation displacements of the cutting system elements [11, 13, 30]. The main directions of improving the control systems of machining are associated with the integration of the machine itself and the computer [30–33]. The problem of controlling the elastic deformation displacements of the tool and the workpiece is formulated in [34]. Finally, the synergetic approach to the analysis and synthesis of control systems for machining processes formulated in [23–25], set the task of building control systems for processing on CNC machines based on the coordination of the program of the machine executive elements and the evolutionarily changing properties of the cutting process. This approach is also used to improve control systems for drilling deep holes of small diameter, as well as to provide the stability of the trajectories of forming movements [25, 35]. Thus, both when controlling the treatment processes on machine tools and when programming the trajectories of forming movements, it is required to know the laws of transforming the controlled trajectories of the machine operating elements into cutting forces, and, as a result, with the given elastic properties of the tool and workpiece subsystems – into their elastic deformations. They directly affect the accuracy parameters of the part-making. The laws of transformation are affected by the rigidity of the mechanical part of the drives of the machine actuators and the parameters that characterize the state of the cutting process. The research given in the paper considers the impact of these parameters on the conversion of programmable trajectories of servomotors into cutting forces. It is aimed at improving the efficiency of control over the precision of parts manufacturing.

Materials and Methods. Consider the longitudinal turning of a shaft of uniform diameter, in which the law of variation of its rigidity in the direction normal to the axis of rotation is given (Fig. 1). When describing the transformation of the trajectories of servomotors into forces acting on the tool, we accept the following hypotheses:

1. Consider the case in which stiffness $c(L)$ of the workpiece set along the axis of rotation is an order of magnitude less than the stiffness of the tool subsystem (Fig. 1). Therefore, the deformations of the tool relative to the machine bearing system can be neglected.
2. We will assume that the rotation paths of the spindle and the caliper drive are set and controlled within the bandwidth of the servomotors. The inertia of the mechanical part of the feed drive is related to the rotor of the feed motor. It affects the transients in the servomotor.
3. The reaction to the speed of the servomotors from the cutting process is neglected. This is true if the cutting power given to the motor rotors is significantly less than the power of the servomotors.
4. We will consider, in addition to the elasticity of the workpiece, the elasticity of the entire mechanical part of the feed drive, which we will take into account through the generalized stiffness c_0 . Since there is no reversal of the feed drive during processing, stiffness c_0 can be considered constant over the entire trajectory of the caliper.
5. For the formation of forces at a constant cutting speed, we assume the hypothesis of their dependence on the area of the cut layer. The delay of forces in relation to the change in the cross-section area is neglected [23–24].

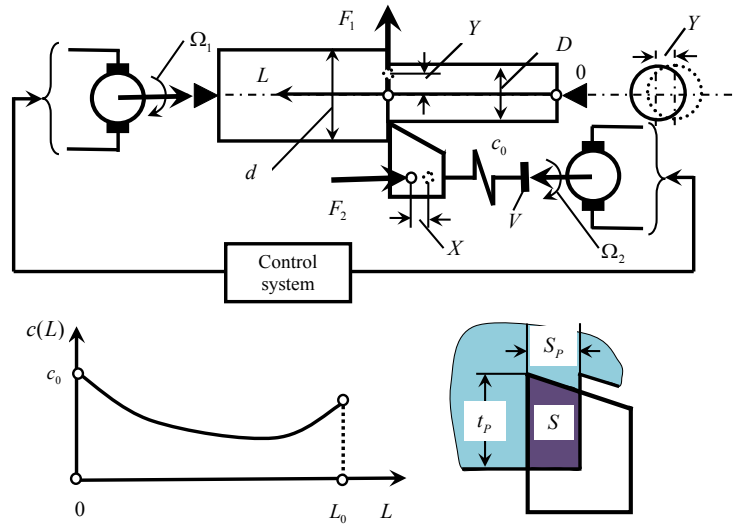


Fig. 1. Diagram of the dynamic system for converting the trajectories of the machine actuators into cutting forces

Then the cutting force modulus is proportional to the area of the cut layer

$$F(t) = F_0 \{ \chi_1, \chi_2 \}^T, \quad (1)$$

where $F_0 = \rho S$ — cutting force modulus in $[kg]$;

ρ — chip pressure on the front surface of the tool in $[kg/mm^2]$;

S — area of the cut layer in $[mm^2]$;

χ_1, χ_2 — nondimensional coefficients. The relationship between the feed rate V and the elastic deformation displacements X and Y is determined from the system (Fig. 1).

$$\begin{cases} c_0 X = \chi_2 \rho (t_p - Y) \int_{t-T}^t [V(\xi) - v(\xi)] d\xi; \\ c(L) Y = \chi_1 \rho (t_p - Y) \int_{t-T}^t [V(\xi) - v(\xi)] d\xi, \end{cases} \quad (2)$$

where $v(t) = dX/dt$; $V(t) = k\Omega_2(t)$;

k — coefficient that determines the relationship between the speed of the feed drive and the speed of the caliper in $[mm]$.

Frequencies Ω_1 and Ω_2 are considered in $[c^{-1}]$. Therefore, the time T in the integral operator of the feed formation is $T = (\Omega_1)^{-1} = const$.

It is convenient to study the conversion of feed rate to cutting forces in the frequency domain. To do this, we can use the Laplace and Fourier transforms [36]. However, system (2) has not only retarded arguments, but also multiplicative terms. The use of the Laplace and Fourier transform methods is possible only for linear systems. Therefore, the study is carried out in two stages. At the first stage, in (2), we put $Y \rightarrow 0$ in comparison with the cutting depth t_p . Then we analyze the conversion of the feed rate to forces based on the expression

$$c_0 X = \chi_2 \rho t_p \int_{t-T}^t [V(\xi) - v(\xi)] d\xi. \quad (3)$$

It is not difficult to show that the transfer function $W(p) = F(p)/V(p)$ is equal to

$$W(p) = c_x \frac{1 - \exp(-Tp)}{p} \frac{1}{1 + \frac{c_x}{c_0} [1 - \exp(-Tp)]} \quad (4)$$

where $c_z = \rho l_p \chi_z$ makes sense of the rigidity of the cutting process. Expression (4) enables to find out the frequency properties of the conversion of the feed rate V to the cutting force F depending on the nondimensional parameter $A = c_z / c_0$. This parameter determines the ratio of the cutting process rigidity to the rigidity of the mechanical part of the feed drive. At $A \rightarrow 0$, the transfer function is $W(p) \Rightarrow c_z \frac{1 - \exp(-Tp)}{p}$. At $A \rightarrow \infty$ $W(p) \Rightarrow \frac{c_z}{p}$. These are two extreme cases. If the case $A \rightarrow 0$ is possible with a significant increase in the rigidity of the mechanical part of the drive compared to the rigidity of the cutting process, then the second case requires reducing the rigidity of the drive to zero, which is impossible for real systems. We give examples $W(j\omega)$ for different A (Fig. 2). The amplitude is considered per unit κ $c_z = 1$.

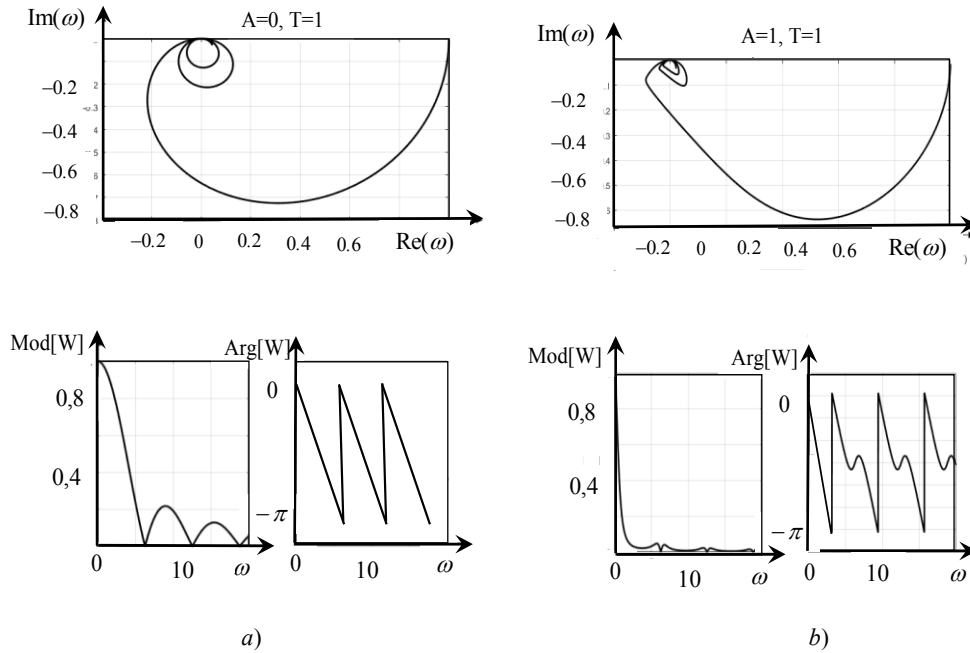


Fig. 2. Example of frequency characteristics of feed rate conversion to the cutting force module

First, let us consider the case when there are no deformations of the mechanical part between the rotor of the feed motor and the movement of the caliper (Fig. 2a). This frequency response is due to the property of the integral operator $\int_{t-T}^t V(\xi) d\xi$ for generating the feed rate, which discloses that the feed rate is the path traveled by the tool relative to the workpiece during the period of its rotation. Naturally, the components of the feed rate variation, whose frequency is equal to or a multiple of the workpiece rotational speed, after integration, turn to zero. These are frequencies at which $Mod[W(j\omega)] = 0$ (Fig. 2). In this case, there is a rapid rotation of the phase at frequencies close to the workpiece rotational frequency, which contributes to the self-excitation of the cutting process control systems. An increase in the compliance of the mechanical part of the drive corresponds to a change in the frequency properties of the conversion of speed into cutting forces. First, the bandwidth of this transformation is noticeably reduced, which should help to increase the transition time when setting a new value of the controlled cutting forces. Second, periodic phase variations are observed in the region of greater amplitude attenuation. Finally, with even greater increases in compliance, the characteristics of the speed-to-force conversion approach the integrator. The transient delaying mechanism is based on the redistribution of forces that affect the deformation displacements, and the deformation displacements that affect the forces. This functionally related process depends on the rigidity of the mechanical part of the feed drive.

The above analysis also enables to estimate the impact of deformation displacements of the workpiece in the direction of the axis of rotation on the dynamics of the conversion of speed V into cutting forces (Y direction in Fig. 1). It is obvious that when the stiffness c decreases, parameter A that affects the dynamics of the conversion of the feed rate into cutting forces also decreases.

Algorithm for calculating the feed rate trajectory. To provide the specified diameter values through controlling the deformation Y , it is required to select such trajectories of velocity at which V at which $Y = const$. For this purpose, instead of the integral operator in (2), let us consider its primitive, that is,

$$\begin{cases} c_0 X = \chi_2 \rho (t_p - Y) [L(t) - L(t-T) - X(t) + X(t-T)]; \\ c(L) Y = \chi_1 \rho (t_p - Y) [L(t) - L(t-T) - X(t) + X(t-T)], \end{cases} \quad (5)$$

where $L(t)$ — the trajectory of the caliper movement without taking into account elastic deformations, that is,

$$L(t) = \int_0^t V(\xi) d\xi. \text{ B (5) } L(t) - L(t-T) = S_p^{(0)}(t) \text{ — the current feed value without taking into account deformation}$$

displacements. If $c(L) = const$ and the steady state is considered ($X(t) = X(t-T)$), then $S_p^{(0)} = S_p = VT$. Here, $S_p(t) = S_p^{(0)} - [X(t) - X(t-T)]$. We emphasize that the feed value $S_p^{(0)}$, which is assessed traditionally, differs from its real value $S_p(t)$.

We will calculate the deformation displacements in (5) sequentially after each turn of the workpiece and determine the sequences $X(iT) = \{X(0), X(T), \dots, X(nT)\}$, $Y(iT) = \{Y(0), Y(T), \dots, Y(nT)\}$, $S_p(t) = \{S_p(T), \dots, S_p(nT)\}$, $c(T) = \{c[S_p(T)], \dots, c[\sum_{i=1}^{i=n} S_p(iT)]\}$. Thus, for n revolutions of the workpiece, the caliper travels the distance

$$L(n) = \sum_{i=1}^{i=n} S_p(iT). \text{ In these sequences, } X(0) = Y(0) = 0. \text{ The solution to two problems can be considered.}$$

The first task of analysis, i.e., determining the trajectories of deformation displacements $X(iT)$ and $Y(iT)$ at a constant feed rate. To calculate values $X(T), Y(T)$ and subsequent values of deformation displacements $X(iT), Y(iT)$, we can use the relations in which all the previous values are known $X[(i-1)T], Y[(i-1)T]$, as well as $c[(\sum_{l=1}^{l=i-1} S_p(lT))]$. Here, $V = const$, it follows that $c[(\sum_{l=1}^{l=i-1} S_p(lT))] = (c(iS_p))$. Thus, for calculating $X(iT), Y(iT)$ we can use the system

$$c_\Sigma Z^{(i)} = F^{(i)}, \quad (6)$$

where $Z^{(i)} = \{Y(iT), X(iT)\}^T$; $F^{(i)} = \rho S_p^{(0)} [t_p + X((i-1)T)] \{\chi_2, \chi_1\}^T$;

$$c_\Sigma = \begin{bmatrix} c_0 + \chi_2 \rho t_p & \chi_2 \rho S_p^{(0)} \\ \chi_1 \rho t_p & [(c(iS_p) + \chi_1 \rho S_p^{(0)})] \end{bmatrix}.$$

In (5), the multiplicative terms of the deformation displacements, which are small quantities, are omitted. At a given speed $V = const$, we are primarily interested in the law of variation of deformation displacements $Y(iT) = \{Y(0), Y(T), \dots, Y(nT)\}$, which characterizes the error of the diameter. On the basis of (6) for deformation displacements $Y(iT)$, that directly affect the diameter of the part, we obtain

$$Y(iT) = \frac{\chi_2 \rho c(iS_p) S_p^{(0)} \{t_p + X[(i-1)T]\}}{c_0 c(iS_p) + \chi_1 \rho c_0 S_p + \chi_2 \rho c(iS_p) t_p}. \quad (7)$$

Thus, $Y(iT)$ depend not only on the law of the distribution of the stiffness of the workpiece $c(L)$ along the cutting path L , but also on $\partial c(L) / \partial L$, that affects $Y(t-T)$. The cutting forces, hence diameter D , are affected by the chip pressure ρ . It changes, for example, as the tool wear increases, due to its geometry variation, processing conditions and properties of the processed material.

The second task of synthesis, i.e., determining the sequence $S_p(t) = \{S_p(T), \dots, S_p(nT)\}$ and the corresponding speed $V(t)$ in such a way that the condition $Y(iT) = const$, $Y(iT) \in Y(iT)$ is met. This is the condition for the consistency of diameter under a given law $c(L)$, other conditions unchanged. Note that the constant components in the deformation displacements $Y(iT)$ are not of fundamental importance, since they can be taken into account using the static tool setup [34]. To determine the law of variation in the feed value at each turn of the workpiece according to the criterion of the consistency of diameter, it is required to put $Y(iT) = const$ in (7). Then we need to calculate the

sequence $S_p(t) = \{S_p(T), \dots, S_p(nT)\}$. The procedure for calculating on i -th turn of the workpiece is to determine $S_p(iT)$, provided that the following parameters are specified $X(iT) = \{X(0), X(T), \dots, X[(i-1)T]\}$, $Y(iT) = \{Y^*(0), Y^*(T), \dots, Y^*[(i-1)T]\}$, therefore, all feed values are determined $S_p(t) = \{[S_p(T) = Y(T) - Y(0)], \dots, S_p[(i-n)T] = [Y((i-1)T) - Y((i-2)T)]\}$. From (7), we obtain

$$S_p(iT) = \frac{Y^* c \left[\sum_{l=1}^{i-1} S_p(lT) \right] \{c_0 + \chi_2 \rho t_p\}}{\chi_1 \rho c_0 \{t_p + X[(i-1)T] - Y^*\}} \quad (8)$$

where $Y^* = \text{const}$ — the specified value of elastic deformation displacements.

In (8), the workpiece stiffness value is taken as the average for each feed. Then, based on the calculated $S_p(t) = \{S_p(T), \dots, S_p(nT)\}$, the law of variation $V(t)$ and, consequently, the programmable trajectory of the feed rate in time or path are determined. The trajectory $V(t)$ is calculated based on the solution to inverse problems of dynamics [37–38].

Research Results. To provide accuracy of the production of low-rigidity shafts, it is required to coordinate the trajectories of the machine actuators with the changing rigidity of the workpiece along the toolpath. The alignment must also be performed if the evolutionary changes in the properties of the cutting process are taken into account, e.g., due to tool wear or thermodynamic processes, as well as regular perturbations, for example, variations in the allowance. For this purpose, first of all, you need to know the laws of converting the programmable feed rate of the caliper into cutting forces and then into the deformations themselves, which change the current value of the workpiece diameter. The performed studies have shown that the transformation law depends on the parameters of the stiffness of the interacting subsystems and the parameters of the dynamic coupling formed by the cutting process.

Among the stiffness parameters, the stiffness characteristics of the mechanical part of the feed drives are of fundamental importance, which can be estimated by the total reduced stiffness c_0 . It changes the amplitude-phase frequency (AFF) response of the conversion of the feed rate to the cutting force (Fig. 2). As you can see, decreasing the drive stiffness significantly reduces the amplitude as the frequency increases, and the initial AFF, which had noticeable spikes, is converted into a characteristic with amplitude attenuation. This characteristic causes the transformation of vibrational transients into monotonic, close to aperiodic ones. As c_0 decreases, there is a decrease in the cutoff frequency in the conversion of the feed rate into cutting forces (Fig. 2), therefore, the transition time increases, e.g., the change in the cutting force when cutting the tool. Figure 3 shows changing the transients of force F_0 setting under turning a shaft made of 20X steel with a diameter of 80 mm. Turning is performed at the following modes: cutting speed is 4.0 m/s (spindle speed — 1000 rpm), cutting depth t_p — 2.0 mm, feed rate S_p — 0.1 mm. for this case, $\rho = 400 \text{ kg/mm}^2$

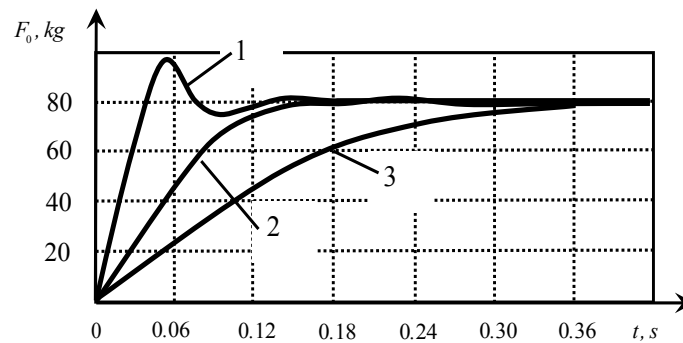


Fig. 3. Example of a change in the transient processes of establishing force –

F_0 : 1 — $c_0 = 1000 \text{ kg/mm}$, 2 — $c_0 = 750 \text{ kg/mm}$, 3 — $c_0 = 500 \text{ kg/mm}$

From the above-mentioned properties of the integral operator for the formation of the feed value, an important conclusion follows on the possibility of controlling the cutting forces, therefore, the elastic deformation displacements of the tool relative to the workpiece. When the feed rate is changed, the frequency components of the disturbances, equal to or multiples of the workpiece rotation frequency, get out of control by varying the feed drive speed. For example, these are variations in the allowance due to misalignment of the workpiece installation, radial spindle runouts,

etc. Besides, the data show that the transients of the feed rate-to-force conversion also depend on the parameters of the dynamic coupling formed by the cutting process, and primarily — on the chip pressure parameter on the front surface of the tool. This parameter changes as tool wear develops. The dynamics of the transformation of the trajectories of the machine actuators into cutting forces are affected by all the factors that connect the cutting forces with the area of the cut layer. These factors limit the ability to control accuracy of manufacturing parts through varying the trajectories of the machine actuators. This applies primarily to the processing of parts of complex geometry.

Discussion and Conclusions. One of the ways to improve accuracy of manufacturing parts on machine tools is associated with the alignment of the CNC program with the changing dynamic properties of the cutting process. Moreover, these changes can be set a priori. For example, the law of variation in the stiffness matrices along the trajectory of the machine actuators can be set a priori. They can develop according to some random law, for example, due to the development of tool wear. In many cases, precision control is based on changes in the elastic deformation displacements of the tool and the workpiece. As shown in the paper, the law of transformation of the feed rate into cutting forces and elastic deformation displacements, first, depends on the elastic parameters of the mechanical part of the feed drives affecting not only the time of transients, but also their shape. Secondly, the regularities of the transformation of the feed rate into forces depend on the evolution of the parameters of the interacting subsystems on the part of the tool and the workpiece, as well as the parameters of the dynamic connection formed by cutting. The disclosed transformation patterns enable not only to find out the limitations imposed by the cutting system on the accuracy control capabilities, but also to increase their accuracy.

References

1. Haken H. Information and Self-Organization: A Macroscopic Approach to Complex Systems. Amsterdam: Elsevier; 2006. 251 p.
2. Prigogine I, George C. The second law as a selection principle: The microscopic theory of dissipative processes in quantum systems. Proceedings of the National Academy of Sciences. 1983;80(14):4590–4594. <https://doi.org/10.1073/pnas.80.14.4590>
3. Ebeling W, Engel A, Feistel R. Fizika protsessov ehvolyutsii. Sinergeticheskii podkhod [Physics of the processes of evolution. Synergetic approach. Translated from German by Yu.A. Danilov]. Moscow: Editorial URSS; 2001. 328 p. (In Russ.)
4. Moiseev NN. Rasstavanie s prostotoi (Put' k ochevidnosti) [Parting with Simplicity (The Path to Evidence)]. Moscow: Agraf; 1998. 472 p. (In Russ.)
5. Nicolis JS, Danilov YuA. Dinamika ierarkhicheskikh sistem. Ehvolyutsionnoe predstavlenie [Dynamics of Hierarchical Systems. Evolutionary View]. Moscow: Mir; 1989. 488 p. (In Russ.)
6. Zakovorotny VL, Flek MB, Ugnich EA. Model' upravleniya sovremennym predpriyatiem na osnove sistemnosinergeticheskogo podkhoda [Model of the modern enterprise management on the basis of system-synergistic approach]. Economics of Contemporary Russia. 2016;4(75):112–128. (In Russ.)
7. Kolesnikov AA. Prikladnaya sinergetika: osnovy sistemnogo sinteza [Applied synergetics: Fundamentals of system synthesis]. Taganrog: TTU YUFU; 2007. 384 p. (In Russ.)
8. Zakovorotny VL, Shapovalov VV. Dinamika transportnykh tribosistem [Dynamics of transport tribosystems]. Assembling in Mechanical Engineering and Instrument-Making. 2005;12:19–24. (In Russ.)
9. Ryzhkin AA. Sinergetika iznashivaniya instrumental'nykh materialov pri lezviinoi obrabotke [Synergetics of tool materials wear during blade processing]. Rostov-on-Don: DSTU; 2019. 289 p. (In Russ.)
10. Ryzhkin AA, Moiseev DV, Bokov AI, et al. Optimizatsiya rezhima rezaniya pri lezviinoi obrabotke [Optimization of the cutting mode during blade processing]. Rostov-on-Don: DSTU; 2017. 34 p. (In Russ.)
11. Starkov VK. Fizika i optimizatsiya rezaniya materialov [Physics and optimization of cutting materials]. Moscow: Mashinostroenie; 2009. 640 p. (In Russ.)
12. Migranov MSh. Issledovaniya iznashivaniya instrumental'nykh materialov i pokrytii s pozitsii termodinamiki i samoorganizatsii [Studies of the wear of tool materials and coatings with regard to thermodynamics and self-organization]. Proceedings of Higher Educational Institutions. Machine Building. 2006;11:65–71. (In Russ.)
13. Bazrov BM. Osnovy tekhnologii mashinostroeniya [Fundamentals of mechanical engineering technology]. Moscow: Mashinostroenie; 2005. 736 p. (In Russ.)

14. Melentyev GA, Skhirtladze AG, Boriskin VP. Rezanie materialov [Cutting materials]. Staryi Oskol: Tonkie naukoemkie tekhnologii; 2019. 512 p. (In Russ.)
15. Kuznetsov VA, Cherepakhin AA, Smirnov AV. Sistemnyi analiz i modelirovanie tekhnologicheskikh metodov izgotovleniya detalei [System analysis and modeling of technological methods of manufacturing parts]. Moscow: KnoRus; 2019. 248 p. (In Russ.)
16. Lapshin VP, Khristoforova VV, Nosachev SV. Vzaimosvyaz' temperatury i sily rezaniya s iznosom i vibratsiyami instrumenta pri tokarnoi obrabotke metallov [Relationship of temperature and cutting force with tool wear and vibration in metal turning]. Metal Working and Material Science. 2020;22(3):44–58. <http://dx.doi.org/10.17212/1994-6309-2020-22.3-44-58> (In Russ.)
17. Lapshin VP, Turkin IA, Khristoforova VV, et al. Modelirovanie vliyaniya temperatury v zone kontakta instrumenta i detali na dinamiku deformatsionnykh dvizhenii instrumenta pri tochenii metallov [Simulation of the influence of temperature in the tool – part contact zone on the dynamics of tool deformation movements under metal turning]. STIN. 2019;10:31–37. (In Russ.)
18. Lapshin VP, Turkin IA, Khristoforova VV. Primer ehksperimental'noi otsenki iznosa na sostavlyayushchie sily rezaniya pri tochenii metallov [An example of an experimental assessment of wear on the cutting force components under metal turning]. STIN. 2020;4:41–44. (In Russ.)
19. Kolesnikov AA. Sinergeticheskaya teoriya upravleniya (invarianty, optimizatsiya, sintez) [Synergetic control theory (invariants, optimization, synthesis)]. Taganrog: TRI; Moscow: Energoatomizdat; 1994. 343 p. (In Russ.)
20. Kolesnikov AA. Sinergeticheskaya teoriya upravleniya [Synergetic control theory]. Moscow: Energoatomizdat; 1994. 344 p. (In Russ.)
21. Kolesnikov AA, Kolesnikov AIA, Kuzmenko AA. Metod AKAR i teoriya adaptivnogo upravleniya v zadachakh sinteza nelineinykh sistem upravleniya [ADAR Method and Theory of Adaptive Control in the Tasks of Synthesis of the Nonlinear Control Systems]. Mechatronics, Automation, Control. 2017;18(9):579–589. <https://doi.org/10.17587/mau.18.579-589> (In Russ.)
22. Kolesnikov AA, Kolesnikov AIA, Kuz'menko AA. Metody AKAR i AKOR v zadachakh sinteza nelineinykh sistem upravleniya [The ADAR method and theory of optimal control in the problems of synthesis of nonlinear control systems]. Mechatronics, Automation, Control. 2016;17(10):657–669. 10.17587/mau.17.657–669 (In Russ.)
23. Zakovorotny VL, Flek MB, Pham Dinh Tung. Sinergeticheskaya kontseptsiya pri postroenii sistem upravleniya tochnost'yu izgotovleniya detalei slozhnoi geometricheskoi formy [Synergetic concept in construction of accuracy control systems for manufacturing parts of complex geometric forms]. Vestnik of DSTU. 2011;11(10):1785–1797. (In Russ.)
24. Zakovorotny V, Gvindhiliya V. Sinergeticheskii podkhod k upravleniyu protsessom obrabotki na stankakh tokarnoi gruppy [Synergetic approach to machining control of lathe group machines]. Science Intensive Technologies in Mechanical Engineering. 2019;11(101):29–38. https://10.30987/article_5d9dc9b8e6bdd8.19855459 (In Russ.)
25. Zakovorotny VL, Panov EYu, Potapenko PN. Svoistva formoobrazuyushchikh dvizhenii pri sverlenii glubokikh otverstii malogo diametra [Properties of forming movements when drilling deep holes of small diameter]. Vestnik of DSTU. 2001;1(2):81–93. (In Russ.)
26. Azarov AS. Vysokoproizvoditel'naya obrabotka valov v mashinostroenii [High-performance shaft machining in mechanical engineering]. Leningrad: Mashgiz; 1951. 224 p. (In Russ.)
27. Bobrovsky AV, Drachev OI. Tekhnologiya mekhanicheskoi obrabotki malozhestkikh osesimmetrichnykh detalei [Technology of processing low-rigid axisymmetric parts]. Izvestia VSTU. 2019;9(232):15–17. (In Russ.)
28. Drachev OI. Sistema avtomaticheskogo upravleniya ehkspluatatsionnoi tochnost'yu dlinnomernykh valov [Automatic control system of the operational accuracy of long shafts]. Izvestia VSTU. 2017;5(200):18–20. (In Russ.)
29. Zholobov AA, Kazakov AV. Prognozirovanie i obespechenie tochnosti tokarnoi obrabotki stupenchatykh valov [Forecasting and ensuring the accuracy of stepped shafts turning]. Vestnik of Belarusian-Russian University. 2014;1(42):6–14. (In Russ.)
30. Plotnikov AL. Upravlenie sistemami i protsessami [Managing systems and processes]. Volgograd: VolGGTU; 2010. 167 p. (In Russ.)
31. Mikheev YuE, Sosonkin VL. Sistemy avtomaticheskogo upravleniya stankami [Automatic control systems for machine tools]. Moscow: Mashinostroenie; 1978. 264 p. (In Russ.)

32. Legaev VP, Generalov LK. Povyshenie ehffektivnosti tokarnoi obrabotki na osnove avtomaticheskogo kontrolya pokazatelei protsessa rezaniya [More efficient lathe operation on the basis of automatic monitoring of the cutting parameters]. Russian Engineering Research. 2011;31(1):44–46. <https://doi.org/10.3103/S1068798X1101014X> (In Russ.)
33. Maksimov S, Kolosov V, Morozov K. Sovremennoe sostoyanie i perspektivy razvitiya sistem CHPU [Current state and prospects of development of CNC systems]. Innovatsii v nauke. 2014;40:40–45. (In Russ.)
34. Bazrov BM, et al. Adaptivnoe upravlenie stankami [Adaptive machine control]. Moscow: Mashinostroenie; 1973. 688 p. (In Russ.)
35. Zakovorotny VL, Gvindjiliya VE. Vliyanie fluktuatsii na ustoychivost' formoobrazuyushchikh traektorii pri tochenii [The influence of fluctuation on the shape-generating trajectories stability with a turning]. University news. North-Caucasian region. Technical Sciences Series. 2017;2(194):52–61. <https://doi.org/10.17213/0321-2653-2017-2-52-61> (In Russ.)
36. Korn G, Korn T. Spravochnik po matematike dlya nauchnykh rabotnikov i inzhenerov [Handbook of Mathematics for Researchers and Engineers]. Moscow: Nauka; 1968. 720 p. (In Russ.)
37. Krutko PD. Obratnye zadachi dinamiki upravlyaemykh sistem: lineinye modeli [Inverse problems of dynamics of controlled systems: linear models]. Moscow: Nauka; 1987. 304 p. (In Russ.)
38. Galiullin AS. Metody resheniya obratnykh zadach dinamiki [Methods for solving inverse problems of dynamics]. Moscow: Nauka; 1986. 224 p. (In Russ.)

Received 28.04.2021

Revised 02.06.2021

Accepted 04.06.2021

About the Authors:

Zakovorotny, Vilor L., professor of the Production Automation Department, Don State Technical University (1, Gagarin sq., Rostov-on-Don, RF, 344003), Dr.Sci. (Eng.), professor, Researcher ID [I-2990-2014](#), Scopus ID: [6507213621](#), ORCID: <https://orcid.org/0000-0003-2187-9897>, vzakovorotny@dstu.edu.ru

Gvindjiliya, Valeriya E., postgraduate student of the Production Automation Department, Don State Technical University (1, Gagarin sq., Rostov-on-Don, RF, 344003), Researcher ID: [AAM-4580-2020](#), Scopus ID: [57204638971](#), ORCID: <https://orcid.org/0000-0003-1066-4604>, sinedden@yandex.ru

Zakalyuzhny, Aleksei A., postgraduate student of the Production Automation Department, Don State Technical University (1, Gagarin sq., Rostov-on-Don, RF, 344003), ORCID: <https://orcid.org/0000-0002-1888-3222>, zakalishnuy-95@yandex.ru

Claimed contributorship

V. L. Zakovorotny: basic concept formulation; research objectives and tasks; academic advising; analysis of the research results. V. E. Gvindjiliya: simulation of the cutting process; text preparation; formulation of conclusions. A. A. Zakalyuzhny: computational analysis; modeling of frequency and transient characteristics.

All authors have read and approved the final manuscript.

MACHINE BUILDING AND MACHINE SCIENCE



UDC 621.791.14

<https://doi.org/10.23947/2687-1653-2021-21-2-163-170>

Technology and equipment for friction stir preweld edge preparation

Y. G. Lyudmirsky¹, A. N. Soloviev¹, M. V. Soltovets¹, R. R. Kotlyshev²,
I. V. Mironov², A. V. Kramskoy³



¹ Don State Technical University (Rostov-on-Don, Russian Federation)

² Main certification body for welding production in the Southern Region (Rostov-on-Don, Russian Federation)

³ Atommash Branch of AEM-technology JSC (Volgodonsk, Russian Federation)

Introduction. Friction stir welding is widely used due to certain advantages of this method. Factors that reduce the strength of joints made of high-strength aluminum alloys are considered. When welding flat sheets, an effective way to increase the strength of the weld is edge thickening. The paper proposes a method for such thickening. A device is developed, calculations and experiments are carried out.

Materials and Methods. Laboratory equipment has been developed to provide simultaneous thickening of two edges to be welded. The main component of this equipment is a steel roller, which is rolled along the edges of two blanks and thickens them due to plastic deformation. The same setup can be used for the friction stir welding process. To calculate the geometry of the thickened edges and the parameters of the deforming roller depending on the value of the edge settlement, a mathematical model based on the contact problem for elastic (roller) and elastoplastic (blank) bodies with a bilinear hardening law has been developed. A three-dimensional simplified geometric model of the facility with account of its symmetry has been constructed. On the contact surfaces, special contact finite elements were selected and the finite element mesh was refined. The numerical implementation of the model was carried out in the ANSYS package.

Results. The theoretical model provides assessing the stress-strain state of interacting elements. On the basis of the developed finite element model, the parameters of the thickened edges are calculated, and the geometry of the thickened edges is defined. Using the developed laboratory equipment, full-scale experiments on thickening the edges of the blanks were carried out. The experimental results confirm the adequacy of the developed theoretical model and calculations based on it. The possibility of adjusting the size of the thickened edges is shown.

Discussion and Conclusion. A technology for obtaining thickened edges in places of welds is proposed. It will reduce the metal consumption of structures and ensure the bearing capacity of welded joints not lower than similar characteristics of the base metal. A theoretical model of the process is developed, and a numerical experiment providing the selection of the process parameters is carried out.

Keywords: friction stir welding, thickened edges, computer model, geometry and dimension of edges, bearing capacity of welded joints.

For citation: Y. G. Lyudmirsky, A. N. Soloviev, M. V. Soltovets, et al. Technology and equipment for friction stir preweld edge preparation. Advanced Engineering Research, 2021, vol. 21, no. 2, pp. 163–170. <https://doi.org/10.23947/2687-1653-2021-21-2-163-170>

© Lyudmirsky Y. G., Soloviev A. N., Soltovets M. V., Kotlyshev R. R., Mironov I. V., Kramskoy A. V., 2021



Introduction. Many researchers¹ [1–5] report on the high level of mechanical properties of joints made by friction stir welding (FSW) and the advantages of this welding method. Issues related to the calculation of temperature fields under FSW are considered in [6]. However, during FSW of aluminum alloys, whose high strength is achieved by

¹ Sergeeva EV. Friction stir welding in the world shipbuilding. Current level of development, prospects, equipment. HSC Consulting. URL: WWW.sergeev-hsc.de (accessed 12.09.2011). (In Russ.)

heat treatment or strengthening deformation, the strength of welded joints is 0.78–0.94 of the strength of the base metal² [7, 8]. In these cases, it is possible to compensate for the missing strength through increasing the thickness of the metal in the places of welds or by introducing a safety factor. The latter increases the weight of the structure and, accordingly, makes it uneconomic. A review of recent studies on the dependence of mechanical and microstructural properties of welds under FSW with the use of cooling is presented in [9]. In [10, 11], the optimization of the FSW process in the connection of aluminum alloys is considered. The effect of cryogenic treatment and annealing on the microstructure of the weld during FSW is considered in [12]. Methods for achieving increased joint strength are investigated in [13]. The impact of the axial force under FSW is studied in [14]. Theoretical and experimental studies of FSW joining dissimilar materials and the effect of technological parameters of the process on its strength are considered in papers [15, 16].

There are several ways to thicken the edges at the welding sites. They are obtained through mechanical or chemical milling^{3,4} by artificial thinning of the base metal, with the exception of the zone where the connection is made by welding. However, these operations cause a reduction in the material utilization factor to 0.5–0.7 and an increase in the construction cost. In addition, these processes are very labor-consuming.

Sometimes the thickening of the welded edges is obtained through surfacing, which causes the appearance of high residual stresses, an increase in welding deformations, and a decrease in the efficiency of the use of high-strength alloys⁵.

The objective of this study is to develop and test the edge thickening technology under FSW, which will increase the material utilization rate, reduce labor costs, increase the bearing capacity of weld joints to the level of the base metal and increase the fatigue strength of the joints.

Materials and Methods. The following requirements are specified to the geometry of the thickened edges shown in Fig. 1.

First, the height of the edge thickening h should compensate for the missing strength of the weld joint caused by the thinning of the weld by the tool shoulders and the softening of the alloys in the heat-affected zone. Usually, for high-strength aluminum alloys, this value is 10–25% of the strength of the base metal. In this regard, $h = (0.1–0.25) S$, where S — thickness of the base metal.

Secondly, the width of the edge thickening b should be greater than the diameter of the tool shoulders for the FSW.

Thirdly, the width of the plastic deformation zone B , as shown in Fig. 1, should overlap the heat-affected zone formed under FSW.

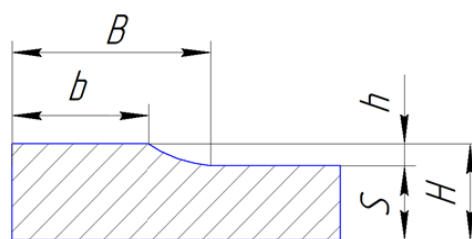


Fig. 1. Thickened edges geometry: S — metal thickness; B — width of plastic deformation zone; b — width of edge thickening; h — height of edge thickening

²Technology. Properties of joints obtained by FSW. Available from: http://referatwork.ru/category/tehnologii/view/492395_svoystva_soedineniy_poluchennyh_stp (accessed 20.08.2018). (In Russ.)

³Chemical milling (contour etching). Available from: <http://megaobuchalka.ru/6/52594.html> (accessed 01.12.2017). (In Russ.)

⁴Karachenkov EM. Improving the quality of body parts of rocket and space technology: Cand.Sci. (Eng.) diss., abstract. Khronichev Space Research Center. Moscow, 2000. (In Russ.)

⁵Kapryin GI, Grishchenko LV, Kurkin SA, et al. Improving the fatigue strength of welded joints. USSR Patent, 1973. (In Russ.)

The process of thickening the welded edges is proposed to be performed by cold rolling. Figure 2 shows the installation scheme for one-sided thickening of two edges that are to be welded at the same time. Moreover, this operation can be performed on the same equipment on which the welding will be carried out later.

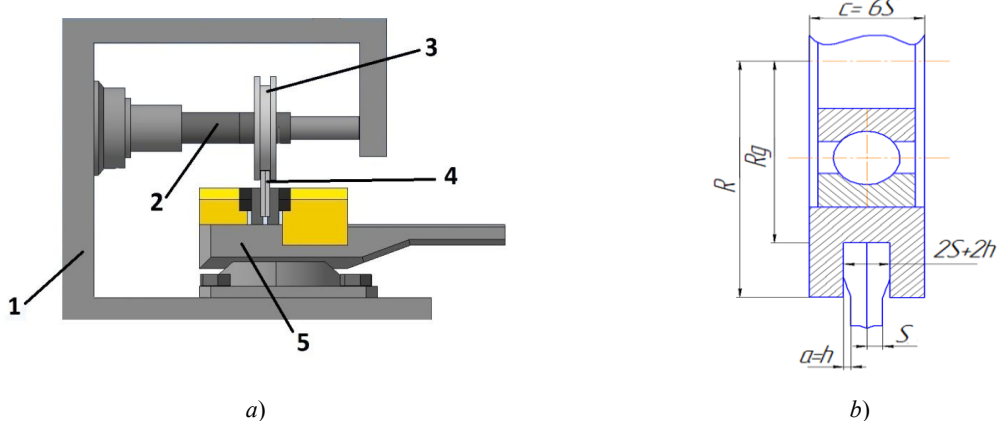


Fig. 2. Installation for edge thickening under FSW:

a) general view of the installation; b) scheme of edge thickening

The installation for edge thickening consists of a universal milling machine 1, on whose rolling pin 2 a deforming roller 3 is installed. Vice 5 is placed on the machine table, in which two blanks 4, whose edges are subjected to thickening, are fixed simultaneously. The installation operates as follows. Thickening blanks are installed along the deforming roller stream. Raising the table creates a predetermined amount of edge settlement. Moving the table along the roller stream is activated. In this case, upsetting of the welded edges occurs by value Δ along the entire length of the blanks.

To calculate the geometry of the thickened edges and the parameters of the deforming roller, depending on the amount of edge upsetting Δ , a computer model has been developed that operates in the finite element package ANSYS. The contact static problem of pressing the roller into the blanks is considered (Fig. 2 b). Due to the symmetry of the problem, a simplified design is considered (Fig. 3 a). It is obtained through dissecting the original with two vertical planes (the plane between the blanks and the plane passing through the roller axis), on which the symmetry conditions are set, and with one horizontal plane (the plane passing through the roller axis), on which a vertical displacement is set (upsetting of the blank edges).

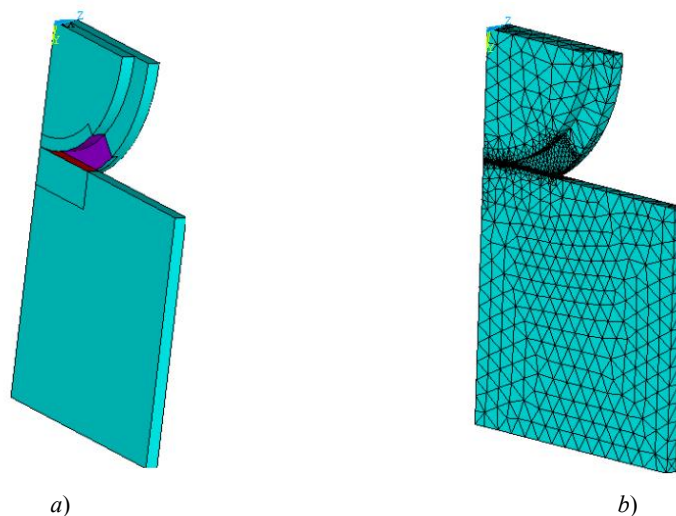


Fig. 3. Model of the contact interaction of the roller and the blank:

a) geometric model; b) finite element model

The developed model uses a linear elastic material for the deforming roller and a bilinear elastic-plastic material without hardening — for an aluminum blank. The surfaces of possible contact are highlighted (Fig. 3 a),

contact elements are set on them, and the finite element grid is refined (Fig. 3 b). The model provides evaluating the stress-strain state of interacting structural elements in the elastic and plastic regions, as well as determining the geometry of thickened edges.

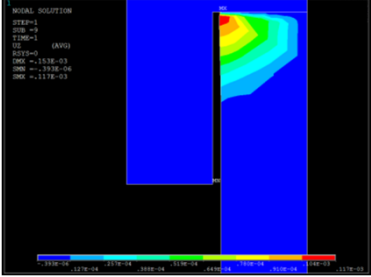
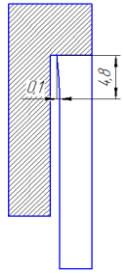
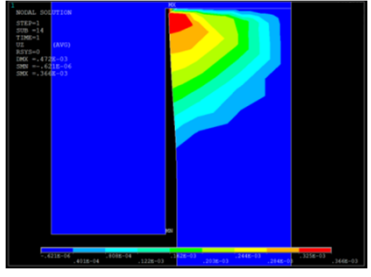
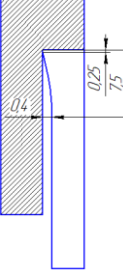
The initial data for the model operation are:

- amount of upsetting of the welded edges Δ , mm;
- thickness of the welded blanks S , mm;
- width of the edge thickening $b \geq d/2$, mm, where d — shoulder diameter;
- plastic deformation zone $B \geq T/2$, where T — heat-affected zone under FSW, mm;
- edge thickening size $h = (0.1–0.25) S$, mm;
- thickness of the preweld edges $H = S + h$, mm;
- deforming roller radius $R_0 \geq 70$ mm;
- roller outer radius $R_0 = R_d + B$, mm;
- gap between the side surfaces of the roller and the blanks $\alpha = (0.1 \dots 0.25) S$, mm;
- width of the roller $C = 6S$, mm;
- elastic modulus of the aluminum blank $E = 0.7 \cdot 10^5$, MPa;
- elastic modulus of the steel deforming roller $E = 2,1 \cdot 10^5$, MPa;
- Poisson's ratio $\mu = 0.33$;
- ultimate strength of the base metal $\sigma_b = 390$ MPa;
- yield strength of the base metal, $\sigma_T = 175$ MPa.

Research Results. The geometry of the thickened edges as a result of their upsetting by value Δ can be inferred by the pattern of the distribution of axial displacements in the deformable edges. Table 1 shows the distribution of stresses in blanks with a thickness of 4.0 mm, the geometry and dimensions of thickened edges with varying degrees of upsetting.

Table 1

Distribution of transverse displacements on deformed blanks with a thickness of 4.0 mm and the geometry of thickened edges with varying degrees of upsetting

Distribution of transverse displacements in the blanks under edge upsetting	Geometry and dimensions of thickened edges, mm	Amount of edge upsetting Δ , mm
		0.1
		0.3

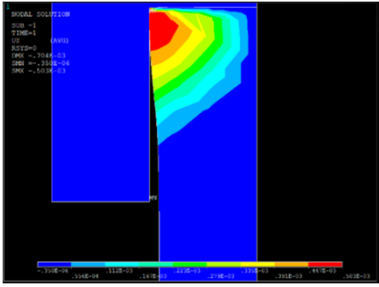
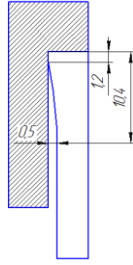
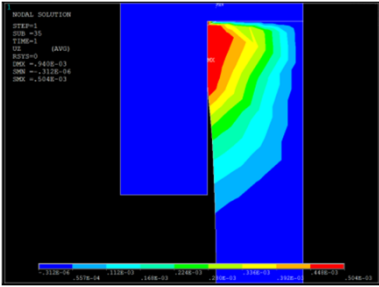
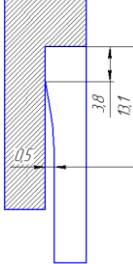
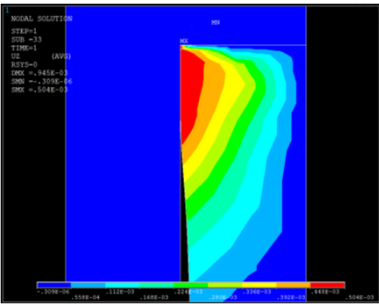
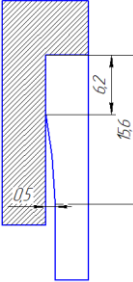
Distribution of transverse displacements in the blanks under edge upsetting	Geometry and dimensions of thickened edges, mm	Amount of edge upsetting Δ , mm
		0.5
		0.8
		1.2

Table 2 shows the parameters that characterize the geometry of thickened edges at varying degrees of upsetting Δ .

Table 2

Dimensions of the thickened edges, depending on the degree of their upsetting

Calculated parameters of thickened edges, mm	Amount of edge upsetting Δ , mm					
	0.1	0.3	0.5	0.8	1.2	1.5
Height of thickened edges h	0.1	0.4	0.5	0.5	0.5	0.5
Width of plastic deformation zone B	4.8	7.5	10.4	13.1	15.6	17.8
Width of thickened edge b	0	0.25	1.2	3.8	6.2	8.65
$B-b$	4.8	7.25	9.2	9.3	9.4	9.15

Figure 4 shows dependences B and b on Δ constructed according to the data presented in Table 2.

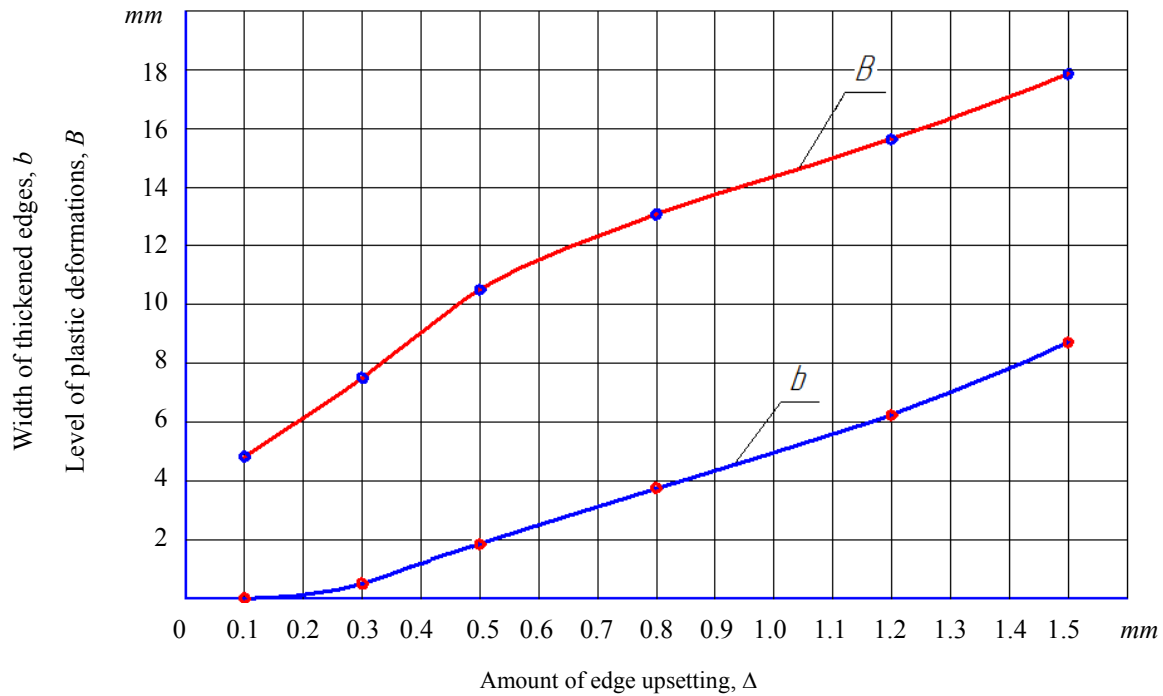


Fig. 4. Width of thickened weld edges b and zone of plastic deformations B , depending on the amount of edge upsetting Δ

It should be noted that at $\Delta \geq 0.5$ the value $(B-b)$ is almost the same and approximately equal to 9.2 mm. With such dimensions, the angle of approach of the weld joint to the base metal ϕ is less than 1 degree. In this regard, the stress concentration coefficient tends to unity.

Thus, it can be argued that weld joints made through FSW along thickened edges will have high resistance to the origin and development of destruction.

To check the adequacy of the edge thickening calculation model using FEM, its consistency with practice was determined. For this purpose, thickened edges were obtained on the above equipment with upsetting of 0.5 and 1.2 mm. Profilograms of thickened edges obtained on a two-dimensional measuring instrument DIP-6 are shown in Fig. 5.

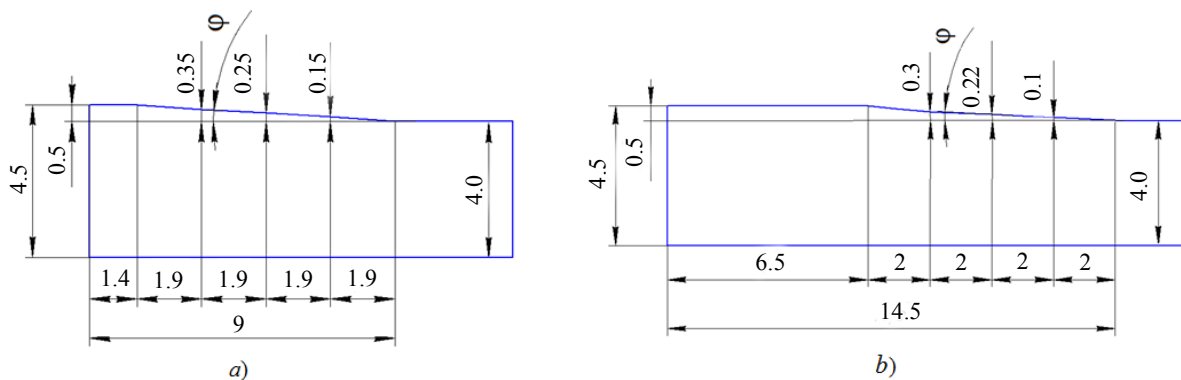


Fig. 5. Geometry of the thickened edges after their upsetting by the value:
a) 0.5 mm; b) 1.2 mm

It can be seen that the dimensions of the thickened edges obtained by calculation using FEM are in good agreement with the experimental data. The discrepancy does not exceed 15 %.

Discussion and Conclusions. The paper proposes a new technology for obtaining thickened edges in the places where welded butt joints are made. A laboratory installation to implement the proposed method has been developed. The main element of this installation is an upsetting roller, which acts on the edges of the welded elements and due to plastic deformation causes thickening of these edges. The dependence of the width of the thickened part on the upsetting of the roller is experimentally investigated. A mathematical model of the deformation process has been developed to select this upsetting for a given thickening width for materials that differ in geometry and mechanical properties. This model is implemented in the finite element package ANSYS. A numerical experiment was carried out for the material and geometry considered in this paper. The results agree with the experimental data and confirm the

proposed model adequacy. Thus, the proposed technology has been validated, which provides reduction of the metal consumption of structures and the strength of joints not lower than the strength of the base metal. The developed computational model of the edge thickening process allows us to find the amount of upsetting of the deforming roller to create the required width of the thickening.

References

1. Frolov VA, Ivanyukhin AN, Sabantsev AN et al. Svarka treniem s peremeshivaniem — plyusy i minusy [Friction stir welding — pros and cons]. Svarochnoe Proizvodstvo. 2008;10:12–19. (In Russ.)
2. Pengfei Yu, ChuanSong Wu, Lei Shi. Analysis and characterization of dynamic recrystallization and grain structure evolution in friction stir welding of aluminum plates. Acta Materialia. 2021;207:116692. <https://doi.org/10.1016/j.actamat.2021.116692>
3. Defalco J. Friction stir welding vs. fusion welding. Welding J. 2006;85(3):42–44.
4. Okamura H, Aota K, Ezumi M. Friction stir welding of aluminum alloy and application to structure. J. of Jap. Institute of Light Metals. 2000;50(4):166–172. <https://doi.org/10.2464/jilm.50.166>
5. Lukyanov VF, Kharchenko VYa, Lyudmirsky YG. Proizvodstvo svarnykh konstruksii (izgotovlenie v zavodskikh usloviyakh) [Production of welded structures (factory fabrication)]. Rostov-on-Don: Terra Print; 2006. 336 p. (In Russ.)
6. Kotlyshev RR, Shuchev LG, Kramskoy AV. Raschet temperatur pri svarke treniem s peremeshivaniem alyuminiyevykh splavov [Temperature calculations in friction stir welding with aluminium alloys]. Vestnik of DSTU. 2010;10(5):693–699. (In Russ.)
7. Kotlyshev RR. Svarka treniem s peremeshivaniem: monografiya [Friction stir welding: monograph]. Rostov-on-Don: DSTU Publ. Centre; 2012. 135 p. (In Russ.)
8. Poklyatskii AG, Ishchenko AYA, Fedorchuk VE. Svarka treniem s peremeshivaniem – ehffektivnyi sposob povysheniya ehkspluatatsionnykh kharakteristik konstruksii [Friction stir welding is an effective way to improve the performance of structures]. Automatic Welding. 2010;4:45–50. (In Russ.)
9. Virendra Pratap Singh, Surendra Kumar Patel, Basil Kuriachen. Mechanical and microstructural properties evolutions of various alloys welded through cooling assisted friction-stir welding: A review. Intermetallics. 2021;133:107122. <https://doi.org/10.1016/j.intermet.2021.107122>
10. Mrinal Sahu, Atanu Paul, Subhas Ganguly. Optimization of process parameters of friction stir welded joints of marine grade AA 5083. Materials Today: Proceedings, 2021. <https://doi.org/10.1016/j.matpr.2021.01.938>
11. Anil Raj, Pratap Kumar Jena, Anil Melwin Rego, et al. Optimization of friction stir welding parameters during joining of AA3103 and AA7075 aluminium alloys using Taguchi method. Materials Today: Proceedings, 2021. <https://doi.org/10.1016/j.matpr.2021.02.246>
12. Xianglai Xu, Xueping Ren, Hongliang Hou, et al. Effects of cryogenic and annealing treatment on microstructure and properties of friction stir welded TA15 joints. Materials Science & Engineering A. 2021;804:140750. <https://doi.org/10.1016/j.msea.2021.140750>
13. Yanying Hu, Yunqiang Zhao, Yongbing Peng, et al. High-strength joint of nuclear-grade FeCrAl alloys achieved by friction stir welding and its strengthening mechanism. Journal of Manufacturing Processes. 2021;65:1–11. <https://doi.org/10.1016/j.jmapro.2021.03.007>
14. Ramamoorthi R, Yuvaraj KP, Gokul C, et al. An investigation of the impact of axial force on friction stir-welded AA5086/AA6063 on microstructure and mechanical properties butt joints. Materials Today: Proceedings. 2021;37(2):3159–3163. <https://doi.org/10.1016/j.matpr.2020.09.050>
15. Sucharitha M, Ravi Sankar B, Umamaheswarrao P. Experimental investigations on the effect of tool rotational speed on mechanical properties and microstructure of friction stir welded AZ31 Mg alloy. Materials Today: Proceedings, 2021. <https://doi.org/10.1016/j.matpr.2020.11.788>
16. Kareem N. Salloomi, Sanaa Al-Sumaidae. Coupled Eulerian-Lagrangian prediction of thermal and residual stress environments in dissimilar friction stir welding of aluminum alloys. Journal of Advanced Joining Processes. 2021;3:100052. <https://doi.org/10.1016/j.jajp.2021.100052>

Received 22.03.2021

Revised 05.04.2021

Accepted 09.04.2021

About the Authors:

Lyudmirsky, Yurii G., professor of the Machines and Welding Fabrication Automation Department, Don State Technical University (1, Gagarin sq., Rostov-on-Don, RF, 344003), Dr.Sci. (Eng.), professor, ORCID: <https://orcid.org/0000-0003-0639-2597>, lyudmirskiy40@mail.ru

Soloviev, Arkadii N., Head of the Theoretical and Applied Mechanics Department, Don State Technical University (1, Gagarin sq., Rostov-on-Don, RF, 344003), Dr.Sci. (Phys.-Math.), professor, ResearcherID: [H-7906-2016](https://orcid.org/0000-0001-8465-5554), ScopusID: [55389991900](https://orcid.org/0000-0001-8465-5554), ORCID: <http://orcid.org/0000-0001-8465-5554>, Solovievarc@gmail.com.

Soltovets, Marat V., associate professor of the Technical Regulation Technology Department, Don State Technical University (1, Gagarin sq., Rostov-on-Don, RF, 344003), Cand.Sci. (Eng.), associate professor.

Kotlyshev, Roman R., Deputy Director, Main certification body for welding production in the Southern Region (2C, Svetlaya St., kh. Kamyshvakha, Rostov Region, RF, 346715), Cand.Sci. (Eng.), kotlyshev@mail.ru

Mironov, Igor V., engineer, “CCBWP SR” Ltd (213, Narodnogo Opolcheniya St., Rostov-on-Don, RF, 344018), mironov_igor_1993@mail.ru

Kramskoy, Aleksandr V., leading welding engineer, Main certification body for welding production in the Southern Region (2C, Svetlaya St., kh. Kamyshvakha, Rostov Region, RF, 346715), Cand.Sci. (Eng.), ORCID: <http://orcid.org/0000-0003-0668-9518>, ingenersvarka@yandex.ru

Claimed contributorship

Y. G. Lyudmirsky: problem statement; development of a laboratory installation scheme; text preparation. A. N. Soloviev: development of a mathematical and computer model; computational analysis; the text revision; correction of the conclusions. M. V. Soltovets: creating a laboratory installation; conducting the experiment. R. R. Kotlyshev: creating a laboratory installation; analysis of the research results. I. V. Mironov: creating a laboratory installation; discussion of the results. A. V. Kramskoy: creating a laboratory installation; discussion of the results.

All authors have read and approved the final manuscript.

MACHINE BUILDING AND MACHINE SCIENCE



UDC 621.876.11

<https://doi.org/10.23947/2687-1653-2021-21-2-171-183>

Improving the maintenance program for passenger elevators based on simulation of their operating modes

D. S. Apryshkin¹, G. Sh. Khazanovich¹, V. O. Gutarevich²¹Don State Technical University (Rostov-on-Don, Russian Federation)²Donetsk National Technical University (Donetsk, Donetsk People's Republic)

Introduction. Elevators in residential and public buildings are the means of vertical transport. An elevator is one of the complex electromechanical devices of increased danger. Therefore, all stages of its life cycle are strictly limited by regulatory documents. The desired levels of safety and comfort are provided through the reasonable choice of the basic parameters and a constant maintenance of the system in good condition. The key factors that affect the implementation of regulatory requirements during the operation of the elevator installation are the quality of manufacturing of critical components, the level of real workload, taking into account the actual value of the spent resource, and the implemented maintenance program. Currently, when determining the maintenance schedule for elevators, such characteristics as the density of occupancy, the level of power loads, the actual operating time of the elevator and the counts of starts of the main drive are not taken into account. This study objective is the scientific rationale of the concept and methodology for developing the program of maintenance of specific elevator installations on the basis of studies of the level and mode of loading of load-bearing units.

Materials and Methods. The use of simulation modeling techniques to assess the load level of power units of an elevator installation and its kinematic indicators under the action of numerous random impacts is validated in the paper. The development of an indicator that characterizes the complex mode of elevator operation, taking into account the joint influence of the level of resource development, net operating time, number of starts, and the power load of the nodes, required the application of an expert method. The final part of the research program is the formation of specific recommendations on the maintenance schedule of elevators. It is based on the ranking of particular indicators.

Results. The performance feature of the elevator installation is that the service time of a customer is a function of many random variables. Mathematical models of the formation of force impacts are based on the representation of an electromechanical elevator as a dynamic one-degree-of-freedom system. Expressions for calculating the static tension of traction ropes and torques on the motor shaft are obtained. The problem of dynamics is solved. The loads whose values are the basis for performing simulation modeling of the operating modes of the elevator installation are determined.

Discussion and Conclusions. Feasibility of the regulations for the maintenance of passenger elevators is an urgent task, the solution to which determines the level of safety and comfort of passengers. Currently, the standards for the design and operation of elevator installations do not link the frequency of maintenance programs with the level of load and the amount of resource development. The paper provides a general statement of the problem and a methodology for the formation of a complex factor of the equivalent load. Mathematical models are given for calculating the power and temporary loads of the elevator, taking into account the nature of numerous random impacts.

Keywords: passenger elevator, random impacts, mathematical models of functioning, dynamic loads, power loading mode, distribution of random factors, kinematic indicators, simulation, complex load factor, maintenance program.

For citation: D. S. Apryshkin, G. Sh. Khazanovich, V. O. Gutarevich. Improving the maintenance program for passenger elevators based on simulation of their operating modes. Advanced Engineering Research, 2021, vol. 21, no. 2, pp. 171–183. <https://doi.org/10.23947/2687-1653-2021-21-2-171-183>

© Apryshkin D. S., Khazanovich G. Sh., Gutarevich V. O., 2021



Introduction. According to the main regulatory document¹, an elevator is a device designed to move people and (or) cargo from one level to another in a cabin moving along rigid guides, whose angle of inclination to the vertical is no more than 15°. The elevator is a unique public transport vehicle. It is operated by the passenger or by personnel who do not require high qualifications [1]. Therefore, the elevator must meet all the requirements of safety and comfort when transporting passengers. The elevator is one of the complex electromechanical devices of increased danger [2]. The design, manufacture, installation and maintenance of elevators during operation are subject to strict requirements formulated in the Technical Regulations and other regulatory documents. Depending on the type of drive, there are electromechanical and hydraulic elevators [3]. In electromechanical elevators, a drive consisting of an electric motor, a gearbox and a traction sheave, is used as a lifting mechanism (Fig. 1), and in hydraulic elevators — a linear hydraulic drive.

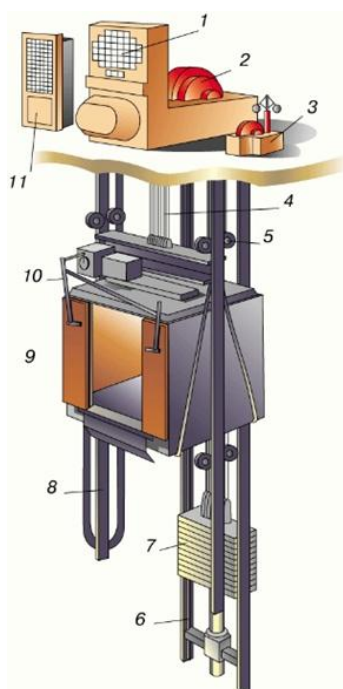


Fig. 1. Elevator design with electromechanical drive: 1 — electric motor; 2 — winch; 3 — speed limiter; 4 — traction ropes; 5 — guide rollers of the cabin; 6 — counterweight guides; 7 — counterweight; 8 — cab guides; 9 — cabin; 10 — door mechanism; 11 — control panel

The most widespread in modern multistorey buildings are electromechanical driven elevators [4]. In this paper, the subject of research is an elevator with geared electromechanical drive.

According to the information of the National Elevator Union, at the end of 2020, there were more than 500 thousand elevators in the Russian Federation operated in the housing stock and various institutions². About 160 thousand of them have worked out the established standard period, but continue to operate. The number of new multistorey buildings across the country is increasing every year, which causes an increase in the fund of elevator equipment.

¹Technical regulations of the Customs Union. Elevator safety. Decision of the Customs Union Commission No. 824 of 18.10.2011 (ed. of 19.12.2019) "On the adoption of the Technical Regulations of the Customs Union "Elevator Safety". URL: <https://docs.cntd.ru/document/902307835/> (accessed: 11.06.2021). (In Russ.)

² Data of the National Elevator Union of the Russian Federation. URL: <http://www.lift.ru/index.php/ru/ebiblio.html/> (accessed: 11.05.2021). (In Russ.)

The most important requirements for elevator equipment are the safety and comfort of passengers, which can be ensured due to the correct selection of parameters of the vertical transport installation and the constant maintenance of the elevator in good condition [4–5].

The following groups of factors have the main influence on the elevator safety indicator:

- quality of manufacturing of elevator equipment;
- load level of the load-bearing elements and its used resource amount;
- ongoing maintenance program.

Safety of the elevator³ is characterized by generally accepted indicators: MTBF, probability of failure-free operation, availability factor.

The indicator “transport comfort” is introduced by the national standard⁴. It characterizes the lift interval, expressed as the time period between two consecutive departures of the elevator cab in a given direction on the main landing floor, where people entering the building have access to the elevators. Thus, the level of comfort is the conditional waiting time the passenger waits for the next flight. Note that the indicator of transport comfort is a random variable, and, naturally, in real conditions, it changes from the minimum to the maximum value. The most representative value of the comfort indicator may be the average value in different periods of daily operation.

Let us turn to the elevator maintenance programs. The elevator equipment servicing is established based on two main documents: the equipment technical passport and the “Rules...”⁵. The frequency is assumed to be the same for all elevator facilities.

In recent years, a number of fundamental studies have been carried out in Russia [4–6]^{6,7,8} and abroad [7–10], related to the reliability and safety of elevator equipment. It should be noted that in the considered works, when determining the maintenance intervals of elevators, such parameters as the density of the population of floors and apartments, as well as the level of power loads, the actual operating time of the elevator, the number of starts of the main drive per unit of time, are not taken into account.

Despite the same number of floors, the same type and number of elevators, similar buildings can significantly differ in the number of residents, as well as in the degree of operation of elevator equipment. This has a significant impact on the net operating time, the equivalent loads experienced by the elevator equipment, which changes the real rate of resource development, the service life of each set of elevator equipment. At the same time, their planned assigned lifespan will be the same.

It is important to note that currently, the normative^{3,4,5} and literary domestic [6]^{6,7,8} and foreign [7–10] sources lack a definition and recommendations for the application of criteria for the loading of elevators. There are also no analytical and engineering methods for designing elevator maintenance programs in the development of research, design and operating organizations. Lack of a methodological base for the design of the elevator maintenance system and program leads in some cases to an excess of the required amount of repair impacts with a simultaneous increase in costs, in others — to an unjustified increase in the repair interval. This affects the reduction of reliability indicators and, in general, safety during the operation of elevator installations.

To maintain the level of safety and comfort of elevator installations with the required and sufficient level of repair impacts, this study provides for research in the following areas:

- use of simulation modeling to establish real equivalent loads and operating modes;

³ National standard of the Russian Federation. Lifts. General safety requirements in service: GOST R 55964-2014. Federal Agency for Technical Regulation and Metrology. Moscow: Standartinform; 2019. 16 p. (In Russ.)

⁴ National standard of the Russian Federation. Passenger lifts. Planning and selection for residential buildings: GOST R 52941-2008. Federal Agency for Technical Regulation and Metrology. Moscow: Standartinform; 2008. 15 p. (In Russ.)

⁵ Regulations for safe use and maintenance of elevators, lifting platforms for the disabled, passenger conveyors (moving pedestrian paths) and escalators, with the exception of escalators in subways. Decree of the Government of the Russian Federation No. 743 of June 24, 2017. URL: <https://docs.cntd.ru/document/436745439#/reg/> (accessed: 11.06.2021). (In Russ.)

⁶ Mechiev AV. Development of ways to ensure safe operation of elevators: Cand.Sci. (Eng.), diss., author’s abstract. Moscow, 2018. 18 p. (In Russ.)

⁷ Gorozheev MYu. Development and research of a device for express diagnostics of elevators during operation: Cand.Sci. (Eng.), diss., author’s abstract. Moscow, 2013. 25 p. (In Russ.)

⁸ Fedyaev RV. Methods of improving the reliability of elevators and lifts: Cand.Sci. (Eng.), diss., author’s abstract. Tomsk, 2013. 23 p. (In Russ.)

- justification of a complex indicator, which helps to form an assessment of the load level of the power elements of the elevator;
- development of recommendations on the maintenance intervals of elevators in both already operated and designed buildings.

This will provide for the control of the correctness of the design decisions made (primarily, according to the parameters of the main drive), and, due to the effective organization of maintenance, the reduction in the likelihood of equipment failures.

It should be noted that when modeling elevator installations in operation, it is possible to use kinematic parameters of the mode obtained as a result of observations of dispatch services: net machine time and specific number of starts [11]. For these elevators, it is crucial to obtain data on power loads as a result of modeling.

Under a complex modeling of the operating modes of the designed elevators, it is required to solve the problem of selecting their key parameters beforehand.

The research objective is to scientifically substantiate the concept and methodology for developing a maintenance program for specific elevator installations based on studies of the level and loading mode of the main load-bearing units during a given or predicted period of operation.

Materials and Methods. Continual problem setting. In accordance with the general concept of the problem solving and to achieve the objective of this study, the structure of tasks and methodological support for each direction are determined. First of all, it is planned to describe the modeling object as a queuing system operating in a cyclic mode and subjected to random external actions. It is required to study a set of random factors affecting the main drive of the elevator installation beforehand.

Simulation modeling is recognized as an effective methodological technique for studying the patterns of work processes under the conditions of random actions. To implement the modeling procedures, it is required to validate mathematical models of the formation of force effects on the elevator installation drive, and models of the formation of random action distributions. The main influencing random factors include the number of passengers in the cabin of a random flight, the numbers of the floors of standing, calling and destination, the number of stops during the cycle, the duration of net machine time, and the total cycle duration.

It is planned to develop algorithms and programs for simulating the impact of the key factors on the equivalent load value and kinematic characteristics of the operating mode of the elevator drive on the basis of one of the modern programming languages.

It is required to assess the adequacy and analyze the results of simulation and power modeling to build generalized dependences of the impact of the key factors on the operating parameters of elevator installations.

For the first time, it is planned to form conceptual approaches to the development of maintenance programs for elevator equipment in connection with the real modes of its loading and the subsequent development of an engineering methodology for the formation of the maintenance regulations for an elevator installation.

The paper gives the results of presenting an elevator as a queuing system, the selection of the equivalent load indicator, the model of the formation of force effects on the main drive shaft. Other stages and results of modeling of kinematic indicators and power modes will be described in the next issues of the journal.

Research Results. Elevator as a queuing system. For an adequate mathematical description of the functioning of a passenger elevator in a multistorey building, it is required to accept some obvious conditions that determine its basic properties. Each elevator installation is characterized by passport parameters that determine the working conditions and its capabilities:

- number of floors of the house, N ;
- maximum load capacity, expressed by the weight of the lifted cargo Q , kg, or the number of passengers, R ;
- steady-state speed of the cab (and counterweight), v , m/s.

First, it should be accepted that the operation of the elevator installation when moving passengers is carried out in separate cycles. Each i -th cycle consists of separate stages: the appearance of users, their random number r , on a random floor M and the call of the elevator; at the end of the previous cycle, the elevator cab is on a random floor L ; the

cab moves at $Q=0$ during the call period from floor L to floor M ; boarding r passengers on floor M and moving to a random destination floor S , $1 \leq r \leq R$; during movement on the section $M \rightarrow S$, there may be intermediate stops random by number Y and location in the building for pick-up and drop-off of individual passengers; passenger drop-off on the destination floor S ; at the end of the cab movement in the i -th cycle, there is a pause of random duration Δ_i — waiting for the next cycle.

It follows from the description that the elevator can be presented as an original single-or multi-channel queuing system (QS) [12], operating in the mode of exposure to a number of random factors — M, L, S, r, Y, Δ . A distinctive feature of the elevator QS is that the duration of the request service from the moment of the call to the passenger's delivery to the final floor of the destination S is a function of many random variables. Each of the random variables (M, L, S, r) are independent. The distribution functions of these quantities can be established either experimentally or on the basis of logical analysis. A separate problem is solved to establish a random variable — number of intermediate stops Y [13,14]. The well-known classical solution can only be used to describe the random waiting time for the next cycle Δ .

In QS theory, it is proved that, if

- a) probability of arrival of another application $p_n(t)$ depends only on the time interval between applications t ,
- b) two events never happen at the same time,
- c) probability that at least one event will occur in a very small-time interval Δt , selected at any moment, then

probability $p_n(t)$ is expressed by the Poisson law [12]:

$$p_n(t) = \frac{(\lambda t)^n e^{-\lambda t}}{n!}.$$

The distribution of the time interval between two consecutive random events T obeys an exponential law, i.e.

$$P(T > \tau) = e^{-\lambda \tau},$$

where the average value of the random variable T is

$$\tau_{cp} = 1/\lambda.$$

Thus, to simulate a flow of applications received at the entrance of a single elevator, we can adopt an exponential distribution law of interval Δ . At the same time, it is required to establish the average waiting time for the next Δ_{cp} application on the basis of experimental observations or regulatory data. The solution to this problem, as well as the justification of the distribution functions of random variables M, L, S, r, Y are given in papers [13, 15].

The selection of the indicator of the equivalent load of the elevator is an independent task. First, it is required to determine the criterion that this indicator should meet. This criterion should be interconnected with the conditions for assigning or changing the frequency of maintenance of the main units of the elevator installation. The basic condition is the accumulated consumption of the unit resource in comparison to its normative value. It is obvious that the resource consumption of a unit or part is determined by two factors: time and power, i.e., the equivalent load indicator should take into account the load distribution during operation so that with an increase in the duration of operation and the magnitude of the perceived loads, the equivalent indicator increases. It is proposed, by analogy with the assessment of the load of an electric motor during long-term operation with a high frequency of starts, to take the standard load for the entire inter-repair period of operation of the elevator⁹ as an indicator of the equivalent load $M_{\text{эКВ}}$ with its correction through introducing the relative frequency of starts into the calculation.

Taking into account the above arguments, the proposed mathematical model for calculating the equivalent load of the power elements of the elevator will have the form:

$$M_{\text{эКВ}} = K(V_{RT}) \cdot \sum_{i=1}^C \left(\sqrt{\frac{\int_0^{t_{Bi}} M_{Bi}^2(t) dt + \int_0^{t_{ПД,i}} M_{ПД,i}^2(t) dt}{\tau_i}} \right),$$

where $M_{Bi}(t)$, $M_{ПД,i}(t)$ — accordingly, the moments on the engine shaft (or in another link of the elevator transmission) in the function of time t in the total periods of the elevator call t_{Bi} of the movement $t_{ПД,i}$ of the elevator cab with passengers;

⁹ Epifanov AP. Fundamentals of electric drive. St. Petersburg: Lan'; 2009. 192 p. (In Russ.).

τ_i — the duration of the full i -th cycle of the installation, including the duration of the cab movement when calling, with passengers, braking, pauses for pick-up and drop-off of passengers, as well as waiting for the next application to use the elevator, s;

C — the total number of cycles for a given period of time T ;

V_{RT} — frequency of the elevator activation cycles for the calculation period T , i.e., the number of cycles per unit of time, 1/hour or 1/day:

$$V_{RT} = \frac{C}{T} = \frac{C_1}{\sum_{i=1}^C \tau_i};$$

$K(V_{RT})$ — correction factor that takes into account the frequency of switching on the elevator; coefficient variation limits $K(V_{RT})_{\min} \leq K(V_{RT}) \leq 1$ are established by experts.

At drive switching frequencies close to the standard ones, $K(V_{RT}) = 1$. With an increase in the switching frequency V_{RT} , the equivalent load increases due to an increase in coefficient $K(V_{RT})$;

C_1 — the number of starts of the main drive for the estimated time T , i.e., during the periods of calling the elevator, movement with passengers and intermediate stops.

It is appropriate to identify repetitive bulk modes, which will mainly determine the equivalent load over the observation period. At this stage of research, it is proposed to divide the daily period of elevator operation on working days into four-time segments [10].

Rationale for mathematical models of the formation of force actions on the elevator installation drive.

Load M during the execution of the elevator operation cycle at a certain time interval τ_i can be presented by random graphs $M(t)$ for the stages of calling and moving with passengers (Fig. 2).

As previously shown, during the same time interval between maintenance, the elevator can perform a different number of operating cycles, which, in turn, will have different characteristics in terms of duration τ_i and the magnitude of loads $M_{экр}$, taken by the engine and other elements of the elevator.

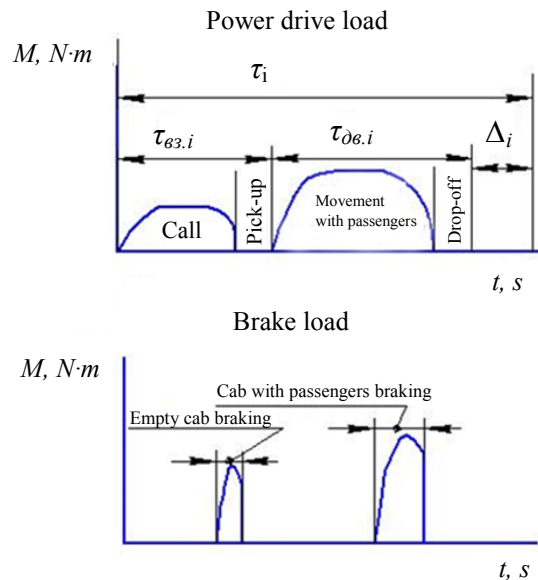


Fig. 2. Elevator operation cycle: τ_i — cycle time; $\tau_{вз.и}$ — call time; $\tau_{дв.и}$ — time of movement with passengers; Δ_i — time after which the application for the use of the elevator is received

after the end of the cycle The duration of the application execution, the amount of load on the drive and power equipment of the elevator will be affected by random variables: $M_i=1, 2 \dots N$; $L_i=1, 2, \dots N$; $S_i=1, 2, \dots, N$, where N — the number of floors of the house; the relative level of loading of the elevator by load capacity; $\gamma=Q_i/Q_{пасп}$, $\gamma_{\min} < \gamma < \gamma_{\max}$, where $Q_{пасп}$ — the nominal (passport) load capacity; the waiting time interval Δ_i .

To find the dependence of the loads on the power units of the elevator on time when exposed to the listed random variables, we will focus on determining the loads that the power parts of the elevator equipment undergo.

Traction ropes (force S_{k1}) and counterweight ropes (force S_{n1}) at any time undergo static loads at the points of run-on and run-off from the traction sheave (TSh), which correspond to the design scheme and are determined from the formulas (Fig. 3):

— when lifting and lowering the cab

$$S_{k1} = \frac{(Q_i + Q_k) \cdot g \pm (F_k + F_r)}{\eta_0^2} + n \cdot q_{TK} \cdot (H - \Delta h_i) \cdot g; \quad (1)$$

— when lifting and lowering the counterweight

$$S_{n1} = [Q_n \cdot g \pm F_n] \cdot \eta_0 + n \cdot q_{TK} \cdot \Delta h_i \cdot g. \quad (2)$$

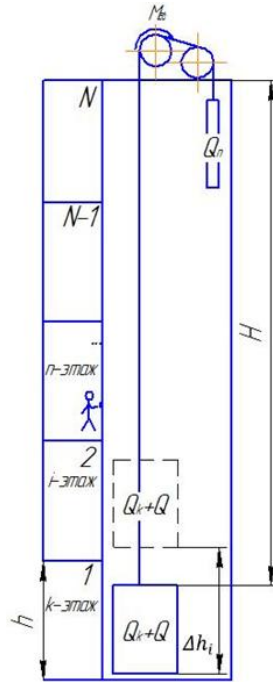


Fig. 3. Scheme for the calculation of forces in traction ropes

The sign “plus” — when the cab or counterweight moves up, “minus” — when the cab or counterweight moves down. The formulas indicate: Q_i — weight of the cargo in the i -th cycle, kg; Q_k — weight of the cab, kg; Q_n — counterweight, kg; F_k — resistance force to the cab movement, N; F_r — resistance force to the movement of the cargo, N; F_n — counterweight movement resistance, N; η_0 — efficiency of the rope system unit; n — the number of traction ropes; q_{TK} — bulk mass of the traction rope, kg/m; Δh_i — the distance between the levels of the first floor and the location of the cab with passengers at a given time (Fig. 3).

As can be seen from formulas (1) and (2), the tension of the branches of the traction ropes and the counterweight ropes at the points of run-in and run-off from the TSh depends directly on the following factors:

- the direction of cab movement and, accordingly, 0 counterweight;
- distance Δh_i , which determines the random location and movement of the cab. In turn, the change of Δh_i occurs depending on the random combination of floor numbers M_i , L_i , S_i in this cycle;
- random value of the mass of the transported passengers Q_i .

In addition to static loads acting on the elevator ropes and transmitted to its drive elements during periods of stationary state and steady motion (TSh, gearbox, engine, braking device), the system also undergoes dynamic loads during periods of unsteady movements during starts, braking, etc.

A typical circuit of the elevator drive and transmission is shown in Fig. 4. In this case, the scheme of the gear drive is considered. Nowadays, gearless drive systems with a motor that has a frequency control to change the speed are spreading. These systems require a separate study that goes beyond the scope of this work.

We will consider the set of kinematically connected elements “engine — gearbox — TSh — ropes — cab — counterweight” as a one-degree-of-freedom system. Under real conditions, the cab and the counterweight suspended on

the ropes can perform, in addition to general kinematically coordinated movements together with all the elements, additional oscillatory movements and cause corresponding loads in the ropes and other elements connected to them.

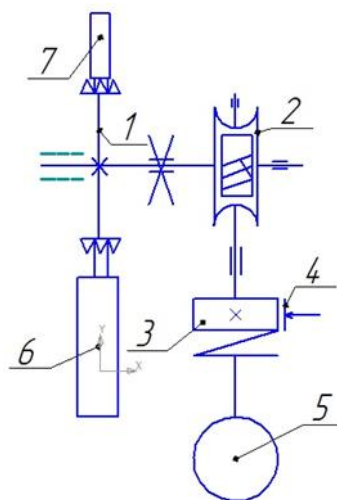


Fig. 4. Calculation kinematic diagram of an elevator with a gear transmission:
1 — TSh; 2 — worm gear; 3 — coupling with a brake pulley; 4 — shoe brake;
5 — electric motor; 6 — cab; 7 — counterweight

To solve such a problem, it is required to present the elevator drive system in at least a three-mass formulation. It should be noted that low-frequency vibrations of the cab during the movement of passengers significantly worsen the level of comfort, therefore, design solutions are provided that exclude the occurrence of oscillatory processes.

In the future, we will consider a set of interrelated parts as a reduced one-mass system¹⁰. The reduction center is the axis of rotation of the electric motor. As can be seen in the diagram shown in Fig. 4, the loads from the gravity forces of the cab and the counterweight are not applied directly to the electric motor, but are transmitted through a number of intermediate elements. Thus, it is possible to write the well-known equation of the dynamics of the electric drive⁷ for the elevator drive.

$$J_{np} \cdot \frac{d\omega}{dt} = M_{dB} - \Sigma M_c, \quad (3)$$

where J_{np} — the moment of inertia of the system “motor–gearbox–drive pulley–ropes–cab–counterweight” reduced to the motor shaft, $\text{kg} \cdot \text{m}^2$;

$M_{dB}(\omega)$ — the torque developed by the engine as a function of the angular velocity, $\text{N} \cdot \text{m}$, this ratio is determined by the mechanical characteristic of the engine;

ΣM_c — the sum of the moments of resistance reduced to the motor shaft from the cab movement, counterweight, ropes and transmission losses, $\text{N} \cdot \text{m}$.

In general,

$$\Sigma M_c = \Sigma_1^2 S_i \cdot r_k / i_{ped}, \quad \text{где} \quad (4)$$

S_i — force in the rope at the points of run-on and run-off from TSh, N , determined from formulas (1) and (2). In these formulas, r_k — radius of the traction sheave, m ; i_{ped} — gear ratio; ω — angular velocity of the motor, $1/\text{s}$; t — current time, s .

From formulas (1), (2), (3) and (4), it follows that the instantaneous value of the total moment M_{dBi} depends on the moment of inertia of the system J_{npi} reduced to the motor shaft, forces in the rope branches S_{n1} and S_{k1} , which, in turn, are determined by a combination of the random variables M , L , S and γ presented earlier.

Along with that, in accordance with the work objective, it is required to establish the influence of all the components of the loads and the mode of their formation as a whole on the elevator servicing intervals. Do this requires determining the so-called representative equivalent load on the elevator, for example, torque M_{9KB} , which will be the value that affects the maintenance program, primarily the frequency of maintenance. The conditional axis in the elevator drive system, relative to which M_{9KB} , is calculated, does not matter in principle, because with the help of known

¹⁰ Epifanov AP. Fundamentals of electric drive. St. Petersburg: Lan'; 2009. 192 p. (In Russ.)

reduction methods, the equivalent load can be recalculated to an arbitrary point. In this work, the main engine shaft is selected as the reduction point.

Elevator motor shaft torque as a function of time $M_{\partial,i}=f(t)$ at every single stage of movement — when calling or moving with passengers — is determined as a result of solving the differential equation (3).

The given moment of inertia of the system J_{npi} will be considered during this i -th cycle as a constant value equal to the sum of the moments of inertia of rotating and translationally moving masses: engine rotor $J_{дв}$, the gearbox including TSh, the cab with the load, the counterweight and the rope branches. Using the well-known rule of reduction of masses and moments of inertia, we obtain a ratio for calculating the reduced moment of inertia of the system in the i -th cycle of the elevator operation:

$$J_{npi} = J_{дв} K_{bp} + [Q_k + Q_n + Q_{пасп} \cdot \gamma_i + q_k \cdot n_k \cdot (N - 1) \cdot h_{эТ}] \frac{r^2}{i_p^2},$$

where K_{bp} — coefficient that considers the rotating masses of the gearbox and TSh;

$Q_{пасп}$ — passport lifting capacity of the elevator, kg;

The sum of the moments of resistance $\sum M_c$, given to the motor shaft, when lifting the cab

$$\sum M_c = (r_k / i_{ред}) (S_{k1} - S_{n1}) \frac{1}{\eta_{ред}} \quad (5)$$

when lowering the cab:

$$\sum M_c = (r_k / i_{ред}) (S_{n1} - S_{k1}) \eta_{ред}. \quad (6)$$

To calculate the sum of the moments on the motor shaft, values S_{k1} and S_{n1} must be substituted from formulas (1) and (2), taking into account the sign rule. Along with that, for the case of lifting the cabin with passengers — according to the formula (5), the sum of the moments will be positive, for the descent of goods (6) — negative. When lifting the cab, in formula (5), values S_{k1} and S_{n1} should be substituted in the following form:

$$S_{k1} = \frac{(Q_i + Q_k) \cdot g + (F_k + F_r)}{\eta_6^2} + n \cdot q_{TK} \cdot (H - \Delta h) \cdot g; S_{n1} = [Q_n \cdot g - F_n] \cdot \eta_6 + n \cdot q_{TK} \cdot \Delta h \cdot g.$$

When descending the cab, values S_{n1} and S_{k1} should be substituted in formula (6) in the following form:

$$S_{n1} = [Q_n \cdot g + F_n] \cdot \eta_6 + n \cdot q_{TK} \cdot \Delta h \cdot g, 0.$$

$$S_{k1} = \frac{(Q_i + Q_k) \cdot g - (F_k + F_r)}{\eta_6^2} + n \cdot q_{TK} \cdot (H - \Delta h) \cdot g.$$

In the latter case, the sum of the resistance moments $\sum M_c$, calculated from formula (6), will be negative, since $S_{k1} > S_{n1}$. When solving differential equation (3), it should be taken into account that the torque developed by the engine during start-up and after the end of start-up, $M_{дв} < 0$.

When solving differential equation (3), it is required to set the initial and final conditions. The initial conditions for all modes of movement with or without a load are the same: for $t=0$, $\varphi=0$, $\omega=0$. As a result of solving the equation, we obtain a change in the moment on the engine shaft $M_{дв}$, the movement of the cab h (m), the angular velocity ω (rad/s) from time. Let us consider the solution to equation (5) to obtain time functions $M_{дв}$, h , t , ω .

The engine parameters and its mechanical characteristic $M_{\partial\omega}(\omega)$ are presented graphically in Fig. 5.

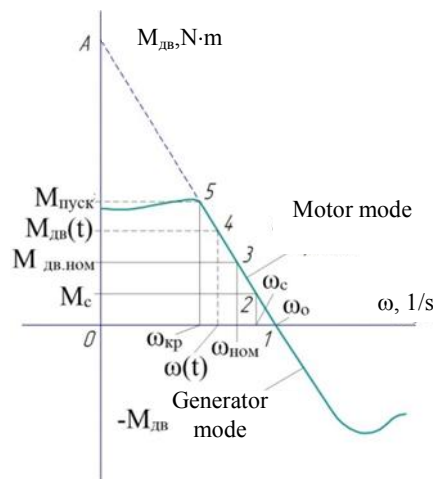


Fig. 5. Mechanical characteristic of an asynchronous squirrel-cage motor:

- 1 — ideal idle speed (synchronous angular velocity); 2 — corresponds to static load ($\sum M_c$) in motor mode;
- 3 — to engine load rating; 4 — to engine current state; 5 — to starting (critical) mode of operation

The process of movement in each cycle (with or without passengers, up or down) generally includes four stages (Fig. 6):

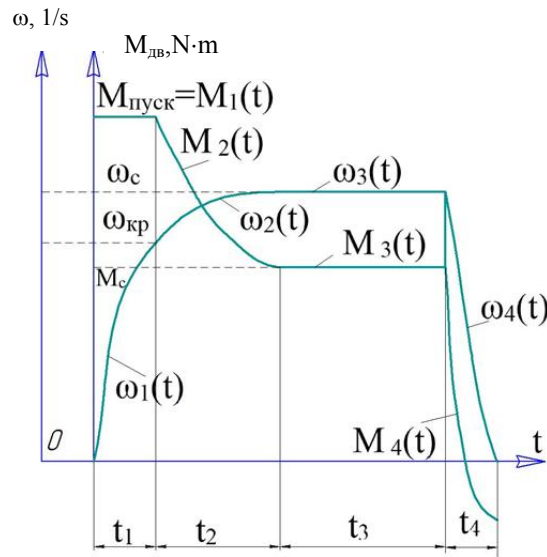


Fig. 6. Qualitative picture of change in angular velocity $\omega(t)$ and torque on the motor shaft $M_{\delta}(t)$ over the periods of the elevator movement

It is necessary to separately consider the solution to the equation when lifting the cab $\sum M_c > 0$ (motor mode) and lowering the cab $\sum M_c < 0$ (generator mode).

Motor mode. At the first stage, the torque developed by the engine is equal to the starting one, $M_{\text{пуск}}$. Its value is maintained throughout the first period $M_{\delta}(\omega) = M_{\text{пуск}}$. Equation (3) takes the form:

$$J_{\text{пр1}} \cdot \frac{d\omega}{dt} = M_{\text{пуск}} - \sum M_{c1}.$$

Solving the differential equation, after the transformations, we get expressions for calculating the engine torque, the time of each stage, and the path traveled by the cab. For the first stage:

$$\begin{aligned} M_{\delta B1}(t) &= M_{\text{пуск}}, \\ t_1 &= \frac{J_{\text{пр1}} \omega_0^2 (1 - S_{\text{кр}})^2 (1 - S_{\text{ном}})}{1000 N_{\delta B} (\lambda_{\text{пуск}} - \lambda_c)}, \\ h_1 &= \frac{J_{\text{пр1}} \cdot \omega_0^3 \cdot (1 - S_{\text{кр}})^2 \cdot (1 - S_{\text{ном}}) \cdot r}{2000 \cdot N \cdot (\lambda_{\text{пуск}} - \lambda_c) \cdot i_{\text{ред}}}. \end{aligned}$$

At the second stage, the start-up continues from angular velocity $\omega_{\text{кр}}$ to angular velocity ω_c , corresponding to the moment of static load $\sum M_c$, i.e., on the segment $\omega_c \leq \omega \leq \omega_{\text{кр}}$ (Fig. 5 and 6). The movement occurs on the working section of the engine characteristic. The results of the solution and transformations on section 2:

$$\begin{aligned} M_{\delta B2} &= M_{\delta B}(\omega_{\text{кр}}) = \frac{M_{\text{ном}}}{S_{\text{ном}}} \left(1 - \frac{\omega_{\text{кр}}}{\omega_{\text{ном}}} \right), \\ t_2 &= \frac{J_{\text{пр}} \cdot \omega_0^2}{1000 N} S_{\text{ном}} \ln \left[20 \left(\frac{\lambda_{\text{пуск}}}{\lambda_c} - 1 \right) \right]; \\ h_2 &= \frac{\omega_{\text{кр}} \cdot r_k}{2 i_{\text{ред}}} t_2, \end{aligned}$$

where $\omega_{\text{кр}} = \frac{\omega_0}{2} (2 - S_{\text{кр}} - \lambda_c S_{\text{ном}})$, $\lambda_{\text{пуск}}$, λ_c – accordingly, the ratio of the starting torque of the engine, the static torque of the resistance to the nominal.

At the end of the second stage, the engine switches to the steady-state mode, the cab speed is determined from the formula:

$$v_2 = \frac{\omega_0 \cdot r_k}{i_{\text{ред}}} (1 - \lambda_c S_{\text{ном}}). \quad (7)$$

At the third stage, the system moves at a steady speed, which is determined from formula (7). To calculate the path of the third stage h_3 it is necessary to: calculate the height of the cab lifting (lowering) when calling or moving with passengers as the difference between the levels of floors $(L-M)h$ or $(M-S)h$, where h – is the interfloor height;

determine the sum of the distances that the elevator passed at the first and second stages: h_1+h_2 ; calculate the path of the third stage: $h_3=(L-M)h-(h_1+h_2)$.

Thus, all the required relations for the power simulation of the elevator operation in the motor mode are obtained.

In the generator mode, when the cab with a load is lowering, $M_c < 0$, the acceleration duration can be neglected. The system “motor – gearbox – TSh – ropes – cab –counterweight” switches to the generator mode in a short time, the engine creates a braking torque, rotating at super-synchronous speed. The descent speed is determined by the mechanical characteristic when substituted $M_{дв} = -M_c$ (Fig. 5):

$$v_{ггн} = \frac{\omega_0 \cdot r_k}{i_{ред}} \left(\frac{M_c}{M_{ном}} S_{ном} + 1 \right).$$

When calculating $M_c < 0$ in formula (6) it is required to enter the efficiency of the gearbox into the numerator. Knowing $v_{ггн}$, we can find, by analogy with the previous one, height $h_{ггн}$ and the duration of cab lowering to height $Kh_{ггн}$, where K — the number of interfloor spans traveled by the elevator.

The simulation of the power modes of the elevator was performed according to the program¹¹. Figure 7 shows fragments of the results of modeling equivalent loads. The graphs show that the torque on the main engine shaft increases proportionally to the square of the number of floors of the house and depends significantly on the observation time.

Discussion. The issues of justification of the regulations for the maintenance of passenger elevator installations remain highly relevant. The essence of the problem is that the maintenance programs recommended in regulatory documents and used in practice do not take into account the actual loading modes of the main nodes in magnitude and in time. To reproduce the real modes of elevator installations operating under the impact of numerous random actions, the need and feasibility of simulation is proved.

The peculiarity of the obtained research results in comparison to the known normative and literary data is that the selection of a specific elevator is associated with correlation relations with the operating characteristics and the residual resource of the installation.

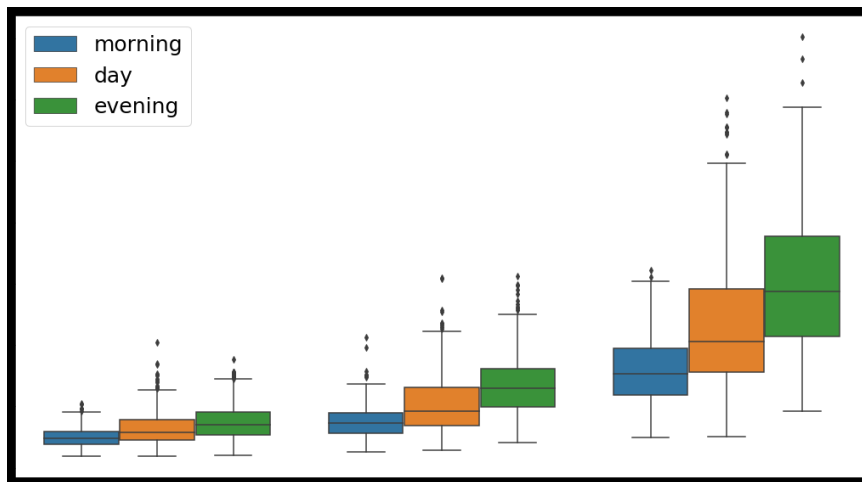


Fig. 7. Dependences of equivalent moment on the elevator engine shaft on the number of floors of a residential building (9, 16, 22 floors) and time interval of observations: morning, day, evening

Conclusion. As a result of the research, a complex indicator of the elevator load is proposed, taking into account the net operating time, the value of the equivalent load, the specific number of starts, and the degree of resource development. In accordance with the indicator value, the maintenance schedule is determined. Mathematical workflow models, including random impact distribution functions, have been developed, providing simulation modeling of elevator operating modes considering the random nature of influencing factors. The relations for calculating the static

¹¹ Otrikov AV, Khazanovich GSh, Apryshkin DS. Simulation of the passenger elevator operation: Certificate of software State registration no. RU 2018664988. Copyright holder: DSTU. 2018. (In Russ.)

and dynamic forces of the elevator drive are described in detail. Basic relations of the impact of the elevator parameters and operating conditions on the power and kinematic parameters of the elevator installation are obtained.

References

1. Sergey Lupin, Than Shein, Kyaw Kyaw Lin, et al. Testing of transport system management strategy. In: Proc. IEEE East-West Design & Test Symposium (EWDTS 2014). <https://orcid.org/10.1109/EWDTS.2014.7027050>
2. Antonevich AI. Analiz sovremennykh konstrukttsii liftov i tendentsii ikh razvitiya [Analysis of modern elevator designs and tendencies of their development]. Vestnik BNTU. 2010;5:18–35. URL: <http://rep.bntu.by/handle/data/1408> (accessed: 21.06.2021). (In Russ.)
3. Yimin D. Permanent Magnet Synchronization Gearless Drive. Elevator World, 2004. P. 108–115.
4. Manukhin SB, Nelidov IK. Ustroistvo, tekhnicheskoe obsluzhivanie i remont liftov [Device, maintenance and repair of elevators]. Moscow: Akademiya; 2004. 336 p. (In Russ.)
5. Shpet NA, Muravyov OP. Issledovanie otkazov passazhirskikh liftov po dannym ehkspluatatsii [Investigation of passenger elevator failures according to operational data]. Bulletin of the TPU Geo Assets Engineering. 2013;323(4):123–125. (In Russ.)
6. Cevat Erdem Imrak, Mustafa Ozkirim. Profilakticheskoe tekhnicheskoe obsluzhivanie liftov [Preventive maintenance of elevators]. Elevator. 2006;4:32–36. (In Russ.)
7. Hongjiu Liu, Jiaxuan Wu. Research on Preventive Maintenance Strategy of Elevator Equipment. Open Journal of Social Sciences. 2018;6(1):165–174. <https://orcid.org/10.4236/jss.2018.61012>
8. Jae-Hak Lim, Dong Ho Park. Optimal Periodic Preventive Maintenance Schedules with Improvement Factors Depending on Number of Preventive Maintenances. Asia Pacific Journal of Operational Research. 2007;24(1):111–124. <https://orcid.org/10.1142/S0217595907001139>
9. Torgny Almgren, Niclas Andréasson, Myrna Palmgren. Optimization Models for Improving Periodic Maintenance Schedules by Utilizing Opportunities. In: Proc. World Conference on Production and Operation Management. Amsterdam, the Netherlands, July 1–5, 2012.
10. Li YH, Liu Z. Maintenance Interval Optimization Method Based on Improvement Factor for System Components. Mechanical Engineering & Automation. 2016;4:6–8.
11. Khazanovich GSh, Apryshkin DS. Otsenka nagruzhennosti silovykh ehlementov passazhirskogo lifta po rezul'tatam regul'yarnogo monitoringa [Assessment of load of load-bearing elements of the passenger elevator based on regular monitoring results]. Safety of Technogenic and natural Systems. 2020;1:32–42. URL: https://bps-journal.ru/upload/iblock/05b/5_103-KHazanovich_32_42.pdf (accessed: 21.06.2021). (In Russ.)
12. Kartashevsky VG. Osnovy teorii massovogo obsluzhivaniya [Fundamentals of the queuing theory]. Moscow: Radio i svyaz'; 2006. 107 p. (In Russ.)
13. Apryshkin DS, Khazanovich GSh. Metodika i algoritm imitatsionnogo modelirovaniya rezhimov raboty passazhirskogo lifta [Method and algorithm of simulation modeling of passenger elevator operation modes]. Engineering and Construction Bulletin of the Caspian Region. 2020;3(33):84–92. (In Russ.)
14. Kudryavtsev EM. GPSS World. Osnovy imitatsionnogo modelirovaniya razlichnykh sistem [GPSS World. Fundamentals of simulation modeling of various systems]. Moscow: DMK Press; 2004. 320 p. (In Russ.)
15. Sergey Lupin, Than Shein, Kyaw Kyaw Lin, et al. Modelling of the Transport Systems in a Competitive Environment. In: Proc. Fifth Int. Conf. on Internet Technologies and Applications (ITA 13). Glyndwr University, Wrexham, North Wales, UK, 10-13 September 2013. P. 516, p. 41–48.

Received 17.05.2021

Revised 31.05.2021

Accepted 04.06.2021

About the Authors:

Apryshkin, Dmitrii S., senior lecturer of the Transport Systems Operation and Logistics Department, Don State Technical University (1, Gagarin sq., Rostov-on-Don, RF, 344003), ORCID: <https://orcid.org/0000-0002-6829-3861>, aprechnik@mail.ru

Khazanovich, Grigorii Sh., professor of the Transport Systems Operation and Logistics Department, Don State Technical University (1, Gagarin sq., Rostov-on-Don, RF, 344003), Dr.Sci. (Eng.), ORCID: <https://orcid.org/0000-0003-3009-4952>, hazanovich@mail.ru

Gutarevich, Viktor O., professor of the Transportation Systems and Logistics Department, Donetsk National Technical University (58, Artema St., Donetsk, Donetsk People's Republic, 283001), Dr.Sci. (Eng.), viktor.gutarevich@mail.ru

Claimed contributorship

D. S. Apryshkin: research objectives, tasks and program formulation; output of mathematical models; design of the graphic part. G. Sh. Khazanovich: generation of the concept of elevator maintenance; verification of the basic operating modes of elevator installations; selection of influencing factors; consultations when developing mathematical models. O. V. Gutarevich: description of the elevator installation operation; selection of materials for the analysis of the issue; participation in the analysis of the operation modes of elevator installations.

All authors have read and approved the final manuscript.

MACHINE BUILDING AND MACHINE SCIENCE



UDC 621.01/03

<https://doi.org/10.23947/2687-1653-2021-21-2-184-190>

Rational Possibility of Generating Power Laws in the Synthesis of Cam Mechanisms


B. Paleva-Kadiyska¹, R. Roussev², V. Galabov³
¹South-West University “Neofit Rilski” (Blagoevgrad, Bulgaria)

²Trakia University (Yambol, Bulgaria)

³Technical University, (Sofia, Bulgaria)

Introduction. The generation of polynomial power laws of motion for the synthesis of cam mechanisms is complicated by the need to determine the coefficients of power polynomials. The study objective is to discover a rational capability of generating power laws with arbitrary terms number under the synthesis of cam mechanisms.

Materials and Methods. A unified formula for determining the values of coefficients of power polynomials with any number of integers and/or non-integer exponents is derived through the so-called transfinite mathematical induction.

Results. A unified formula for determining the values of coefficients, which gives correct results for any number of even and/or odd exponents, is presented. The correctness of the derived formula is validated by the results on the multiple checks for different numbers, even and odd values of the exponents of quinquinomial and hexanomial power functions.

Discussion and Conclusions. A unified formula for determining the values of coefficients of power polynomials makes it possible to rationally define the laws of motion without finite and infinite spikes in the synthesis of elastic cam-lever systems. This provides a rational determination of the laws of motion without finite and infinite spikes in the synthesis of elastic cam-lever systems, and simple verification of the accuracy of the results obtained. The functions are particularly suitable for the synthesis of polydyne cams, as well as cams, since one polynomial can be used throughout the entire geometric mechanism cycle.

Keywords: cam mechanisms, laws of motion, power functions.

For citation: B. Paleva-Kadiyska, R. Roussev, V. Galabov. Rational possibility of generating power laws in the synthesis of cam mechanisms. *Advanced Engineering Research*, 2021, vol. 21, no. 2, pp. 184–190. <https://doi.org/10.23947/2687-1653-2021-21-2-184-190>

© Paleva-Kadiyska B., Roussev R., Galabov V., 2021



1. Introduction

One of the most important tasks in the design of cam mechanisms [1–4] and in the planning of industrial robots movements [5–7], is undoubtedly the selection of the law of motion, as the law affects the basic kinematic, force and dynamic characteristics of the generated movements [8–11].

It is generally assumed that the units are rigid bodies connected without a gap clearance, whereby the mechanism generates the desired basic law of motion. In fact, real laws of motion of the mechanisms differ significantly from the baselines as the speed of the cam, the load, the deformations, and the clearances of the cam-lever systems are greater.

The cams, synthesized according to polynomial laws of motion taking into account the dynamics and deformations of the mechanical system driven by the cam, are called polydyne cams. The design of such cams is required for the construction of high-speed and insufficiently rigid mechanical systems.

The development of methods for the synthesis of polydyne cams was started in 1948 by Dudley [12], supplemented and developed by many other authors mainly in connection with dynamic studies of cam-lever systems [13–18]. The main purpose of the methods is to exclude the acceleration breaks (jerks), resp. of the inertial load of resiliently susceptible mechanical systems to achieve more precise target movements with minimum oscillations.

The design of polydyne cams is required not only for cam-lever valves of automobile engines [17–19], but also for many other high-speed and insufficiently rigid mechanical systems of various technological machines [15], [19–22].

Power-polynomial laws of motion with four or more terms have great advantages in achieving the desired boundary conditions at the beginning and at the end of the phases of movement of the output at the cam mechanisms [15], [20, 21]. Such motion laws are suitable for the synthesis of mechanisms with polydyne cams [1–3], [5]. These laws make providing the laws of motion without finite and infinite spikes with better dynamic characteristics of high-speed, elastic cam-lever systems than the power trinomial and quadrinomial laws of motion. However, the derivation of power laws of motion with four or more terms is difficult due to the need to solve systems with four and more equations, respectively.

The aim of the study is to explore a rational possibility for generating basic power laws with arbitrary number of terms when formulating design laws of motion for the synthesis of cam mechanisms.

2. Materials and Methods

The basal law of motion of polydynamic cam mechanisms is most significantly affected by the basal second transfer function and its derivatives. This function, multiplied by the dynamic constant of the cam-driven mechanical system, changes the output displacement, as the inertial load generated by the acceleration deforms the system components elastically. In other words, the second derivative (the basal second transfer function) also participates in the real displacement function.

Therefore, in order to avoid spikes in the first two real transfer functions, it is required to avoid spikes in the next two basal transfer functions — the third and the fourth. This cannot be achieved for the limits of the phases of movement of the output unit if a power trinomial or quadrinomial displacement function is selected. These spikes will be avoided if the displacement function and its first four derivatives are continuous functions.

The displacement function of the output link of the cam mechanism may, in any law of motion, be written in summary form $B = B_0 + \Delta B(\varphi) = B_0 + H \cdot u(\xi)$, where B is the output coordinate formed by its initial value B_0 , which determines the initial position of the output link, to which the *displacement function* of the output link is added — a product of the follower motion $H \equiv \Delta B_{\max}$ and the normalized function $u(\xi)$. The velocity, acceleration and the subsequent derivative (jerk) of the follower's motion correspond to the transfer functions $B'(\varphi)$, $B''(\varphi)$, $B'''(\varphi)$, which differ by only one factor H/Φ_1 , H/Φ_1^2 and H/Φ_1^3 (Φ_1 is the cam angle of the follower rise) respectively from the derivatives u' , u'' and u''' of the normalized function $u(\xi) \in [0; 1]$ in the argument $\xi = \varphi / \Phi_1 \in [0; 1]$:

$$\begin{cases} \Delta B = H \cdot u(\xi); \\ B' = \frac{H}{\Phi_1} u'(\xi); \\ B'' = \frac{H}{\Phi_1^2} u''(\xi); \\ B''' = \frac{H}{\Phi_1^3} u'''(\xi) \dots \end{cases} \quad (1)$$

For a **binomial power function** with the exponents k and m , the coefficients a_k and a_m are determined by the relations:

$$a_k = \frac{m}{(m-k)}; \quad a_m = \frac{k}{(k-m)}.$$

For a **trinomial power function** with the exponents k , m and p , the coefficients a_k , a_m and a_p are determined by the relations:

$$a_k = \frac{m p}{(m-k)(p-k)}; \quad a_m = \frac{k p}{(k-m)(p-m)}; \quad a_p = \frac{k m}{(k-p)(m-p)}$$

There are known formulas for determining the coefficients of normalized power functions up to four integers and/or non-integer power exponents.

For a **quadrinomial power function** with the exponents k, m, p and q , the coefficients a_k, a_m, a_p and a_q are determined by the relations:

$$a_k = \frac{m p q}{(m-k)(p-k)(q-k)}; a_m = \frac{k p q}{(k-m)(p-m)(q-m)};$$

$$a_p = \frac{k m q}{(k-p)(m-p)(q-p)}; a_q = \frac{k m p}{(k-q)(m-q)(p-q)}.$$

A formula for determining the coefficients of normalized power functions with an arbitrary number of integer and non-integer exponents is derived.

According to the method of the so-called transfinite mathematical induction, it can be assumed that the formulas for determining the values of the coefficients of the input normalized power functions are valid for any plurality of integer and non-integer exponents. The known formulas for determining the values of the coefficients are true for two, three and four even and odd exponents, from which the **inductive assumption** follows that for any number of even and/or odd exponents, a formula for the values of the coefficients is inductively obtained

$$a_j = \frac{k \cdot m \cdot p \dots v}{(k-j)(m-j)(p-j) \dots (v-j)}, \quad (2)$$

in which j consistently takes n in the number of values k, m, p, \dots, v . The numerator of (2) excludes the exponent j (it is assumed that $j = 1$), and in the denominators of any value of exponents (except j), the value of j is subtracted. In other words, the value of each unknown coefficient a_j of the normalized power function is determined by the relation (2) with the numerators, which is the product of the exponents, excluding j , and the denominator, which is the product of the difference between the exponents (except j) and the exponent j .

3. Results

To verify the results obtained, the sum of the values of the calculated coefficients must be equal to one:

$$k + m + p + \dots + v = 1.$$

An **inductive inference** for (2) is reached if it is also proved that an arbitrary number n is odd and/or odd values of exponents. The correctness of formula (2) is validated by the results on the multiple checks for different numbers of n , even and odd values of the exponents of quinquinomial and hexanomial power functions. Two functions have been selected from them.

Example 1. Let the power function be quinquinomial with integers and non-integers exponents. For example, at $k = 5; m = 5.5; p = 6; q = 6.5; s = 7$ from formula (2), it is obtained:

$$a_k = 1001; a_m = -3640; a_p = 5005; a_q = -3080; a_s = 715.$$

The results are true since $a_k + a_m + a_p + a_q + a_s = 1$.

Thus, for the normalized power function and its derivatives, we obtain:

$$\begin{cases} u = 1001\xi^5 - 3640\xi^{5.5} + 5005\xi^6 - 3080\xi^{6.5} + 715\xi^7, \\ u' = 5005(\xi^4 - 4\xi^{4.5} + 6\xi^5 - 4\xi^{5.5} + \xi^6), \\ u'' = 10010(2\xi^3 - 9\xi^{3.5} + 15\xi^4 - 11\xi^{4.5} + 3\xi^5), \\ u''' = 15015(4\xi^2 - 21\xi^{2.5} + 40\xi^3 - 33\xi^{3.5} + 10\xi^4), \\ u'''' = 15015(8\xi - 52.5\xi^{1.5} + 120\xi^2 - 115.5\xi^{2.5} + 40\xi^3) \end{cases} \quad (3)$$

Indeed, for the interval boundaries $\xi \in [0, 1]$, the function $u(\xi)$ has values of 0 and 1, respectively, and all derivatives functions of $u(\xi)$ are zeroing.

Figure 1 presents the power polynomial $u(\xi)$ with the first three derivatives.

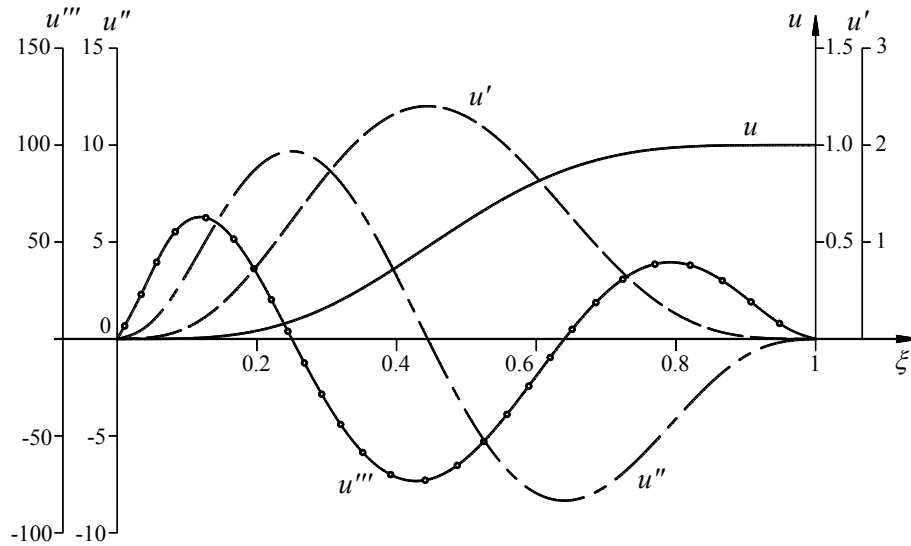


Fig. 1. Graphs of the quinquinomial $u(\xi)$ and the first three derivatives by equation (3)

Example 2. Let the power function be hexanomial with integer power, for example:

$k = 6$; $m = 7$; $p = 8$; $q = 9$; $s = 10$; $v = 11$. From formula (2), we obtain $a_k = 462$; $a_m = -1980$; $a_p = 3465$; $a_q = -3080$; $a_s = 1386$; $a_v = -252$, and therefore:

$$\begin{cases} u = 462\xi^6 - 1980\xi^7 + 3465\xi^8 - 3080\xi^9 + 1386\xi^{10} - 252\xi^{11}, \\ u' = 2772(\xi^5 - 5\xi^6 + 10\xi^7 - 10\xi^8 + 5\xi^9 - \xi^{10}), \\ u'' = 13860(\xi^4 - 6\xi^5 + 14\xi^6 - 16\xi^7 + 9\xi^8 - 2\xi^9), \\ u''' = 27720(2\xi^3 - 15\xi^4 + 42\xi^5 - 56\xi^6 + 36\xi^7 - 9\xi^8), \\ u^{(4)} = 166320(\xi^2 - 10\xi^3 + 35\xi^4 - 56\xi^5 + 42\xi^6 - 12\xi^7), \\ u^{(5)} = 332640(\xi - 15\xi^2 + 70\xi^3 - 140\xi^4 + 126\xi^5 - 42\xi^6). \end{cases} \quad (4)$$

Expectedly, for the boundaries of the interval $\xi \in [0, 1]$, the function $u(\xi)$ has values of 0 and 1, respectively, and all derivatives functions of $u(\xi)$ by the fifth line are zeroing. This means that the polynomial has one common point and 5 infinitely close common points with the axis ξ at $\xi = 0$ and $\xi = 1$ in the positive direction to the axis ξ and another 5 infinitely close common points with the axis ξ at $\xi = 0$ and $\xi = 1$ in the opposite direction to the axis ξ . In practice, this means 11 infinitely close common points of the polynomial with the ξ axis or an oscillation (tangent) of 10 lines of the polynomial with the ξ axis. Although infinitely close, the common points generally lead to an approximate, but sufficiently accurate, in some cases dwell of the output link. Figure 2 presents the power polynomial $u(\xi)$ with the first three derivatives.

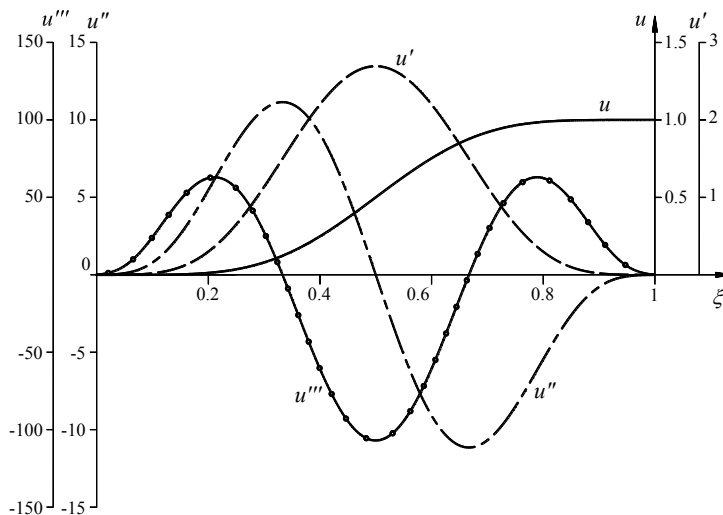


Fig. 2. Graphs of the hexanomial polynomial $u(\xi)$ and the first three derivatives by equation (4)

For values of the exponents $k = 7$; $m = 8$; $p = 9$; $q = 10$; $s = 11$; $v = 12$ from formulas (2), it is obtained: $a_k = 792$; $a_m = -3465$; $a_p = 6160$; $a_q = -5544$; $a_s = 2520$; $a_v = -462$.

Then the normalized function and its derivatives are specified in the form:

$$\begin{cases} u = 792\xi^7 - 3465\xi^8 + 6160\xi^9 - 5544\xi^{10} + 2520\xi^{11} - 462\xi^{12}, \\ u' = 5544(\xi^6 - 5\xi^7 + 10\xi^8 - 10\xi^9 + 5\xi^{10} - \xi^{11}), \\ u'' = 5544(6\xi^5 - 35\xi^6 + 80\xi^7 - 90\xi^8 + 50\xi^9 - 11\xi^{10}), \\ u''' = 55440(3\xi^4 - 21\xi^5 + 56\xi^6 - 72\xi^7 + 45\xi^8 - 11\xi^9), \\ u^{(4)} = 166320(4\xi^3 - 35\xi^4 + 112\xi^5 - 168\xi^6 + 120\xi^7 - 33\xi^8), \\ u^{(5)} = 665280(3\xi^2 - 35\xi^3 + 140\xi^4 - 252\xi^5 + 210\xi^6 - 66\xi^7), \\ u^{(6)} = 665280(6\xi - 105\xi^2 + 560\xi^3 - 1260\xi^4 + 1260\xi^5 - 462\xi^6). \end{cases} \quad (5)$$

The check $a_k + a_m + a_p + a_q + a_s + a_v = 1$, the normalized function $u(\xi)$, and its derivatives show the accuracy of the results obtained, because of the interval's boundaries $\xi \in [0; 1]$, the function $u(\xi)$ has values of 0 and 1, respectively, and all derivative functions are zeroing.

The graphs of $u(\xi)$, $u'(\xi)$, $u''(\xi)$, and $u'''(\xi)$ are presented in Figure 3, which shows that at the beginning and at the end of the cam angle Φ_1 in the rise phase distance phase (rise phase, outstroke phase), the follower remains practically stationary — an approximate dwell of the follower is realized. In the cam angle Φ_3 in the return phase (reverse move, return stroke) of the follower, the normalized power functions $u(\xi)$, $u'(\xi)$, $u''(\xi)$ and $u'''(\xi)$ are retained by type with a new argument $\xi = 1 - \xi$, where $\xi \in [0, 1]$.

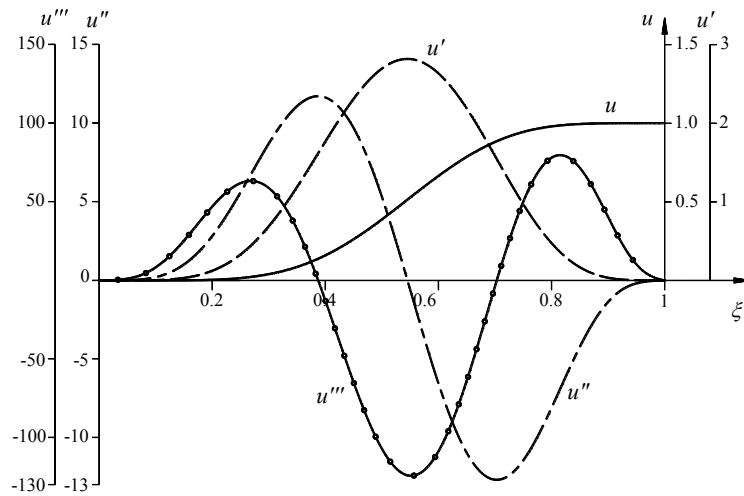


Fig. 3. Graphs of the hexanomial $u(\xi)$ and the first three derivatives by equation (5)

A detailed solution to the question of the laws of motion and synthesis of cam mechanisms was made by Galabov, Roussev, and Paleva-Kadiyska in [4].

4. Discussion and Conclusions

The spikes in the first two transfer functions in high-speed, resilient (elastic) cam-lever systems are avoided if the displacement function and its first four derivatives are continuous functions. This cannot be achieved for the limits of the phases of movement of the output unit if a power trinomial or quadrinomial displacement function is selected. However, the derivation of power laws of motion with four or more terms is complicated by the need to solve systems with four or more equations, respectively. Therefore, by the method of the so-called transfinite mathematical induction, a unified formula for determining the values of coefficients of power polynomials with any number of integers and/or non-integer exponents is derived. It gives a rational possibility for defining the laws of motion without finite and infinite spikes in the synthesis of elastic cam-lever systems and easy verification of the accuracy of the results obtained.

The functions (3), (4), (5) and other polynomial power polynomials are especially suitable for the synthesis of polydyne cams, as well as cams, since one polynomial can be used throughout the geometric mechanism cycle.

References

1. Levitsky NI. Kulachkovye mekhanizmy [Cam mechanisms]. Moscow; Mashinostroenie; 1964. 287p. (In Russ.)
2. Rothbart HA. Cams. Design, Dynamics and Accuracy. New York: John Wiley & Sons Inc.; 1965. 336 p.
3. Chen FY. Mechanics and Design of Cam Mechanisms. Pergamon Press, 1982. 523 p.
4. Galabov V, Roussev R, Paleva-Kadiyska BL. Synthesis of cam mechanisms I. Sofia: New Man Publishing House; 2020. 253 p. (In Bulgarian).
5. Skenderov I, Shivarov N, Galabov V. Synthesis of Power-Polynomial Motion Laws. Problems of technical cybernetics and robotics. Sofia: Academies of Sciences of Bulgaria. 2008;59:74–81.
6. Galabov V, Roussev R, Shivarov N. Planning of Movement Laws Using Trigonometric Polynomials. BAS, Theor. & Appl. Mechanics, 2010;3:3–12.
7. Galabov V, Savchev S, Slavov G. Planning of Motion Laws Using Power-Trigonometric Polynomials. Conferences & Symposia IFAC-PapersOnLine. 2015;48-24:134–137.
8. Erdman AG, Sandor GN. Mechanism Design: Analysis and Synthesis. New Jersey: Prentice-Hall Inc.; 1984. Vol. 1. 2nd ed., 1991.
9. Norton RL. Design of Machinery. New York: McGraw-Hill Inc.; 1992. 306 p.
10. Erdman AG (ed). Modern Kinematics. New York: John-Wiley & Sons, Inc.; 1993. 604 p.
11. Uicker JJ, Pennock GR, Shigley JE. Theory of Machines and Mechanisms. 3rd ed. Oxford University Press, 2003. 768 p.
12. Dudley WM. New Methods in Valve Cam Design. SAE Transactions. 1948;2(1):19–33.
13. Thoren TR, Engemann HH, Stoddart DA. Cam Design as Related to Valve Train Dynamics. SAE Transactions, 1952, vol. 6. <https://doi.org/10.4271/520208/>
14. Stoddart DA. Polydyne Cam Design. Machine Design. 1953;25:121–149.
15. Berzak N, Freudenstein F. Optimization Criteria in Polydyne Cam Design. In: Proc. Fifth World Congress on TMM, Canada, Toronto, 1979. P. 1303–1306.
16. Cardona A, Lens E, Nigro N. Optimal Design of Cams. Multibody System Dynamics. 2002;7:285–305. <https://doi.org/10.1023/A:1015278213069/>
17. Moreno D, Mucchi E, Dalpiaz G, et al. Multibody analysis of the desmodromic valve train of the Ducati MotoGP engines. In: Proc. Multibody Dynamics 2007, ECCOMAS Thematic Conference, Italy, Milano, 2007.
18. Tounsi M, Chaari F, Walha L, et al. Dynamic behavior of a valve train system in presence of camshaft errors. WSEAS Transactions on Theoretical Mechanics. 2011;6(1):17–26.
19. Korchemny LV. Dinamika gazoraspredeitel'nogo mekhanizma i profilirovanie kulachkov bystrokhodnykh dvigatelei [Dynamics of the gas distribution mechanism and the profiling of the cams of high-speed engines]. Moscow: Trudy NAMI. 1960;91;100. (In Russ.)
20. Sadek KSH, Daadbin A. Improved Cam Profiles for High-Speed Machinery Using Polynomial Curve Fitting. J. of Process Mechanical Engineering. Part E. 1990;204(2):127–132.
21. Blechsmidt JL, Lee CH. Design and Analysis of Cam Profiles Using Algebraic Functions. New York: ASME, DE. 1991;32(2):451–459.
22. Norton RL. Design of Machinery. New York, McGraw-Hill Inc.; 1992. 306 p.

Received 01.04.2021

Revised 25.04.2021

Accepted 13.05.2021

About the Authors:

Paleva-Kadiyska, Blagoyka I., chief assistant, mechanical engineer, Faculty of Engineering, South-West University “Neofit Rilski” (66, Ivan Mihaylov St., Blagoevgrad, Bulgaria, 2700), Cand. Sci. (Eng.), ORCID: <https://orcid.org/0000-0002-8514-4542>, paleva-kadiyska.bl@abv.bg

Roussev, Rumen A., associate professor, mechanical engineer, Faculty of Technics and Engineering, Trakia University (38, Graf Ignatiev St., Yambol, Bulgaria, 8600), Cand. Sci. (Eng.), roussev_r@abv.bg

Galabov, Vitan B., professor, mechanical engineer, Faculty of Mechanical Engineering, Technical University (8, Kliment Ohridski Blvd St., Sofia, Bulgaria, 1000), Dr. Sci. (Eng.), vgalabov@abv.bg

Claimed contributorship:

B. I. Paleva-Kadiyska: preparation of the text; preparation of the results and graphs; formulation of conclusions; translation of the paper into English; translation of the abstract and keywords into Russian. R. A. Roussev: review of literature sources; calculations; computational analysis; analysis of the research results. V. B. Galabov: basic concept formulation; formulation of the research purpose and tasks; academic advising; text processing; correction of the conclusions; approval of the final version of the paper before submitting it for publication.

All authors have read and approved the final manuscript.

INFORMATION TECHNOLOGY, COMPUTER SCIENCE, AND MANAGEMENT



UDC 620.179

<https://doi.org/10.23947/2687-1653-2021-21-2-191-199>

Control algorithm for an elastic-viscoplastic model to study processes of shock interaction of bodies

V. L. Lapshin¹, E. V. Zenkov^{1,2}

¹ Irkutsk National Research Technical University (Irkutsk, Russian Federation)

² Irkutsk State Transport University (Irkutsk, Russian Federation)



Introduction. In engineering practice, dynamic processes, with the help of which mechanics of interaction of machine components and structural elements are described and studied, are of great importance. These dynamic processes are the cause of large deformations leading to the destruction. The research objective is to develop a more accurate shock simulation algorithm through the controlled transformation of the mechanorheological shock process model from elastic-viscous to elastic-viscoplastic.

Materials and Methods. Differential equations of the model movement are proposed. The conditions for the transformation of the model during the transition from elastic to plastic deformations, from the stage of loading the model to the stage of unloading under the shock interaction with the surface, are considered. When calculating deformations, the assumption is made that elastic and plastic deformations occur simultaneously from the very onset of the impact. The model functioning method is considered in detail, the algorithm of the model operation is developed, the logic of its functioning is described in detail.

Results. To study shock processes, a mechanorheological elastic-viscoplastic model was developed. An important parameter of the model is the force corresponding to the onset of plastic deformation. As a result of the research, a more perfect algorithm was created, and a new computer program was developed to study the shock process using an elastic-viscoplastic model with an adjustable elastic-plastic transformation.

Discussion and Conclusions. The results obtained can be used to improve the accuracy and reliability of simulation of shock processes in order to further develop the techniques for determining the physical and mechanical characteristics of materials by shock methods. Knowledge of the mechanical characteristics of materials is required when solving various research problems through mathematical modeling of vibration and shock processes. At the same time, an important task is to adapt the design model to the real shock process, for which it is required to develop appropriate methods and techniques.

Keywords: elastic-viscoplastic model, shock interaction of bodies, mathematical modeling of shock process.

For citation: V. L. Lapshin, E. V. Zenkov. Control algorithm for an elastic-viscoplastic model to study processes of shock interaction of bodies. Advanced Engineering Research, 2021, vol. 21, no. 2, pp. 191–199. <https://doi.org/10.23947/2687-1653-2021-21-2-191-199>

© Lapshin V. L., Zenkov E. V., 2021



Introduction. In engineering practice, dynamic processes (shock, vibration) are critical. They are used to describe and study the mechanics of interaction of machine parts and structural elements. At the same time, much attention is paid to the shock process since, in this case, the bodies are exposed to high dynamic loads. They can cause

large deformations and damage to equipment. These circumstances explain the increased attention of scientists and engineers to modeling and research of dynamic processes [1–14]. The development of express methods and techniques for determining the physical and mechanical characteristics of materials by shock methods is of particular practical interest. At the same time, a crucial task is to adapt the computational model to the real shock process. In this regard, the study objective is to create a more accurate algorithm for modeling a shock process due to the controlled transformation of the mechanorheological model of the shock process from elastic-viscous to elastic-viscoplastic. The developed algorithm allows for the transformation of the model at the loading stage based on the specified conditions, which provides a better and more reliable simulation of the shock process, taking into account the real plasticity of the material. The previous development did not allow this transformation to be carried out, and the model under the impact interaction was elastic-viscoplastic from the very beginning of loading.

Materials and Methods. One of the areas of scientific research at Irkutsk National Research Technical University is the modeling and study of the processes of dynamic interaction of solids. To study the dynamics of these processes in order to solve practical problems, an elastic-viscoplastic model was developed and studied [15]. The model is constructed using the rheological and inertial elements m_1 and m_2 , combined in two blocks (Fig. 1). One of the blocks is elastic-viscous K_1-C . It is designed to simulate elastic deformations of the body. They arise under the impact of an external load and disappear in its absence. The elastic-plastic block K_2-f_2 simulates the plastic deformations remaining after the load is removed. The mass of the body is taken into account by the inertia element m_1 . The mass m_2 is introduced to describe the motion dynamics of an elastic-viscoplastic model using two second-order differential equations. To exclude the influence of m_2 on the dynamics of the process, its value was assumed to be small ($m_2 \leq 0,001 m_1$). As the calculations showed, under this condition, you can accept $N_1 \approx N_2$ (4).

Consider the shock process on the example of a spherical body. When a body is loaded, internal forces arise in it that prevent changes in the shape and size of the body, that is, prevent (2) its deformation. One of them is the elastic resistance force. In this case, additional deformation resistances, which are called viscous, may occur. They are related to the rate of deformation of the body. On the model, the data of the resistance to deformation of the body is described by the expressions:

$$\begin{aligned} N_1 &= F_v + F_{E1}, \\ F_v &= C(\dot{y}_1 - \dot{y}_2)^{s1} (y_1 - y_2)^{s2}, \\ F_{E1} &= K_1 (y_1 - y_2)^{n1}. \end{aligned} \quad (1)$$

where $y_1, y_2, \dot{y}_1, \dot{y}_2$ — dynamic characteristics of the model describing the movement and velocity of the inertial elements m_1 and m_2 ; K_1 — the model parameter, which characterizes the elastic properties of the material (elastic-viscous block of the model); C — the model parameter, which characterizes the viscous (dissipative) properties of the material in the same block of the model (3).

The deformation resistance forces that occur in the elastic-plastic block of the model are described by the following expressions:

$$\begin{aligned} N_2 &= F_p + F_{E2}; N_2 \approx N_1; \\ F_{E2} &= K_2 y_2^{n2}; \\ F_p &= f_2 y_2^{n3} + F_{ST}. \end{aligned} \quad (2)$$

Here, F_{ST} — the loading force of the model, under which the elastic-plastic block of the model starts to work, taking into account the plastic deformations of the material; K_2 — the model parameter that characterizes the elastic properties of the material under plastic deformation (elastic-plastic block of the model); f_2 — the model parameter that characterizes the plasticity of the material in the same block of the model (3).

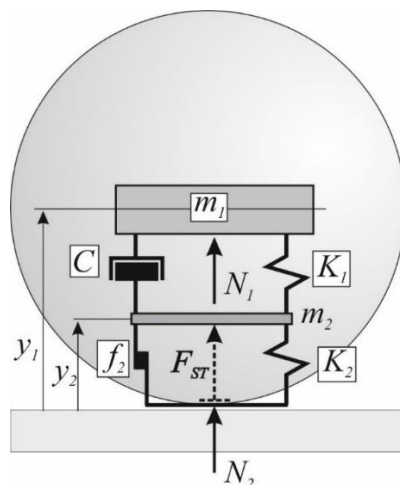


Fig. 1. Elastic-viscoplastic mechanorheological model

The variables y_1, \dot{y}_1 describe the amount and rate of total deformation. The variables y_2, \dot{y}_2 describe the amount and rate of plastic deformation. Hence, the rate and amount of elastic deformation is specified as $\dot{y}_1 - \dot{y}_2$; $y_1 - y_2$.

The rheological elements of the model (elastic, viscous, plastic) have nonlinear characteristics, that is, elastic, viscous, and plastic resistances of deformation are proportional to the rate and amount of deformation to a given degree (s_1, s_2, n_1, n_2, n_3). As a recommendation, it can be noted that for elastic resistances upon impact of a spherical body, $n_1=n_2=3/2$ [2–4] should be used, for viscous and plastic resistances, a value equal to one can be taken [2, 3].

Research Results. Consider how the model works. At the initial stage of using the model in scientific research, a simplified version of its functioning was used. It was assumed that under the deformation of the body, elastic and plastic deformations occur simultaneously from the very beginning of loading. This allowed us to develop and test in practice a simpler algorithm for the model functioning. On its basis, a research computer program¹, was developed, a complex of scientific studies of the shock process was carried out on the model², including those presented in paper [16].

However, this simplification limits the capabilities of the model and does not allow to fully perform studies of shock processes. Therefore, as a result of further research, a more advanced algorithm was created, and a new computer program was developed to study the shock process using an elastic-viscoplastic model with an adjustable elastic-plastic transformation³. Consider this algorithm of the model functioning in greater detail.

The developed algorithm provides the following sequence of functioning of the model blocks. At the initial stage of the shock process, only the elastic-viscous block of the model K_1 – C is involved in the operation. It enables to calculate the elastic deformations of the body at the loading stage (Fig. 2). In this case, the elastic-plastic block of the model does not function, since up to a certain point, plastic deformations in the body may be absent. The appearance of plastic deformations corresponds to the specified force F_{st} . When the calculated loading force N_1 reaches the set value ($N_1=F_{st}$), the elastic-viscous model is converted to an elastic-viscoplastic mode. The elastic-plastic block of the model starts to function. When the loading force reaches its maximum value N_{max} , the growth of deformation stops, and the loading stage ends. Due to the material elasticity, the body starts to restore its original shape and size, and the stage of unloading the model comes. During this process, elastic deformations disappear, while the resulting plastic deformations remain in the body and, accordingly, on the model. Thus, at the stage of unloading the model, only the elastic-viscous block works.

¹ Glukhov AV. Impact of an elastic-viscoplastic model of a spherical body. Certificate of registration software no. 2011619238. 2011. (In Russ.)

² Lapshin VL, Glukhov AV, Rudykh AV. Method for determining the elasticity modulus of a material. RF Patent no. 2526233. 2014. (In Russ.)

³ Lapshin VL, Zenkov EV. Impact of an elastic-viscoplastic model with adjustable elastic-plastic transformation. Certificate of registration software no. 2019618137. 2019. (In Russ.)

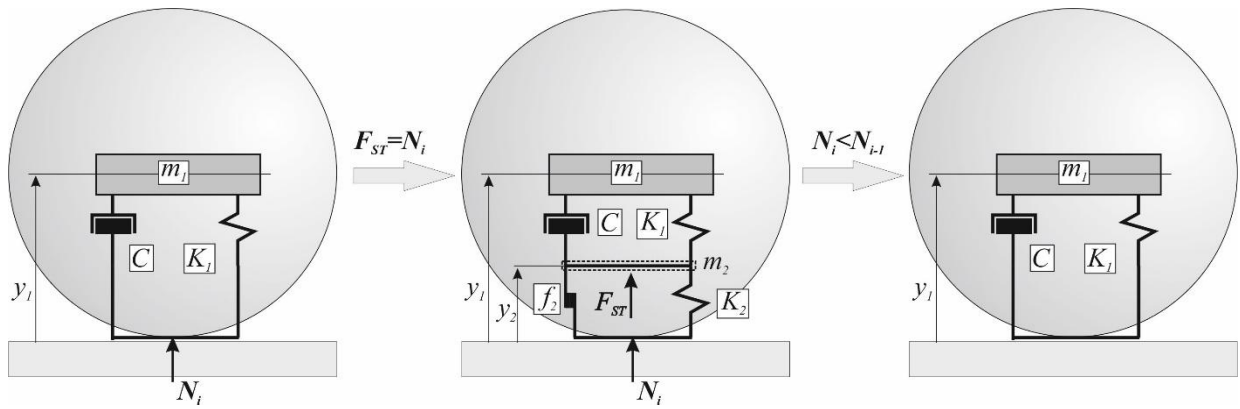


Fig. 2. Model transformation diagram

The contact interaction stage ends when the normal reaction force N , defined by equations (1) and (2), becomes zero. The body bounces off the surface to a height of h .

The process of loading the model at various stages of deformation is described using differential equations, which are given below:

$$m_1 \ddot{y}_1 + C_1 \dot{y}_1^{s1} + K_1 y_1^{s2} = -m_1 g, \quad (3)$$

$$m_1 \ddot{y}_1 + C_1 (\dot{y}_1 - \dot{y}_2)^{s1} (y_1 - y_2)^{s2} + K_1 (y_1 - y_2)^{n1} = -m_1 g, \quad (4)$$

$$m_2 \ddot{y}_2 + K_2 y_2^{n2} + f_2 y_2^{n3} + C_1 (\dot{y}_2 - \dot{y}_1)^{s1} (y_2 - y_1)^{s2} + K_1 (y_2 - y_1)^{n1} = -m_2 g + F_{ST}. \quad (5)$$

The elastic deformations of the model at the loading and unloading stages are calculated using equation (3). Using equations (4) and (5), the elastic and plastic deformations of the model are calculated when it is loaded at the stage of plastic deformation of the material.

The strength of the normal reaction at the elastic deformation stage is determined from the formula:

$$N_i = C_1 \dot{y}_1^{s1} + K_1 y_1^{s2}. \quad (6)$$

The normal reaction force at the stage of plastic deformation is determined from the formula:

$$N_i = K_2 y_2^{n2} + f_2 y_2^{n3} + F_{ST}. \quad (7)$$

The calculation is performed with the specified time step dt . The impact time is determined from the formula:

$$T = dt \cdot i, \quad (8)$$

where i — the number of steps.

The condition for the transition from elastic to plastic deformation has the form:

$$N_i > F_{ST} \quad (9)$$

The condition for the end of the loading stage and the beginning of the unloading stage of the model:

$$N_{i-1} > N_i \quad (10)$$

The condition for the end of the contact interaction stage of the model:

$$N_i = 0 \quad (11)$$

Consider the algorithm for studying the shock process (Fig. 3).

1. Block 1 forms the initial data of the process under study.

2. Block 2 enters the initial data of the process: the initial impact time $t = 0$, the initial deformation of the body (models) $y = 0$, the initial rate of the deformation $\dot{y} = \dot{y}_s$, the initial impact force $N = 0$.

3. Block 3 calculates the values of the coefficients of the model K_1, K_2, f_2, C .

4. Block 4 calculates the impact time and records the number of calculation steps at the loading stage under elastic deformation.

5. Block 5 calculates the parameters of the impact interaction of bodies using the elastic-viscous block of the model. The elastic deformation y_1 and the deformation rate are calculated (equation (3)). The impact force N_i is determined (equation (6)).

6. Blocks 6 and 16 perform the check according to condition (11). If the condition is not met, the calculation continues at the next step of the shock interaction stage. If the condition is met, then the calculation is completed, and the transition to the rebound stage of the model is performed.

7. Blocks 7 and 12 control the moment of completion of the loading process of the model. The fulfillment of condition (10) means that the loading stage of the model has completed, and the force of the contact interaction N_i starts to decrease. The calculation is performed at the stage of the model unloading. The calculation is passed to block 4 or 14. If condition (10) is not met, the contact force N_i continues to increase. The loading stage of the model continues, and the calculation is performed by blocks 8 or 13.

8. Block 8 records the largest value of the contact force N_{max} , the corresponding time in the process of impact T_{Nmax} and transmits control to block 9.

9. Block 9 determines the end of the elastic deformation stage when the model is loaded. If condition (9) is satisfied, it means that the force of the normal reaction of the model N_i exceeds the specified force F_{st} , corresponding to the beginning of the formation of plastic deformations. The elastic deformation stage is completed, the elastic-plastic deformation stage begins, and control is transferred to unit 10. If condition (9) is not met, it means that the normal reaction force of the model N_i is less than the set value F_{st} , and there are no plastic deformations. The calculation is transferred to block 4 to perform the calculation in the next step of the elastic deformation stage.

10. Block 10 calculates the current time and the number of the calculation step at the elastic-plastic deformation stage.

11. Block 11 calculates the parameters of the process of impact interaction of bodies at the stage of plastic deformation. Deformation rates and amount of the model $y_1, \dot{y}_1, y_2, \dot{y}_2$ are calculated (equations (4) and (5)), and the contact interaction force N_i is determined (equation (7)). Then the control is transferred to block 12.

12. Block 12 determines the end of the loading stage of the model. If condition (10) is satisfied, it means that the normal reaction force N_i decreases, the loading stage of the model is over, and the transition to the unloading stage of the model is performed. Control is transferred to block 14. If condition (10) is not met, it means that the force of the normal reaction N_i continues to increase, the loading stage of the model is in progress, and control is transferred to the block 13.

13. Block 13 records the largest value of the contact force N_{max} and the corresponding time in the process of impact T_{Nmax} , and transmits control to block 10 for calculation at the next step of the elastic-plastic deformation stage.

14. Block 14 calculates the current time and the number of the calculation step at the elastic deformation stage when unloading the model. Control is transferred to block 15.

15. Block 15 calculates the parameters of the process of impact interaction of bodies using an elastic-viscous model under unloading: elastic deformation y_1 , deformation rate \dot{y}_1 according to equation (3), normal reaction force N_i according to equation (6). Control is transferred to block 16.

16. Block 16 checks condition (11). If the condition is not met, the impact interaction stage continues, and control is transferred to unit 14. If the condition is met, the calculation at the impact interaction stage is completed, and the transition to the model rebound stage is performed. Control is transferred to block 17.

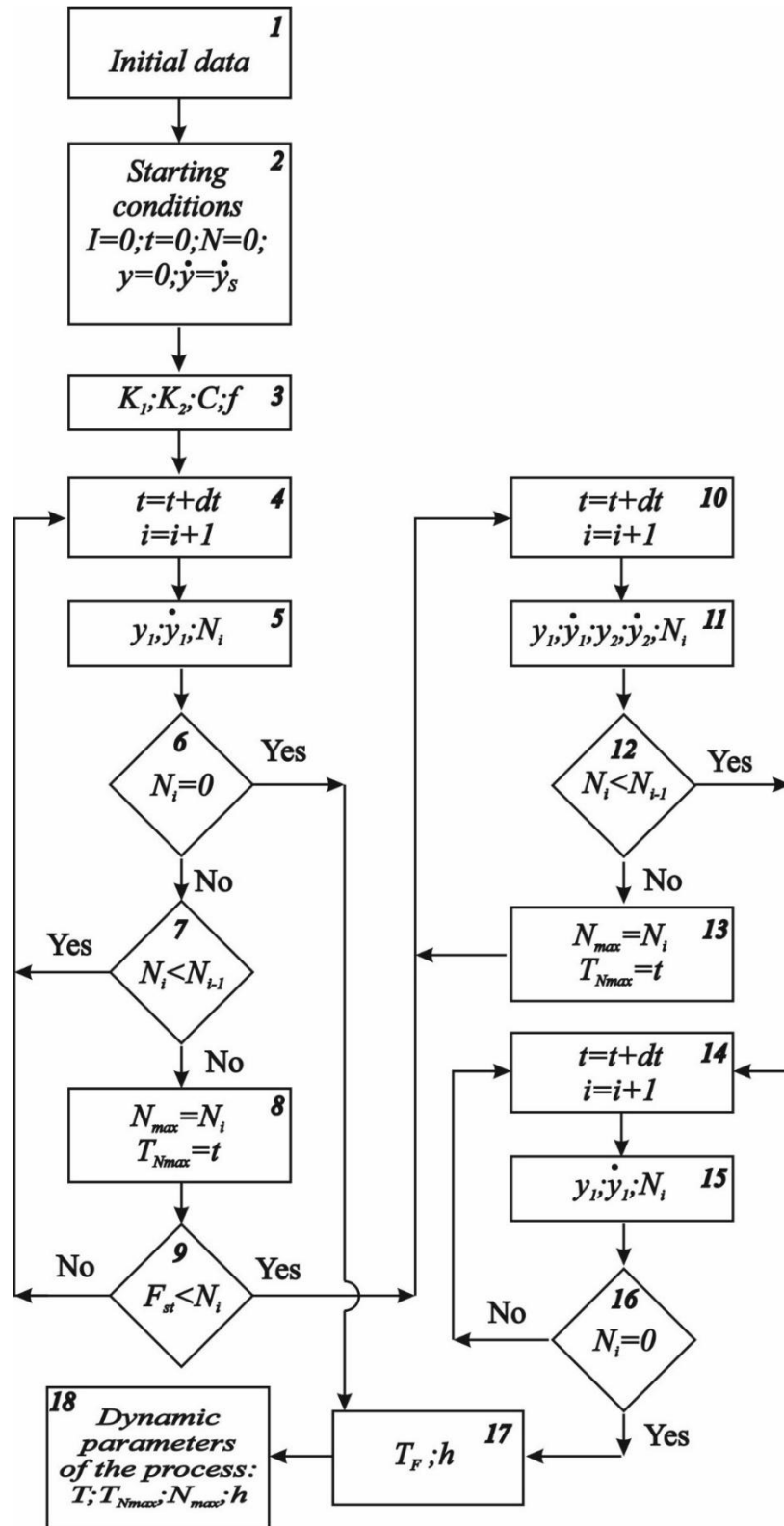


Fig. 3. Algorithm diagram

17. Block 17 determines the height of the body bounce h , the bounce flight time T_F , and transfers control to block 18.

18. Block 18 generates and outputs the main characteristics of the shock process: the time of the impact interaction of bodies (model) T (equation (8)); the force of the impact interaction of bodies N_{max} ; the time in the process of impact T_{Nmax} , corresponding to N_{max} ; the body rebound height (model) h .

On the basis of the created algorithm, a research computer program⁴ has been developed. The author's program was used to study the process of impact interaction of bodies [17]. The effect of various factors on the dynamics of the shock process was investigated. In particular, the influence of the mechanical properties of the material (elasticity, viscosity, plasticity) on the time and force of the impact interaction of a spherical body with the surface, the amount and rate of deformation, and the rebound height after impact, was studied on the model. At the same time, various options of the elastic-plastic transformation of the research model reflecting the transition from the elastic to the elastic-plastic state of the material under loading were considered

Let us compare the operation of the elastic-viscoplastic model according to the previous algorithm (Graph 1, Fig. 4) and the new one (Graph 2, Fig. 4).

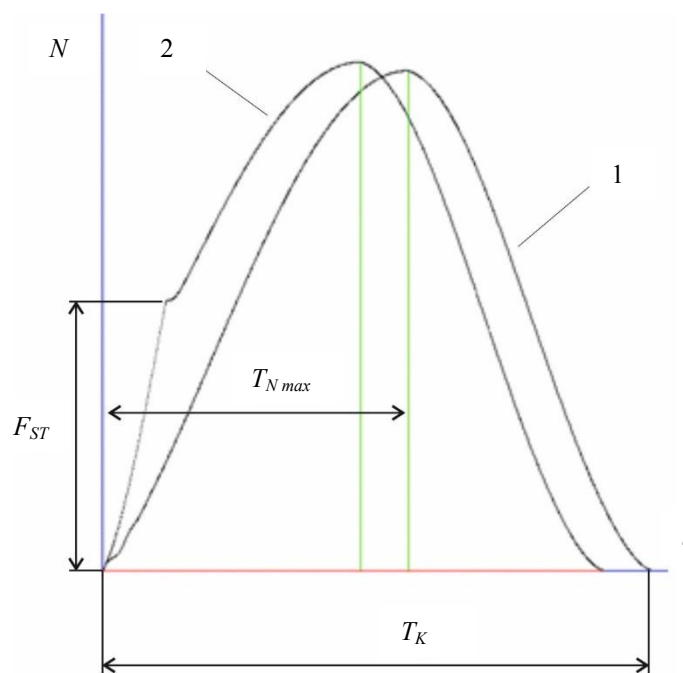


Fig. 4. Change in the force of the impact interaction of bodies N

When modeling the shock process of the interaction of bodies, the new algorithm provides the transition from the elastic-viscous model to the elastic-viscoplastic model for a given force of the impact interaction F_{ST} . This transition to the model corresponds to the beginning of the formation of plastic deformations in the material, which makes it possible to describe the shock process more reliably and accurately

It is clearly seen that the regularity of the change in the strength of the normal reaction calculated by the new algorithm (Graph 2, Fig. 4) differs significantly from a similar pattern (Graph 1, Fig. 4) obtained on the previous version of the algorithm. The impact time T_K and the time from the beginning of the impact to the maximum of the impact force T_{Nmax} differ (Fig. 4). The value N_{max} can also change significantly. Thus, the developed algorithm provides a better solution to the problems of adapting the elastic-viscoplastic model to the real processes of impact interaction of bodies taking into account their mechanical properties.

Conclusion. As a result of the research, a more advanced algorithm has been created and a new computer program has been developed to study the shock process using an elastic-viscoplastic model with an adjustable elastic-plastic transformation. The differential equations of model motion are presented. The conditions for the model transformation under the transition from elastic to plastic deformations, from the loading stage of the model to the unloading stage in the process of the impact interaction with the surface are considered. The methodology of the model functioning is considered in detail, the algorithm of the model operation is compiled, the logic of its functioning is described in detail.

The advantage of the new algorithm is that it provides a more accurate description of the process at the moment of the onset of the formation of plastic deformations in the material when it is loaded. The moment of the onset of plastic deformations on the model can be precisely set and fully correspond to the actual behavior of the material. For this, for example, data from experimental studies of the shock process can be used. This feature was not available in previous versions of the algorithm and the program.

⁴ Lapshin VL, Zenkov EV. Impact of an elastic-viscoplastic model with adjustable elastic-plastic transformation. Certificate of registration software no. 2019618137. 2019. (In Russ.)

So, for example, to study the shock process of interaction of a spherical body and a surface, an algorithm for adapting the elastic-viscoplastic model to the conditions of the shock process of interaction of bodies⁵ was developed.

In this algorithm, a condition was implemented under which elastic and plastic deformations occur simultaneously from the very beginning of the impact interaction. However, this simplification of the real process limits the possibilities of modeling, especially when studying the effect of material plasticity on the dynamics of the shock process.

The improved algorithm enables to implement the capabilities of the elastic-viscoplastic model in full. The elastic-plastic transformation of the model can be performed according to a given plan, which will provide a better adaptation of the model to the real shock process. At the same time, the actual plastic deformations can be simulated more reliably.

Thus, the new parameter of the model F_{ST} (the loading force corresponding to the appearance of plastic deformations in the material), introduced through the developed algorithm, expands the possibilities of adapting the model to real shock processes and increases the accuracy of the model in describing plastic deformations. The algorithm performance was validated in the course of studies of the shock process using the model [18].

Practical application of the developed program can significantly improve the accuracy and reliability of modeling shock processes. In particular, the results of studies on shock processes can be used for improving methods and techniques for evaluating the mechanical properties of structural materials based on the shock principle of action. Thus, using the previous version of the algorithm, a new method for determining the elastic modulus of a material has been developed, based on the impact interaction of bodies [16]. Knowledge of the mechanical properties of materials is required when performing research to form mathematical models of the processes of vibration and shock interaction of mechanical systems. At the same time, to adapt the computational model to the real shock process, which requires the development of appropriate methods and techniques, is a challenge. The solution to these problems is possible on the basis of the obtained research results.

References

1. Panovko YaG. Osnovy prikladnoi teorii kolebanii i udara [Fundamentals of the applied theory of vibration and impact]. Leningrad: Politekhnik; 1990. 272 p. (In Russ.)
2. Batuev GS. Inzhenernye metody issledovaniya udarnykh protsessov [Engineering methods for studying shock processes]. Moscow: Mashinostroenie; 1977. 240 p. (In Russ.)
3. Kil'chevskii NA. Dinamicheskoe kontaktnoe szhatie tverdykh tel. Udar. [Dynamic contact compression of solids. Shock.]. Kiev: Naukova dumka; 1976. 319 p. (In Russ.)
4. Lapshin VL, Rudykh AV, Yashchenko VP. Issledovatel'skaya model' protsessa udarnogo vzaimodeistviya sfericheskogo tela s ploskoi poverkhnost'yu rudnogo materiala [Research model of the process of impact interaction of a spherical body and flat surface of an ore material]. Proceedings of Irkutsk State Technical University. 2006;2(26):110–115. (In Russ.)
5. Eliseev SV, Piskunova VA, Savchenko AA. Vzaimodeistvie tverdykh tel v kolebatel'nykh sistemakh s uprugimi svyaziyami i sochleneniyami pri deistvii vneshnego vibratsionnogo vozmushcheniya [Interaction of rigid bodies in oscillatory systems with elastic linkages and couplings under external vibrations]. Science and Education. 2013;2:41–49. (In Russ.) <https://doi.org/10.7463/0113.0486817>
6. Stankevich IV, Yakovlev ME, Si Tu Htet. Matematicheskoe modelirovanie kontaktnogo vzaimodeistviya uprugoplasticheskikh sred [Mathematical simulation of contact interaction of elasto-plastic environments]. Science and Education. 2012;4:39–45. (In Russ.)
7. Vozhzhov AA, Khudaimuratov MA. Analiz odnositel'nykh vynuzhdennykh kolebanii instrumenta i detali pri fasonnom tochenii [Analysis of the relative forced vibrations of the tool and the part during shaped turning]. Vestnik Sovremennykh Tekhnologii. Sevastopol State University. 2016;3:16–27. (In Russ.)
8. Kuznetsov NK, Lapshin VL, Eliseev AV. Some problems of control of dynamical conditions of technological vibrating machines. IOP Conf. Series: Earth and Environmental Science. 2017;87:082027. <https://doi.org/10.1088/1755-1315/87/8/082027>
9. Petrov IB. Modelirovanie deformatsionnykh protsessov v slozhnykh konstruktsiyakh pri ikh intensivnom dinamicheskom nagruzhении [Simulation of deformation processes in complex constructions under dynamic intensive loadings]. Mathematical Models and Computer Simulations. 2006;18(5):91–11. (In Russ.)
10. Vroniuk MN, Iakobovski MV. Adaptatsiya algoritmov modelirovaniya dinamicheskikh protsessov fil'tratsii v perkolyatsionnykh reshetkakh dlya graficheskikh uskoritelei [Adaptation for GPU of numerical algorithms

⁵ Lapshin VL, Glukhov AV. Algorithm for adapting the mechanorheological model to the conditions and parameters of the process of impact interaction of a spherical body and a surface. Topical issues of the development of science in the world: Proc. IV Int. Sci. Conf., Moscow. 2015;1(4). (In Russ.)

for dynamic filtration processes in percolation grids]. Mathematical Models and Computer Simulations. 2012;24(12):78–85. (In Russ.)

11. Beklemysheva KA, Petrov IB, Favorskaya AV. Numerical simulation of processes in solid deformable media in the presence of dynamic contacts using the grid-characteristic method. Math Models Comput. Simul. 2014;6(3):294–304. <https://doi.org/10.1134/S207004821403003X>

12. Petrov IB, Vasyukov AV, Beklemysheva KA, et al. Chislennoe modelirovanie dinamicheskikh protsessov pri nizkoskorostnom udare po kompozitnoi stringernoi paneli [Numerical modeling of low energy strike at composite stringer panel]. Mathematical Models and Computer Simulations. 2014;26(9):96–110. (In Russ.)

13. Miryaha VA, Sannikov VA, Petrov IB. Discontinuous Galerkin method for numerical simulation of dynamic processes in solids. Math. Models Comput. Simul. 2015;7(5):446–455.

14. Burago NG, Zhuravlev AB, Nikitin IS. Kontinual'naya model' i metod rascheta dinamiki neuprugoi sloistoi sredy [Continuum model and method of calculating for dynamics of inelastic layered medium]. Mathematical Models and Computer Simulations. 2018;30(11):59–74. (In Russ.)

15. Lapshin VL, Demakov EI. Uprugo-vyazko-plastichnaya mekhanoreologicheskaya model' dlya otsenki uprugovo-vyazkikh svoystv mineralov pri modelirovanii protsessov vibroseparatsii [Elastic-viscoplastic mechanorheological model for evaluating the elastic-viscous properties of minerals under the simulation of vibration separation processes]. Mechanical Engineers to XXI century. 2007;6:67–71. (In Russ.)

16. Lapshin VL, Rudykh AV, Glukhov AV. Razrabotka udarnogo sposoba opredeleniya modulya uprugosti materiala [Developing impact method for elasticity modulus of a material]. Systems. Methods. Technologies. 2015;2(26):37–43. (In Russ.)

17. Lapshin VL. Study on the dependence of the force of shock interaction on the body size using a mechanorheological model. IOP Conf. Series: Materials Science and Engineering. 2019;667:012055. <https://doi.org/10.1088/1757-899X/667/1/012055>

18. Lapshin VL, Eliseev AV. Studies on the dynamics of impact interaction of the mechanoreological model under elastic plastic transformation of its mechanical system. Journal of Physics: Conference Series. 2018;1050:012040. <https://doi.org/10.1088/1742-6596/1050/1/012040>

Received 22.03.2021

Revised 05.04.2021

Accepted 12.04.2021

About the Authors:

Lapshin, Vladimir L., professor of the Mechanics and Strength of Materials Department, Irkutsk National Research Technical University (83, Lermontov St., Irkutsk, RF, 664074), Dr.Sci. (Eng.), professor, Scopus ID: [57196257405](https://orcid.org/0000-0002-2345-2275), ORCID: <https://orcid.org/0000-0002-2345-2275>, lapshin@istu.edu

Zenkov, Evgeniy V., associate professor of the Mechanics and Strength of Materials Department, lecturer-researcher, Irkutsk National Research Technical University (83, Lermontov St., Irkutsk, 664074, RF), associate professor of the Quality Management and Engineering Graphics Department, Irkutsk State Transport University (15, Chernyshevskogo St., Irkutsk, RF, 664074), Cand.Sci. (Eng.), associate professor, Researcher ID: [E-4990-2017](https://orcid.org/0000-0003-4414-0307), ScopusID: [57056173700](https://orcid.org/0000-0003-4414-0307), ORCID: <http://orcid.org/0000-0003-4414-0307>, jovanny1@yandex.ru

Claimed contributorship

V. L. Lapshin: development of the logic and mechanics of the model functioning; determination of the research objectives and tasks; development of an algorithm for computer modeling of the impact process; formulation of conclusions. E. V. Zenkov: development of a mathematical model; development of a new block of a computer program; writing the paper.

All authors have read and approved the final manuscript.

INFORMATION TECHNOLOGY, COMPUTER SCIENCE, AND MANAGEMENT



UDC 004.42

<https://doi.org/10.23947/2687-1653-2021-21-2-200-206>

Theoretical foundations of the organization of branches and repetitions in programs in the logic programming language Prolog



D. V. Zdor

Primorskaya State Academy of Agriculture (Ussuriysk, Russian Federation)

Introduction. The organization of branches and repetitions in the context of logical programming is considered by an example of the Prolog language. The fundamental feature of the program in a logical programming language is the fact that a computer must solve a problem by reasoning like a human. Such a program contains a description of objects and relations between them in the language of mathematical logic. At the same time, the software implementation of branching and repetition remains a challenge in the absence of special operators for the indicated constructions in the logical language. The objectives of the study are to identify the most effective ways to solve problems using branching and repetition by means of the logic programming language Prolog, as well as to demonstrate the results obtained by examples of computational problems.

Materials and Methods. An analysis of the literature on the subject of the study was carried out. Methods of generalization and systematization of knowledge, of the program testing, and analysis of the program execution were used.

Results. Constructions of branching and repetition organization in a Prolog program are proposed. To organize repetitions, various options for completing a recursive cycle when solving problems are given.

Discussion and Conclusions. The methods of organizing branches and repetitions in the logic programming language Prolog are considered. All these methods are illustrated by examples of solving computational problems. The results obtained can be used in the further development of the recursive predicates in logical programming languages, as well as in the educational process when studying logical programming in the Prolog language. The examples of programs given in the paper provide using them as a technological basis for programming branches and repetitions in the logic programming language Prolog.

Keywords: logical programming, branching, repetition of predicates, recursive rule, recursion termination condition.

For citation: D. V. Zdor. Theoretical foundations of the organization of branches and repetitions in programs in the logic programming language Prolog. Advanced Engineering Research, 2021, vol. 21, no. 2, pp. 200–206. <https://doi.org/10.23947/2687-1653-2021-21-2-200-206>

© Zdor D. V., 2021



Introduction. Logical programming languages are used as tools for solving problems in building artificial intelligence systems [1]. One of the languages of non-procedural logic programming is Prolog. The program in this language uses the predicate calculus theory, it is a sequence of facts and rules that describe objects and define relationships between them. Then the goal is formulated, which is a statement that must be proved during the execution of the program. The program execution mechanism is based on the implementation of an attempt to prove the goal based on the facts and rules of the program using a standard backtracking and matching engine [2].

These circumstances significantly affect the approach used in the program preparation. In traditional procedural programming, the construction of the program is based on the algorithm for solving the problem. Procedural languages provide the software implementation of the compiled algorithm using operators. At the same time, structural procedural programming languages enable to implement basic algorithmic structures. Object-oriented programming is an evolutionary continuation of the development of this technology. The program is based on an object, its properties, methods and events. However, it should be noted that the event handler, which is a procedure executed when an event occurs in object-oriented programming languages, also contains a sequence of operators that solve a specific task. Here, in Prolog logic programming language, it is required to describe the problem and set the rules for its solution in the language of mathematical logic, taking into account the features of the program execution mechanism [3].

Thus, the composition of a program for solving a simple computational problem in Prolog will require the development of a separate approach related to the specifics of logic programming. Despite the fact that Prolog language has found its main application in the field of building expert systems, the software implementation of calculations is also a challenge, since computational tasks are included as elements of information processing systems, as well as intelligent ones [4].

A number of papers consider various aspects of programming in Prolog. The paper by Adam Lally and Paul Fodor describes the rules for matching with samples in Prolog. In particular, the authors suggest using backtrace instead of pattern matching, since it is required to check a lot of conditions during parsing, i.e., there is a need for a query language in which conditions can be included or excluded depending on some context. Prolog is recognized as an effective solution to the pattern matching problem, as well as the problems of depth-first search and backtracking. The researchers believe that despite its simplicity, Prolog is very expressive and allows recursive rules to represent reachability in parse trees, perform and treat the negation operation as a failure to check for absence of conditions [5].

N. I. Tsukanova examines in detail the subject area of using programming through logical models, demonstrates the connection of the basic logical concepts of predicates and Prolog basic language constructions. The paper discusses in detail the basics of logic programming and the program structure, basic algorithms, while using Visual Prolog 7 language as an example [6].

E. Costa considers Prolog as a logical programming language; he also describes in detail its main constructions, the program structure, the types of sentences on Prolog, the features of the program execution [7].

I. Bratko considers artificial intelligence algorithms in Prolog. The main value of the work is that the researcher demonstrates the use of Prolog in various areas of artificial intelligence, including for performing heuristic search, programming under constraints, machine learning, etc. [8].

The solution to logical problems in Prolog is studied in the paper of A. N. Adamenko. It is of fundamental importance, since the author considers recursion as a way of organizing the repetition of predicates [9].

In the paper of V. T. Tarushkin, P. V. Tarushkin, L. T. Tarushkina and A.V. Yurkov, the logic of predicates and Prolog is considered, which allows us to draw a number of valuable theoretical conclusions about the basics of using a program language [10].

O. P. Soldatova and I. V. Lezina consider Prolog as an element of logical programming and axiomatic systems. The paper also discusses the main strategies for solving problems, the procedural nature of the program, in particular, repetition and recursion of the language [11].

Michael A. Covington, Roberto Bagnara, Richard A. O'Keefe, Jan Wilemaker and Simon Price consider the problem of coding in Prolog. The researchers' work contains guidelines for code markup, naming conventions, documentation, proper use of Prolog functions, program development, debugging and testing. Each guide provides its justification, and where there are controversial points, illustrations of the relative pros and cons of each alternative are given [12].

V. N. Markov presents an overview of new and traditional logic programming tools, and also analyzes the main paradigms of functional programming, which is organically implemented in Visual Prolog 7.5 version. Basic methods of processing and further representation of arrays, branches, repetitions, graphs, are also considered [13].

In their paper, Gopal Gupta, Enrico Pontelli, Khayri A.M. Ali, Mats Carlsson and Manuel V. Hermenegildo present a comprehensive overview of the problems of parallel implementation of logical programming languages, as well as the most relevant approaches. The researchers focus on the problems that arise when running Prolog programs in parallel, in particular, the organization of branches and repetitions. The paper describes basic methods of parallelism and shared memory parallelism, as well as their combinations [14].

It is also necessary to note the paper of O. N. Polovikova, V. V. Shiryaev, N. M. Obrabin and L. L. Smolyakova, where the features of performing logical tasks in Prolog are analyzed, in particular, a state-generated approach to finding answers and validation procedure, during which repetitions are performed and branches are organized. The paper presents a solution to a logical problem, which in practice illustrates the approach developed by the researchers [15].

The analysis has shown that the literature sources consider the solution to computational problems in which it is required to implement branching or repetition according to the algorithm. In all the analyzed works there are direct or indirect descriptions of the organization of branches and repetitions in Prolog. However, there is no data on the maximum rationality of any approach, which indicates the incompleteness of knowledge about the use of the language and its capabilities when composing programs in the context of logical programming.

The study objective is to determine the most rational theoretical basis for the organization of branches and repetitions in programs in Prolog language.

Materials and Methods. The analysis of specialized literature on the research topic for the last 15 years has been carried out. Methods of comparative analysis, generalization and systematization of knowledge, the program testing, analysis of the program execution, were used.

Research Results. Based on the analysis of literary sources, the most rational method of organizing branches and repetitions in programs in Prolog is determined. The theoretical background for the organization of branches and repetitions in programs in this language is formulated. It should be noted that the process of proving the program purpose is reduced to comparing the statements included in the purpose to the facts and rules from the program knowledge base. The truth of the statements included in the purpose is established in the order of their sequence in the purpose from left to right. In this case, the comparison with the predicates of the program knowledge base is carried out in the order of their sequence from top to bottom. If at some step of the program execution, i.e., the proof of the problem solution, the comparison of some predicate fails, the Prolog system uses a second process — backtracking.

To control the search for a solution in Prolog, there is a number of standard predicates that provide changing the standard search mechanism. These predicates include the predicate fail, which has the value “false”, and the cut predicate, which can be written as the “!” sign.

When organizing a branch, it is required to construct it. Mutually exclusive conditions must be included as tail predicates in the rules that make up the branching structure. Let us consider an example of finding the largest of two numbers. It is known that the maximum of two numbers in mathematics can be determined as follows:

$$\max(x, y) = \begin{cases} x, & x \geq y \\ y, & x < y \end{cases}.$$

In Prolog, the finding of $\max(x, y)$ can be set as follows:

predicates

`max (real, real, real) /* triadicpredicate */`

clauses,

`max (X, Y, X) :- X >= Y.`

`max (X, Y, Y) :- X < Y.`

The knowledge base does not contain facts, but contains two rules. The first rule can be read as follows: “Maximum of values X, Y is X, if $X \geq Y$ ”, the second rule: “Maximum of values X, Y is Y, if $X < Y$ ”.

If you set an external goal

goal

`max (15, 10, Max). /* X=15, Y=10 */`

Prolog will find the solution:

Max = 15

1 solutions.

When finding a solution, Prolog needed only the first rule, because for given values $X > Y$. Since the goal is external, Prolog will also check the second rule for finding another solution and spend time on it. The conditions in the rules are mutually exclusive, so if you add cut predicate: $X > Y$.

$\text{max}(X, Y, X) :- X > Y, !.$ or $\text{max}(X, Y, Y) :- X < Y, !.$

$\text{max}(X, Y, Y) :- X < Y.$ $\text{max}(X, Y, X) :- X > Y.$

Prolog, having found maximum value according to the first rule, will no longer check the second one. In this example, the presence of the cut predicate is due to the logic of the program.

Let us consider the ways of organizing repetitions in the program in Prolog language. To organize the repetition of actions, you need to set a cyclic construction:

repeat.

repeat:- repeat.

This construction sets an infinite loop. You can use a predicate with any name as a loop predicate. The predicate repeat is not standard in this case and should be described in the section predicates. The program must provide for an exit from the cyclic design.

We consider as an example a program for finding function values $y = x^2$ for arguments that the user enters sequentially from the keyboard:

predicates

tab

repeat

test(real)

clauses

repeat.

repeat:-repeat.

tab:-repeat, readreal(X), test(X).

test(10e10):-nl.

test(X):-Y=X*X, write("X=",X," Y=",Y), nl, fail.

goaltab.

If you enter numbers from the keyboard, the values of the argument will be displayed on the screen, and the calculated value of the function will be displayed next to it. The program execution will end if a number in the exponential form 10e10 is entered. Until the specified number is entered, the tail predicate test(X) will have the value "false" due to the presence of the predicate **fail** in the tail of the rule test(X). In this case, Prolog uses backtracking, and the predicate **repeat** loops the process on entering a new number. If you enter a number in exponential form 10e10, the goal will be proved.

In this example, the organization of repetitions is implemented through a construction using the rule **repeat:-repeat**, which, in fact, is recursive, since both the head and the body there is a predicate with the same name.

Now let us consider the organization of repetitions directly using a recursive rule on the example of the task of tabulating function $y = x^2$ on segment $[a; b]$ with step h :

predicates

tab(real,real,real)

clauses

tab(A,B,H):-A<=B, X=A, Y=X*X, write("X=",X," Y=",Y),nl,

A1=A+H, B1=B, H1=H, tab(A1,B1,H1).

goal

```
write("a="), readreal(A), write("b="), readreal(B),
write("h="), readreal(H), nl, tab(A,B,H).
```

When the program is executed, a table of function values will be displayed on the screen for a user-defined segment with a specified step.

This program contains recursive rule `tab(A,B,H)`. To exit the recursion, the program uses the tail condition `A<=B`. `tab (A, B, H). A<=B`. The disadvantage of this method of exiting recursion is the fact that the predicate of the goal `tab(A,B,H)` after the program execution will have the value “false” because of the tail condition `A<=B` in the body of the recursive rule `tab(A,B,H)` after variable `A` reaches a value that exceeds the value of variable `B`. This disadvantage can be corrected by adding a non-recursive rule with the same name as the recursive one to the program. The program will take the following form:

```
predicates
tab(real,real,real)
clauses
tab(A,B,_):-A>B.
tab(A,B,H):-A<=B, X=A, Y=X*X, write("X=",X," Y=",Y),nl,
    A1=A+H, B1=B, H1=H, tab(A1,B1,H1).
goal
write("a="), readreal(A), write("b="), readreal(B),
write("h="), readreal(H), nl, tab(A,B,H).
```

Note that in this case, the recursive rule, which is responsible for repeating predicates, and the non-recursive rule, which is responsible for correct exit from recursion, use mutually exclusive conditions.

Here is another example of organizing repetition using a recursive rule. Let us consider a program for calculating the sum of k of the first terms of a series $S = 1 + x + x^2 + x^3 + \dots + x^n + \dots$:

domains

```
k=integer
x=real
n=real
s=real
```

predicates

```
sum(x,k,n,s)
clauses
sum(_,1,N,S):-N=1, S=N.
sum(X,K,N,S):-K1=K-1, sum(X,K1,N1,S1), N=N1*X, S=S1+N.
```

goal

```
write("X="), readreal(X),
write("K="), readint(K),
sum(X,K,N,S), nl,
write("S=",S).
```

In this program, k — the number of members of the series, whose sum must be calculated. Variable n is necessary to find the i -th term of the series, this variable contains the desired sum.

When trying to prove the statement of the goal, `sum(X,K,N,S)` the recursive rule `sum(X,K,N,S)` will be executed, provided that $K \neq 1$, as the tail condition of which there is recursive call `sum(X,K1,N1,S1)`, in this case, the value of the variable is $K1 = K - 1$. So, the value of variable k will decrease to 1 during the direct course of recursion. After matching with the rule `sum(_,1,N,S):-N=1, S=N` the reverse recursion will start, at each turn of which the next term of the series will be calculated by multiplying the previous term by the value of argument x . The value of the sum of the series will be accumulated in variable s .

Thus, the organization of repetitions in the program in Prolog is implemented using recursion. A recursive rule sets an infinite loop. This loop is used to solve a computational problem. Here, the completion of the loop and the exit from the recursion can be implemented in different ways:

- input of a predefined variable value by the user from the keyboard;
- using a logical expression as one of the conditions of a recursive rule;
- using a non-recursive rule with the same name as the recursive one, but true statements must act as predicates of the body in this rule.

Discussion and Conclusions. The most effective ways of organizing branches and repetitions in the logic programming language Prolog, identified as a result of a comparative analysis of literary sources, are presented. The given tasks are for educational and training purposes. Their solution contributes to the understanding of the logical programming theory based on the application of analogy, taking into account the specifics of building a program in Prolog and a special mechanism for its execution.

The given examples of programs allow us to use them as a technological basis for programming branches and repetitions in Prolog. The obtained results can be used in the further development of the application of recursive predicates in logical programming languages, as well as in the educational process when studying logical programming in Prolog.

References

1. Adir E, Almog L, Fournier E, et al. Genesys-Pro: Innovations in Test Program Generation for Functional Processor Verification. *IEEE Design & Test of Computers*. 2014;21(2):84–93. <https://doi.org/10.1109/MDT.2004.1277900>
2. ARM Architecture Reference Manual. ARM DDI 0487A.f. ARM Corporation, 2015. 5886 p.
3. Kent D. Lee. *Foundations of Programming Languages*. Springer, 2017. 370 p.
4. Ute Schmid. *Inductive Synthesis of Functional Programs: Universal Planning, Folding of Finite Programs, and Schema Abstraction by Analogical Reasoning*. Springer Science & Business Media, 2013.
5. Adam Lally, Paul Fodor. *Natural Language Processing with Prolog in the IBM Watson System*. Association for Logic Programming, 2011.
6. Tsukanova NI, Dmitrieva TA. *Teoriya i praktika logicheskogo programmirovaniya na yazyke Visual Prolog 7 [Theory and practice of logic programming in Visual Prolog 7]*. Moscow: Hot Line – Telecom, 2013. 232 p. (In Russ.)
7. Eduardo Costa. *Visual Prolog 7.3 for Tyros*. 2010. 270 p. URL: <http://visual-prolog.com/download/73/books/tyros/tyros73.pdf>
8. Bratko I. *Algoritmy iskusstvennogo intellekta na yazyke Prolog [Artificial intelligence algorithms in the Prolog language]*. 3rd ed. Moscow: Williams; 2004. 637 p. (In Russ.)
9. Adamenko AN, Kuchukov AM. *Logicheskoe programmirovaniye i Visual Prolog [Logic programming and Visual Prolog]*. Saint Petersburg: BKhV-Peterburg, 2003. 982 p. (In Russ.)
10. Tarushkin VT, Tarushkin PV, Tarushkina LT, et al. *Logika predikatov i yazyk Prolog [Predicate logic and the Prolog language]*. *Modern High Technologies*. 2010;4:62–63. (In Russ.)
11. Soldatova OP, Lezina IV. *Programmirovaniye na yazyke PROLOG [Programming in the PROLOG language]*. Samara: Samara University Repository; 2008. 52 p. URL: <http://repo.ssau.ru/handle/Metodicheskie-ukazaniya/Programmirovaniye-na-yazyke-PROLOG-Elektronnyi-resurs-metod-ukazaniya-k-lab-rabotam-53131?mode=full> (accessed: 20.06.2021). (In Russ.)
12. Michael A. Covington, Roberto Bagnara, Richard A. O’Keefe, et al. *Coding guidelines for Prolog. Theory and Practice of Logic Programming*. 2011;12(6):889–927.
13. Markov VN. *Sovremennoe logicheskoe programmirovaniye na yazyke Visual Prolog 7/5. [Modern logic programming in Visual Prolog 7/5]*. Saint Petersburg: BKhV-Peterburg; 2016. 541 p. (In Russ.)

14. Gopal Gupta, Enrico Pontelli, Khayri A.M. Ali, et al. Parallel Execution of Prolog Programs: a Survey. ACM Transactions on Programming Languages and Systems. 2011;23(4):472.

15. Polovikova ON, Shiryayev VV, Oskorbin NM, et al. Osobennosti programmnoi realizatsii logicheskikh zadach na yazyke PROLOG [Features of software implementation of logical tasks in PROLOG]. Izvestia of Altai State University. 2021;1(117):116–120. URL: <https://cyberleninka.ru/article/n/osobennosti-programmnoy-realizatsii-logicheskikh-zadach-na-yazyke-prolog> (accessed: 24.05.2021). (In Russ.)

Received 01.04.2021

Revised 14.04.2021

Accepted 04.06.2021

About the Author:

Zdor, Dmitrii B., associate professor, Engineering Institute, Primorskaya State Academy of Agriculture (44, Bluhera St., Ussuriysk, RF, 692510), Cand.Sci. (Pedagogy), associate professor, ORCID: <https://orcid.org/0000-0003-1131-6708>, jevgeniya.999.gn@mail.ru

The author has read and approved the final manuscript.

INFORMATION TECHNOLOGY, COMPUTER SCIENCE, AND MANAGEMENT



UDC 004.94

<https://doi.org/10.23947/2687-1653-2021-21-2-207-217>

Prospects of IoT technology

M. V. Yadrovskaya¹, M. V. Porksheyana¹, A. A. Sinelnikov²

¹Don State Technical University (Rostov-on-Don, Russian Federation)

²Russian Foreign Trade Academy (Moscow, Russian Federation)



Introduction. Internet of Things (IoT) is one of the promising innovative technologies. Every year more and more people are involved in the use of smart things. At the same time, a relatively small number of papers are devoted to the study of the social value of technology and the experience of human interaction with this technology. It is important to study the features and prospects of the technology, to analyze the attitude and willingness of people to use it.

Materials and Methods. We have conducted an Internet survey, in which special attention is paid to the place of IoT in the life of modern people, their attitude to the concept of devices. The obtained data is processed and systematized.

Results. The analysis of the survey results allowed us to draw conclusions regarding the attitude and willingness of young people to apply this technology. In the course of the study, the IoT concept was defined, the conditions required for the existence and functioning of the technology were described, the advantages of IoT technology were generalized, information technologies interacting with this technology were specified, the tasks that require solutions for the successful and effective implementation of IoT into Russian reality were listed.

Discussion and Conclusions. The Internet of Things is a technology that, with a consistent and systematic solution to a number of problems, can become a significant factor in the development of both individual spheres of life and activity, and the country as a whole. At the same time, it is important to study and consider the social impact of technology dissemination. This will increase trust in the IoT and eliminate negative impacts. The survey shows that young people tend to use smart things more widely. It is necessary to expand the range of smart things, to more confidently introduce the basics of practical application of IoT technology into educational programs, to discuss issues, ways to solve the tasks and pilot projects related to this technology widely in the media. This will enable to train not only people who are practically interested in IoT, but also qualified personnel who are able to solve problems in a new way.

Keywords: smart things, networks, innovative technology, IoT, Internet of things technology, online survey.

For citation: M.V. Yadrovskaya, M.V. Porksheyana, A.A. Sinelnikov. Prospects of IoT technology. Advanced Engineering Research, 2021, vol. 21, no. 2, pp. 207–217. <https://doi.org/10.23947/2687-1653-2021-21-2-207-217>

© Yadrovskaya M. V., Porksheyana M. V., Sinelnikov A. A., 2021



Introduction. The Internet of Things (IoT) is a relatively new concept and a multidisciplinary field of activity, a revolutionary technology that consists in connecting people, devices, physical and virtual things, processes and systems that can interact with each other through data transmission using networks. The simplest example is the control of such things as a coffee maker, washing machine, air conditioning, indoor light switches, etc. via an application on the phone and the network. The implementation of such interaction is possible thanks to special means of identifying and measuring the characteristics of things, communication technologies that transmit data to the storage, as well as

information technology that provides performing information processes for storing, processing, analyzing, presenting, and transmitting data to things.

The means of identifying things that are not connected to the Internet include radio frequency tags, optically recognizable identifiers — barcodes, Data Matrix, QR codes, infrared tags, and means of determining the location in real time. The means of identifying objects that are connected to the Internet network include the MAC address of the network adapter, which enables to identify the device at the channel level. The means of measuring the parameters of objects include sensors, smart meters, integrated systems. The means of data transmission include wireless and wired networks. Data processing tools include special applications, information and computing systems.

To implement smart things projects, a technical platform is required — a tool that will manage things and monitor their condition. A platform for remote monitoring and management of devices that have an Internet connection can be made, for example, in the form of a web server written in Java, whose prototype is called IOPT (Internet Of Pretty Things) [1]. Platforms can have free access or be commercial. Specifically, Intel® IoT Platform is a platform for the Internet of Things in the automotive industry, energy, healthcare, industrial systems, retail, smart buildings and homes; SAP HANA Cloud Platform for the Internet of Things is designed for the transport industry, energy, construction, medical systems, retail, telecommunications, oilfield services, metallurgy, fleet management and asset management [2].

Interaction of smart things with the user is carried out through the interface, which can be made in the form of an information panel of the service, a mobile or WEB application.

Internet of Things devices are elements of equipment that have mandatory communication capabilities and additional capabilities for measuring, triggering, as well as data input, storage and processing. The device, as a rule, includes a sensor, a radio module, a microcontroller, an actuator, a power source. Sensors are sensitive elements that interact with the system, constantly measure the physical parameters of the system objects in real time and form a signal. They are combined into nodes and equipped with microcontrollers. A microcontroller is a simple computer that, receiving a signal from a sensor, implements the logic of the entire device. Microcontrollers read the information and, according to the algorithms embedded in them, send the information to the server. A sensor, e.g., can generate a signal about the reading once per second, and a microcontroller will decide whether to transfer data to the server and with what time interval to do it. An actuator is an executive device that switches the device by a signal from a microcontroller or by a remote command that can be received by a radio module. If the task of the Internet of Things is only to monitor the system, then an actuator is not required. And, conversely, when reconciliation tasks are performed, sensors in the Internet of Things devices are not needed.

Special application protocols are used to interact with all these elements and perform their tasks. There are many protocols due to various ways of organizing the interaction of the Internet of Things and a diverse element base. According to [3, 4], issues of standardization and practical implementation of these protocols are handled by international organizations (ITU-T, IEEE, ETSI, OASIS), non-governmental associations (oneM2M), alliances of manufacturers and operators (IERC, ISO/IEC), partner projects.

The use of the Internet of Things can create a number of advantages. Indeed, light sensors will provide saving electricity; smoke sensors — fighting smoking in public places; it will be possible to reasonably control the temperature in the room with easily controlled air conditioners and batteries; radio tags on cars will allow you to control cargo transportation; video surveillance system optimizes the activity of identifying outsiders and people who are late for work; medical sensors will allow you to measure the pulse, pressure and other characteristics of the human condition, which will simplify the diagnosis and increase the effectiveness of treatment; in the retail sector, timely acquisition of information about the preferences of the buyer will allow the company to adapt to his needs and requirements; in those industries where expensive equipment, perishable products are used, and financial or other risks arise, the analysis of up-to-date information from IoT sensors will reduce the risks. Thus, the use of the Internet of Things in many industries will provide comprehensive information in a timely manner in real time, the analysis of which can affect the quality of work to optimize it.

It is established that the American continent currently makes a greater contribution to health care and smart supply chains projects, and the European continent — to smart cities projects [5]. It is also known that IoT projects related to industry and intelligent vehicles, as well as smart cities and smart energy have a large market share today [5].

When considering IoT in detail, there are questions that require study and scientific analysis. First, the functioning of the IoT is associated with the formation of large volumes of information, which are called “big data” because of the huge flow of data. There is a problem of limited computing power, which is required for processing and analyzing big data on dedicated servers. The solution to this problem is to switch to cloud and fog/edge computing, which support such processing, monitoring and analysis in IoT systems [5].

Data management requires technology to protect them well from unauthorized access, cyberattacks, risks, and vulnerabilities. According to experts, insufficient authorization and authentication, insecure software, microcode software and web interface, poor transport layer encryption are important issues of trust in IoT technology [5]. Cryptographic information protection for mobile devices is an important step towards understanding the data protection of the Internet of Things. A key security goal in an IoT cloud application is to ensure that unauthorized users do not have access to sensitive private data coming from devices. The application must also prevent sending unauthorized commands to devices [6]. Approaches to data protection should be adopted through design development [7] and the formation of special optimal containers for the protection of IoT devices that can be printed on 3D printers [8].

Other problems include: the lack of consistent approaches and concepts of IoT, the presence of different ways to connect things to the network, the lack of microelectronics components, the high price of smart devices and systems, the lack of uniform standards for the production of equipment and data transmission protocols, the immaturity of hardware and software, high energy consumption of IoT systems, etc. Accordingly, the problem of interoperability, which arises due to the heterogeneous nature of various technologies and solutions used for the development of the Internet of Things, needs to be solved. These solutions are required at four levels — technical, semantic, syntactic, and organizational. They can be based on adapters/gateways, virtual networks/overlay [5]. The task of developing high-quality materials to create new IoT devices with lower energy consumption needs research [5].

Today, the Internet of Things is a set of networks that are still loosely interconnected, each of which solves its own tasks and works according to different standards, which creates difficulties when combining them into one network. A significant part of their equipment was designed for special purposes, so it is quite difficult to combine all systems using IoT, it takes time and money. It is difficult to make changes when production applications, business processes, user interaction systems and data are isolated and fragmented. But there are grounds for solving problems. These include the declining cost of computing equipment and data transfer technologies, the development of cloud technology, the increasing number of smart devices, the availability of networks. Technologies are becoming much cheaper and easier to use, therefore, there are fewer obstacles to their implementation. It is necessary to develop standards for communication, interaction, confidentiality, and security [2].

Materials and Methods. Industry analysis company Gartner estimated that 8.4 billion Internet-connected things were used in 2017, which is 31% more than in 2016 [9]. Every year, an increasing number of people are involved using smart things, such as mobile devices, smartphones, tablet computers and portable devices, fitness trackers and smart watches, industrial machines and transport systems, continuous blood glucose monitoring monitors and digital blood pressure monitors [9]. Therefore, it is important to analyze people's attitude to the Internet of Things technology, their readiness to use devices that can see, hear, feel and create new data. According to analysts, only a relatively small number of studies have investigated the life experience of people using IoT technology [9].

To get answers to some questions related to IoT, an Internet survey was conducted, in which 102 people took part. Let us characterize a group of respondents through graphically presenting data about them. The majority of respondents are young people (65 %) (Fig. 1). They will implement the concept of the Internet of Things in life and use its results.

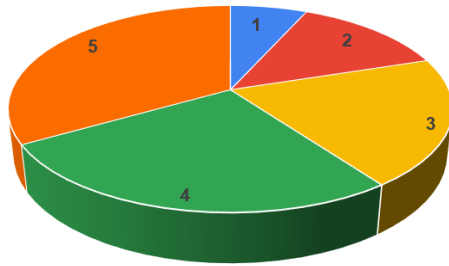


Fig. 1. Ratio of respondent categories: 1) student; 2) student-worker; 3) schoolboy; 4) worker; 5) unemployed

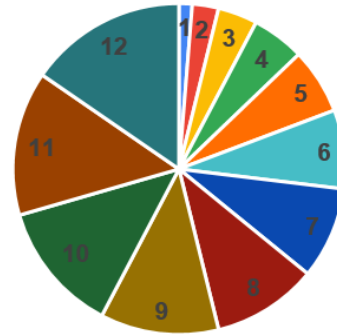


Fig. 2. Ratio of respondents by city of residence: 1) Rostov-on-Don; 2) St. Petersburg; 3) Novocherkassk; 4) Kamensk-Shakhtinsky; 5) Vladimir; 6) Glubokiy; 7) Moscow; 8) Kiev; 9) Bataysk; 10) Aksai; 11) Volgograd; 12) Volgodonsk

Most of the respondents (75 people) are residents of Rostov-on-Don (Fig. 2). Residents of Moscow, St. Petersburg, Vladimir, Volgograd and Kiev are presented in the group (Fig. 3). Global networks are ideal for conducting surveys.

The average age of the respondents is 20 years, the minimum age is 10 years, the maximum is 33 years. The average salary of respondents is 8,778 rubles, the maximum is 50,000 rubles.

The gender ratio of respondents is shown in Fig. 4: men (44 %) and women (56 %) make up the group of respondents in approximately equal proportions.



Fig. 3. Cities whose residents took part in the survey are marked in red

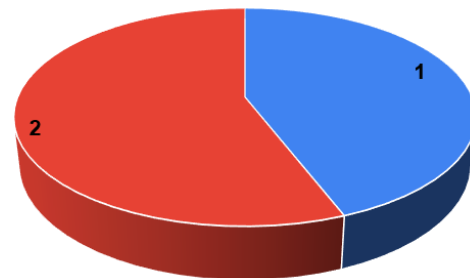


Fig. 4. Gender ratio of respondents: 1) men; 2) women

According to the histogram shown in Fig. 5, most respondents are moderately busy with work or study. It can be assumed that the survey participants are active and educated people who follow the development of technology. This is confirmed by the diagram in Fig. 6. About 83% of respondents rated their level of activity highly.

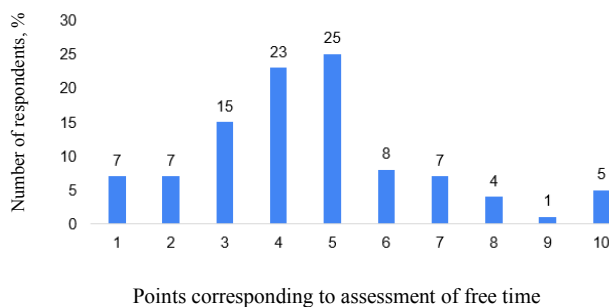


Fig. 5. Ratio of respondents by the availability of free time

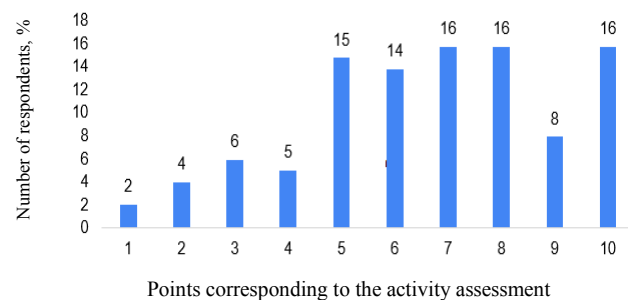


Fig. 6. Ratio of respondents by activity level

According to the diagram shown in Fig. 7, most of the respondents have a good command of a computer. Indeed, the respondents are young people who study information technologies at all levels of education and widely apply them in life and activities.

The presented data allow us to form a social portrait of a group of respondents.

Survey Findings. In the process of statistical analysis of the survey data, the following results were obtained regarding the use of the Internet of Things.

Figure 8 shows the ratio of respondents by the number of smart things at their disposal. These include: a smartphone; a smart watch / bracelet; a smart vacuum cleaner; a speaker with a voice assistant; a smart refrigerator; a smart washing machine; a car with artificial intelligence (autopilot). As you can see, in most cases, the respondents have 2, 3 or 4 smart things at their disposal. The maximum number of such things is 16.

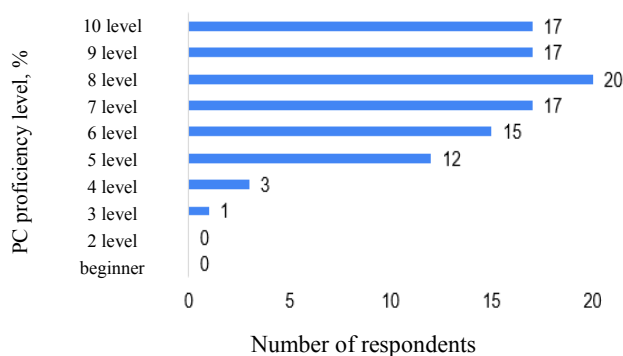


Fig. 7. Ratio of respondents by the level of computer proficiency

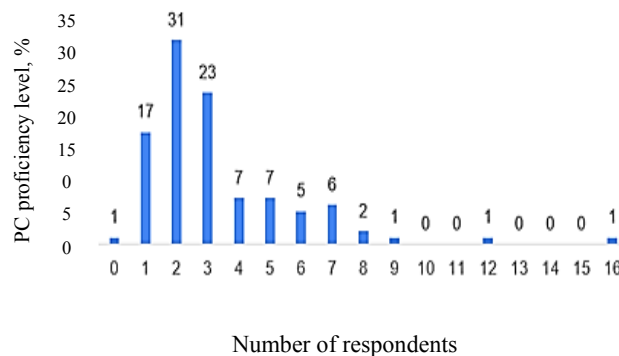


Figure 8. Ratio of respondents by the number of smart things at their disposal

Influence of the factor of the level of personal computer proficiency on the number of smart things available to respondents is not statistically proven (p-value of one-way analysis of variance is 0.73).

There is a weak correlation between the number of smart things and the average monthly income of respondents (0.141). Probably, the smart things that are noted in the survey were purchased on the income of all family members of the respondents. At the same time, there is an average degree of correlation between the age and the average monthly income of the respondents (0.52).

There is no correlation between the factors of age and the number of smart things that are available to respondents (-0.036). Accordingly, during the one-way analysis of variance, the influence of the age factor on the number of smart things available to respondents was not proved (p-value of one-factor analysis of variance is 0.55).

The influence of the factor of the sphere of activity to which the respondents refer themselves on the number of smart things at their disposal was statistically proved during a one-way analysis of variance (p-value is 0.03) (Fig. 9).

According to the diagram in Fig. 10, the majority of respondents believe that smart things can be used for work, training, entertainment (29.4 %), for training and entertainment (23.5%), or for training (16.7%). This suggests that the use of the Internet of Things is still poorly implemented in production, only 8.8 % of respondents use smart things for work. Indeed, many experts note such problems of the spread of the Internet of Things in our country as the lack of understanding of the results from using IoT, the unwillingness of business to change, the lack of real experience in implementing and serious research on the effectiveness of investments in the Internet of Things.

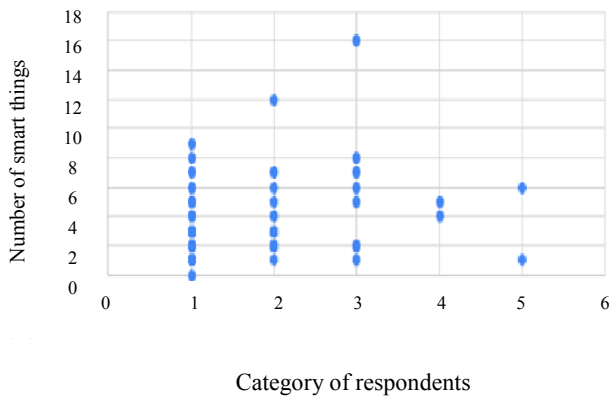


Fig. 9. Scatter chart of the number of smart things that respondents have: 1) student; 2) student-worker; 3) schoolboy; 4) worker; 5) unemployed

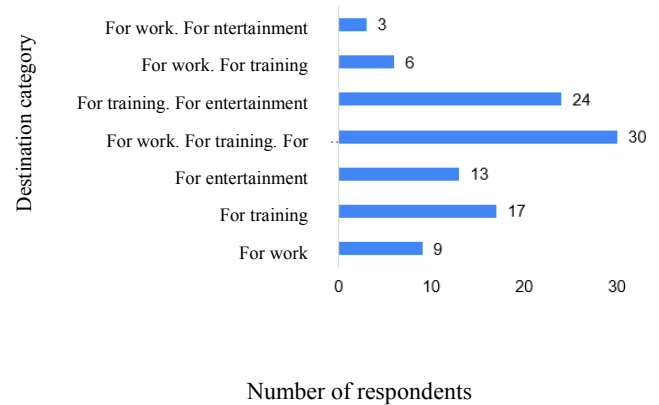


Fig. 10. Ratio of respondents according to the nature of the use of smart things

Linking smart things into a network provides a system of things that interact with each other and with the outside world, which can increase the significance of their use separately. According to previous surveys, 30 % of respondents say that the issue of implementing the Internet of Things in the activities of enterprises is not very important or not at all important. On the contrary, 34 % believe that the introduction of the IoT is very important. According to the survey (Fig. 11), the overwhelming majority of respondents (94 %) have a positive attitude to the idea of sharing smart things and turning them into Internet things.

The majority of respondents rather highly assess the security of data obtained through the Internet of Things (microphone in the speaker, GPS in the bracelet, sensors that measure pulse, temperature, etc.) (Fig. 12). There is such an opinion along with the fact that currently, the issues of the need to improve the security of electronic data are widely discussed in society. Probably, the results obtained are due to the lack of a deep understanding of the functioning of the IoT and its still small practical application.

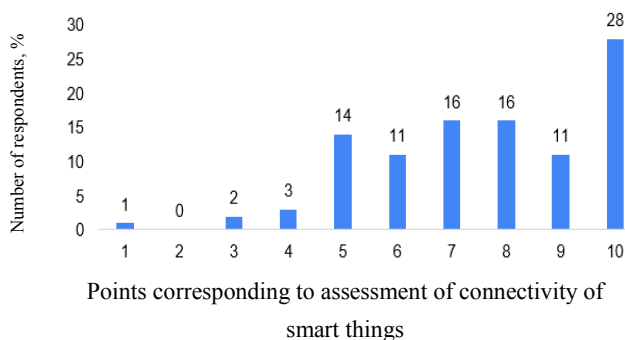


Fig. 11. Ratio of respondents according to the opinion about the connectivity of smart things

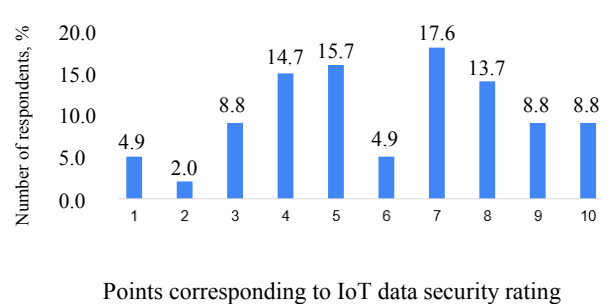
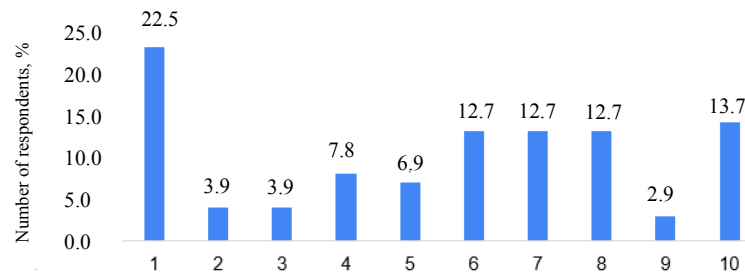


Fig. 12. Ratio of respondents in their opinion about the IoT data security rating

To this date, according to the survey, 22.5% of respondents believe that the problems of the Internet of Things are currently very poorly discussed. On the contrary, 53 % of respondents gave ratings from 6 to 10 on a ten-point scale to the level of discussion of IoT issues (Fig. 13). Indeed, the mass media pay sufficient attention to new solutions of smart things, giving examples of their practical application in various fields of activity: medicine, service, training, logistics, etc.



Points corresponding to the assessment of breadth of discussion of the IoT problems in society

Fig. 13. Ratio of respondents according to the opinion on breadth of discussion of the IoT problems in society

Based on the results of the information received, it can be concluded that:

- in most cases, the respondents have 2, 3 or 4 smart things at their disposal, maximum number of such things is 16;
- there is no correlation between the factors of age and the number of smart things that are available to respondents;
- there is weak correlation between the number of smart things and the average monthly income of respondents;
- influence of the sphere of activity factor on the number of smart things has been statistically proven;
- influence of the factor of the level of personal computer ownership on the number of smart things available to respondents has not been statistically proven;
- the number of smart things that respondents have tends to increase due to the increasing discussion of IoT technology in society;
- respondents aged 20 to 30 years are more likely to use smart things for work and entertainment;
- respondents under the age of 20 are more likely to use smart things for training;
- only 8.8 % of respondents use smart things for work;
- respondents who have little free time are more likely to use smart things for work and training in practice;
- respondents who have a lot of free time are more likely to use smart things for entertainment;
- the more the respondent plans his activities, the more smart things he owns;
- the vast majority of respondents (94 %) have a positive attitude to the idea of sharing smart things and turning them into Internet things;
- as the level of computer proficiency increases, the importance of linking smart things to the network grows;
- the more attention is paid to the discussion of the IoT technology in society, the more respondents have hopes for linking smart things together;
- 22.5% of respondents believe that the problems of the Internet of Things are currently very poorly discussed;
- 53 % of respondents gave ratings from 6 to 10 on a ten-point scale to the level of discussion of IoT issues;
- the majority of respondents quite highly appreciate the security of data obtained through IoT (microphone in the speaker, GPS in the bracelet, sensors that measure pulse, temperature, etc.).

Results and Discussion. According to popular belief, the most effective development tool is the Internet of Things technology [10–12]. It is an integral attribute of the information society, a form of communication between people and things. Linking smart things into a network can be characterized by different levels of complexity and coverage of interaction. Experts point to the prospects of “smart” homes, factories, hospitals, cities, agriculture, transportation, retail, the environment, the planet, etc. [13].

IoT technology can seriously affect production, the nature of business processes, and an ordinary human life. Its joint use with other information solutions (Table 1) will multiply the pace and determine innovative ways of the desired transformations [14, 15]. If we consistently and systematically solve a whole range of tasks, the IoT technology can become a significant factor in the development of Russia (Table 1).

Table 1

Characteristics of the Internet of Things technology

IoT advantages	Solving IoT problems in Russia	Technologies interacting with IoT
Data consolidation	State support for technology	Automatic data processing
Analyzing large amounts of data	Development of the legislative framework	Big Data solutions
Up-to-date receiving of comprehensive information	Tax incentives for enterprises	High performance networks
Condition monitoring and prediction	Development of a unified ontology, codifiers, reference books	Distributed computing
Automated quality control	Building an open technical dictionary technology	Machine learning
Interaction automation	Development of own production of IoT devices	Virtual reality (VR)
Remote process control	Formation and regulation of IoT market	Augmented Reality (AR)
Automatic diagnostics	Development of IoT standards	Robotics
Uninterrupted manufacture	Development of unified data transfer protocols	Cloud technologies
Production output in automatic mode	Development of technologies for cryptographic information protection	Video analysis
Mobile interaction of personnel	Creation of unified IoT information collection centers	Neural networks
Improving the quality of interaction between different departments of the enterprise	Creation of industry databases for IIoT	Artificial intelligence
Selection of the optimal mode of equipment operation	Development of mobile technologies	Cybersecurity
Reducing risks and incidents	Forming public opinion	Mobile technologies
Optimization of logistics and production chains	Building real IoT experience	Computer simulation
Reducing the significance of human factor in production	Research on the effectiveness of investments in IoT	Manufacturing of high-tech hand prostheses
Immersive training of specialists	Creating service-oriented business models	Digital Twin technology
Creating a complete portrait of the consumer	Short pilot projects	3D modeling
Provision of product quality monitoring services	Development of high-quality materials with lower energy consumption	3D scanning and printing
Introduction to agriculture (greenhouses, etc.)		Virtual SIM cards (eSIM)
		Digital workplace
		Machine-to-machine interaction
		Additive manufacturing technology

In addition, it is important to study and take into account the social impact of the spread of technology [12]. Reliable conclusions of this study will increase confidence in IoT and eliminate negative impacts, such as: blurring the

boundaries between private and public; possibility that algorithmic decision-making processes in IoT will be preconceived and will exacerbate social inequality and social marginalization; concentration of smart city technologies on rich cities or districts that are able to pay for their services; possibility of not meeting expectations from the use of technology [9, 12, 16], etc.

Conclusions. The survey has shown that young people are ready to practically use IoT. Young people aged 20 to 30 years are more likely to use smart things for training and leisure activities, and not just in everyday life. Schoolchildren use smart things to a greater extent for learning. These are undoubtedly important areas of smart things application. The most significant would be the use of IoT in production and support activities, in which currently, for objective reasons, the use of Internet of Things technology is low. Positive steps towards the use of IoT are critical. It is required to further expand the range of smart things that could be used in the educational and entertainment spheres to form the skills of young people to use this technology in practice and turn it into a reasonable need. It is important to introduce into educational programs the basics of practical application of the Internet of Things technology in parallel with other technologies that work effectively together. This will contribute, on the one hand, to the deepening and expansion of knowledge of innovative information technologies; and on the other hand, it will help to interest young people, provide an indicative basis for practical application, further development and implementation of this technology in various fields of activity. It is also essential to widely discuss problems, ways to solve them and pilot projects related to Internet of Things technology in the media. This will allow us to train not only people who are practically interested in IoT, but also qualified personnel who are able to solve problems in a new way.

References

1. Yakimenko AA, Belov AI, Goncharuk PS, et al. Razrabotka platformy dlya upravleniya infrastrukturoi interneta veshchei [Development of platform for controlling the infrastructure of the Internet of Things]. Proceedings of the Samara Scientific Center of the RAS. 2017;19(6):97–104. URL: <https://cyberleninka.ru/article/n/razrabotka-platformy-dlya-upravleniya-infrastrukturoy-interneta-veschey/viewer> (accessed: 13.02.2021). (In Russ.)
2. Goikhman V, Saveleva A. Analiticheskii obzor protokolov Interneta veshchei [Analytical review of the Internet of Things protocols]. Communication Technologies & Equipment Magazine. 2016;4:32–37. URL: <http://lib.tssonline.ru/articles2/reviews/analiticheskii-obzor-protokolov-interneta-veschey> (accessed: 11.02.2021). (In Russ.)
3. Shcherbinina MYu, Stefanova NA. Kontseptsiya internet veshchei [Concept of Internet of Things]. Creative Economy. 2016;10(11):1323–1336. URL: https://www.researchgate.net/publication/311863315_Koncepcia_internet_vesej (accessed: 12.02.2021). (In Russ.)
4. Anna Gerber, Jim Romeo. Connecting all the things in the Internet of Things IBM Developer, 2020. URL: <https://developer.ibm.com/technologies/iot/articles/iot-lp101-connectivity-network-protocols/> (accessed: 30.03.2021).
5. Sachin Kumar, Prayag Tiwari, Mikhail Zymbler. Internet of Things is a revolutionary approach for future technology enhancement: a review. Journal of Big Data. 2019;6:111. URL: <https://journalofbigdata.springeropen.com/articles/10.1186/s40537-019-0268-2> (accessed: 30.03.2021).
6. Joy Patra, Amitranjan Gantait, Ayan Mukherjee. Securing IoT applications. IBM Developer, 2018. URL: <https://developer.ibm.com/technologies/iot/articles/iot-trs-secure-iot-solutions3/> (accessed: 30.03.2021).
7. Dave Whitelegg. Application privacy by design. IBM Developer, 2018. URL: <https://developer.ibm.com/technologies/iot/articles/s-gdpr2/> (accessed: 30.03.2021).
8. Ori Pomerantz. 3D Printing for IoT Developers. IBM Developer, 2018. URL: <https://developer.ibm.com/technologies/iot/articles/3d-printing-for-iot-developers/> (accessed: 30.03.2021).

9. Deborah Lupton. The Internet of Things: Social dimensions. *Sociology Compass*. 2020;14(4). URL: https://www.researchgate.net/publication/338576609_The_Internet_of_Things_Social_dimensions (accessed: 30.03.2021).
10. Dovgal VA, Dovgal DV. Internet Veshchei: kontseptsiya, prilozheniya i zadachi [Internet of Things: concept, applications and tasks]. *Bulletin of Adyghea State University (Mathematical-Natural and Technical Sciences)*. 2018;1(216):129–135. URL: <https://cyberleninka.ru/article/n/internet-veschey-kontseptsiya-prilozheniya-i-zadachi/viewer> (accessed: 11.02.2021). (In Russ.)
11. Markeeva AV. Internet Veshchei. Vozmozhnosti i ugrozy dlya sovremennykh organizatsii [Internet of Things (IoT): opportunities and threats for contemporary organizations]. *Society: Sociology, Psychology, Pedagogics*. 2016;2:42–46. URL: <https://cyberleninka.ru/article/n/internet-veschey-iot-vozmozhnosti-i-ugrozy-dlya-sovremennykh-organizatsiy/viewer> (accessed: 12.02.2021). (In Russ.)
12. Markeeva AV. Sotsial'nye posledstviya razvitiya interneta veshchei (IoT) [Social consequences of the development of the Internet of Things (IoT)]. *Modern Information Technologies and IT-Education*. 2016;12(2):236–240. URL: <https://cyberleninka.ru/article/n/sotsialnye-posledstviya-razvitiya-interneta-veschey-iot/viewer> (accessed: 12.02.2021). (In Russ.)
13. Cvetkov VJ. Internet veshchei kak global'naya infrastruktura dlya informatsionnogo obshchestva [Internet of Things as a global infrastructure for the information society]. *Modern Management Technology*. 2017;6(78):3. URL: <https://sovman.ru/article/7803/> (accessed: 12.02.2021). (In Russ.)
14. Anna Gerber, Jim Romeo. Key concepts and skills for getting started in IoT. IBM Developer, 2020. URL: <https://developer.ibm.com/technologies/iot/articles/iot-key-concepts-skills-get-started-iot/> (accessed: 30.03.2021).
15. Anna Gerber, Jim Romeo. Choosing the best hardware for your next IoT project. IBM Developer, 2020. URL: <https://developer.ibm.com/technologies/iot/articles/iot-lp101-best-hardware-devices-iot-project/> (accessed: 30.03.2021).
16. Gorodischeva AN, Zamyatina EV. Internet veshchei i ego mesto v informatsionnom obshchestve [Internet of Things and its place in the information society]. *Social and economic and humanitarian magazine of Krasnoyarsk SAU*. 2015;1:134–141. (In Russ.)

Received 01.04.2021

Revised 29.04.2021

Accepted 04.05.2021

About the Authors:

Yadrovskaya, Marina V., lecturer of the Media Technologies Department, Don State Technical University (1, Gagarin sq., Rostov-on-Don, RF, 344003), Cand.Sci. (Phys.-Math.), associate professor, ORCID: <https://orcid.org/0000-0002-4469-1603>, marinayadrovskaya@rambler.ru

Porksheyan, Markos V., programmer, Digital Educational Technologies Department, Don State Technical University (1, Gagarin sq., Rostov-on-Don, RF, 344003), ORCID: <https://orcid.org/0000-0001-6772-487X>, marinayadrovskaya@rambler.ru

Sinelnikov, Anton A., Director of Informatization, Russian Foreign Trade Academy (6A, Vorobiyovskoye Sh., Moscow, RF, 119285), ORCID: <https://orcid.org/0000-0003-2522-4900>, antal@vavt.ru

Claimed contributorship

M. V. Yadrovskaya: basic concept formulation; research objectives and tasks setting; literature analysis; computational analysis; text preparation; formulation of conclusions. M. V. Porksheyan: conducting a survey and calculations; literature analysis; text preparation. A. A. Sinelnikov: preparation of the questionnaire for the survey; literature analysis; formulation of conclusions.

All authors have read and approved the final manuscript.